This PDF file including Research Plan and 5 Papers

Xin Wu

1. Research Plan: p 2 - 3
2. Papers: p4 - 57

(1) 3: related to heart (including arrhythmia study)
(2) 2 related to vessel

The career development plan of research

Xin Wu, MD

A. Research Interests:

1. *Mechanotransduction* in cardiovascular (both heart and vessel) system and *neuroplasticity* in nervous system: Using atomic force microscopy, cell stretching in physiological and pathological conditions (e.g. diabetes mellitus, hypertension, and heart failure; aging and epilepsy).
2. *Electrophysiology* with/without immunofluorescence in cardiovascular (both heart and vessel-blood vessel and lymphatic vessel) and nervous systems: ion channels (e.g. Ca^{2+}, K^{+} and GABA channels) regulation in physiological and pathological condition.
3. *Cell adhesion, integrins, extracellular matrix and cellular signaling*.
4. *Signal transduction in cardiovascular systems*: Including calcium signal, cytoskeleton, second messengers, and protein phosphorylation, etc.
5. *Functional studies*: Including ECG and EEG in physiological and pathological condition in vivo.

I have conducted highly sophisticated studies on the cardiovascular (both heart and vessel, including lymphatic vessel) and nervous systems for more than 20 years using techniques at the nano-molecular, cellular, organic, and systemic levels. My current research interest is to study the mechanisms of integrin-mediated mechanotransduction in the process of diabetic related cardiovascular diseases. **I am eager to learn new concepts, master new tasks quickly and come up with 'better and easy ways'**.

There are is an estimated 21 million Americans have diabetes. 65% of the deaths from diabetes are related to cardiovascular causes. **Type 2 diabetes mellitus (DM. Or metabolic syndrome)** increases the risk for cardiovascular diseases 2 to 4 times. More than 50% treated DM or hypertension patients are uncontrolled by using current treatment regimens. We need develop new technology (e.g. nanotechnology) on research and discover new medications (e.g. integrin ligands). Most anti-DM and anti-hypertension drugs target on cell components. However, during progress of hyperglycemia, diabetes, hypertension, and myocardial infarction, there is an increase in expression and deposition of fibronectin (FN) and collagen in non-cell compartments. Extracellular matrix (ECM) proteins communicate with intracellular molecules including cytoskeleton and Ca^{2+} signaling systems through integrins. **The roles of integrin-mediated intracellular signaling in cardiac and vascular system from diabetes (or/and hypertension) are still not well understood.** In addition to cardiovascular disease, integrins are central to the pathophysiology of many nervous diseases, such as stroke, Alzheimer, diabetic neuropathy and epilepsy.

My research interests are how integrin modulate mechanotransduction in cardiovascular system and neuroplasticity in nervous system. My NIH R21 (1, PI/MPI-Received a priority score and will be resubmitted) and NIH RO1 (2, in preparation) proposals cover both systems.

Because integrin pathway is a potential new target in **cardiovascular** and nervous diseases and integrin ligands may hold promise to produce disease-modifying effect for the prevention of **cardiovascular** and nervous diseases**,** my **long-term goal** is to understand the mechanisms of integrin function in the development of **cardiovascular** and nervous diseases.

B. To investigate this hypothesis, the techniques I will employ (details on CV) are as follows: (1) **Nano-technique** (atomic force microscopy with/without immunofluorescence. > 5 years experience) in fresh isolated living cells to address mechanical properties in physiological and pathological condition (e.g. DM, hypertension); (2) **Electrophysiology** and optical imaging techniques (>15 years experience) in native or gene transfected cells, and in tissues to probe the ion channels involved signaling pathways; (3) Histocytochemistry, PCR, and co-expression of ion channels, and/or intracellular molecules in HEK cells or fresh isolated cells, and site-directed mutagenesis strategies to understand the details in the signaling pathways; (4) Single fresh cell isolation techniques including isolating VSM cells, endothelial cells, neuronal cells, cardiomyocytes, etc; and isolated and canulated blood and lymphatic vessels (diameter <100 micrometer) methods and Langendorff heart preparations to allow interpretation of biological responses; (5) Single cell stretching (I modified in

VSM) using two or three microelectrodes and application of protein-coated microbeads to single cells (I developed) while performing electrophysiological recording to document characteristics of mechanosensitivity; (6) Imaging and cardiovascular monitoring (e.g. Echocardiogram, ECG, MRI, EEG) to deal with systemic functional changes in human or animal model; (7) Designing customized programs and research equipments to ensure efficiencies, compliance and productivity gains in data analysis and research. (8) I can also perform other techniques that mentioned in my CV on different systems because I was well-trained as a physiologist with clinical experience. I have taught and trained many medical students and scientists in the past.

I have studied that integrins modulated mechanotransduction signaling including ion channels, such as Ca^{2+}, K^{+} and mechanosensitive channels for more than 15 years using combination of patch-clamp (whole cell and single channel) and immunofluorescence system, gene expression and confocal microscopy in fresh isolated and cultured arteriolar smooth muscle cells, cardiomyocytes, neuronal cells, ion channel gene expressed HEK cells. I have also studied the cardiac mechanical properties, and contractility for more than 5 years using combination techniques of atomic force microscopy, and force-Ca^{2+} measurements. Three grants as PI and Co-PI have been received to support my researches on cardiovascular researches. Almost 30 articles were published in top-quality high impact journals including the J Cell Biol, Pharmacology & Therapeutics, J Biol Chem, and Circ Res (Editorial and Cover Story) with citation more than 800. At least 9 papers are in preparations. Many other Labs asked for the help for the techniques of patch clamp and fresh single cell isolation (see CV). Our paper was the first paper in the world to show Ca^{2+} currents in cremaster arterioles (not arteries, mentioned by other scientist in the paper). I am the only person followed Dr. Mike Davis using two or three microelectrodes to stretch single vascular smooth muscle cell (Dr. Davis developed and I modified) in America because of the difficulty that mentioned by many papers. I also developed the technique for applying protein-coated microbeads to single cells while performing electrophysiological recording. I have participated and helped Drs. Davis and Muthuchamy receive at least four NIH RO1 grants and other grants. I will focus on translational researches of integrin regulation on cardiovascular and nervous systems in the future.

C. Collaborative arrangement:

Co-lab with Drs. Muthuchamy, Carl Tong, Samba Reddy and Chaodong Wu (Texas A&M); Drs. Mike Davis and Gerald Meininger (University of Missouri); and Dr. Haodong Xu (Department of Pathology and Laboratory Medicine, University of Rochester School of Medicine and Dentistry) and other faculty members in the Institute for genetic animal models and specific expressed ion channels. **We have several transgenic (TG) mouse lines including vinculin-KO mouse, and tropomyosin-KO mouse**.

Significance: Cardiovascular and nervous diseases are the major cause of death in US. The integrin ligands might be the potential drug candidates for cardiovascular and nervous diseases. **These studies will provide important new functional information about the mechanotransduction process between integrins and intracellular signaling in cardiovascular and nervous diseases.** Since investigations on how integrin mediated mechanotransduction involved in the cardiovascular and nervous systems are limited**, these studies may have far reaching medical implications.**

Am J Physiol Heart Circ Physiol 298: H2071–H2081, 2010.
First published April 9, 2010; doi:10.1152/ajpheart.01156.2009.

Cardiomyocyte contractile status is associated with differences in fibronectin and integrin interactions

Xin Wu,[1] Zhe Sun,[2] Andrea Foskett,[1] Jerome P. Trzeciakowski,[1] Gerald A. Meininger,[2]* and Mariappan Muthuchamy[1]*

[1]*Department of Systems Biology and Translational Medicine, Texas A&M Health Science Center College of Medicine, College Station, Texas; and* [2]*Dalton Cardiovascular Research Center, Department of Medical Pharmacology and Physiology, University of Missouri-Columbia, Columbia, Missouri*

Submitted 9 December 2009; accepted in final form 6 April 2010

Wu X, Sun Z, Foskett A, Trzeciakowski JP, Meininger GA, Muthuchamy M. Cardiomyocyte contractile status is associated with differences in fibronectin and integrin interactions. *Am J Physiol Heart Circ Physiol* 298: H2071–H2081, 2010. First published April 9, 2010; doi:10.1152/ajpheart.01156.2009.—Integrins link the extracellular matrix (ECM) with the intracellular cytoskeleton and other cell adhesion-associated signaling proteins to function as mechanotransducers. However, direct quantitative measurements of the cardiomyocyte mechanical state and its relationship to the interactions between specific ECM proteins and integrins are lacking. The purpose of this study was to characterize the interactions between the ECM protein fibronectin (FN) and integrins in cardiomyocytes and to test the hypothesis that these interactions would vary during contraction and relaxation states in cardiomyocytes. Using atomic force microscopy, we quantified the unbinding force (adhesion force) and adhesion probability between integrins and FN and correlated these measurements with the contractile state as indexed by cell stiffness on freshly isolated mouse cardiomyocytes. Experiments were performed in normal physiological (control), high-K^+ (tonically contracted), or low-Ca^{2+} (fully relaxed) solutions. Under control conditions, the initial peak of adhesion force between FN and myocyte $\alpha_3\beta_1$- and/or $\alpha_5\beta_1$-integrins was 39.6 ± 1.3 pN. The binding specificity between FN and $\alpha_3\beta_1$- and $\alpha_5\beta_1$-integrins was verified by using monoclonal antibodies against α_3-, α_5-, α_3 + α_5-, or β_1-integrin subunits, which inhibited binding by 48%, 65%, 70%, or 75%, respectively. Cytochalasin D or 2,3-butanedione monoxime (BDM), to disrupt the actin cytoskeleton or block myofilament function, respectively, significantly decreased the cell stiffness; however, the adhesion force and binding probability were not altered. Tonic contraction with high-K^+ solution increased total cell adhesion (1.2-fold) and cell stiffness (27.5-fold) compared with fully relaxed cells with low-Ca^{2+} solution. However, it could be partially prevented by high-K^+ bath solution containing BDM, which suppresses contraction by inhibiting the actin-myosin interactions. Thus, our results demonstrate that integrin binding to FN is modulated by the contractile state of cardiac myocytes.

integrins; extracellular matrix protein; mechanobiology; atomic force microscopy; cell mechanics

IN CARDIAC MUSCLE, a salient example of the link between mechanical strain and physiological function is the regulation of cardiac output in response to increasing ventricular pressure. This interaction defines the cardiac pressure-volume relationship (i.e., the Frank-Starling law of the heart). The mechanism for this relationship is believed to involve stretching of the myocytes within the cardiac wall, which impacts the myofilament overlap in such a way that filament interaction and, hence, contractile performance are affected (44). In addition to the acute effects of mechanical load, prolonged mechanical loading of the myocardium leads to hypertrophy as well as changes in cardiac wall and myocyte stiffness (54, 56, 69, 71). These changes are accompanied by significant alterations in integrin and extracellular matrix (ECM) protein expression (4, 8, 38, 58, 75, 78, 80, 81). Fibronectin (FN) is one of the major ECM proteins that promotes the adhesion of cardiomyocytes. FN is normally expressed in the heart and undergoes increased expression in the hypertrophic and injured myocardium (1, 7, 30, 38, 74). Moreover, an accumulation of immunoreactive FN is seen in the ischemic injured myocardium during the early stages of acute myocardial infarction and may have functions related to the repair process and fibrotic remodeling of the ventricular wall (6, 32). An imbalance in the production and degradation of ECM proteins may lead to structural alterations such as basement membrane thickening and ECM protein deposition in tissues during the development of cardiovascular diseases (2, 5, 8, 17, 20, 31, 38, 40, 52, 58, 63, 64, 75, 78, 80, 81). These studies have implied that FN is potentially of major importance to the functioning of the myocardium. However, the roles of FN in the myocardium with respect to its interaction with integrins and other downstream signaling events have not been addressed. In this study, our aim was to characterize the relationship between integrin adhesion and FN in normal myocytes as an essential starting point in understanding its functional significance.

$\alpha_3\beta_1$-Integrin and $\alpha_5\beta_1$-integrin are two important adhesion receptors for FN, and both bind to the arginine-glycine-aspartic acid (RGD) motif in FN domain III (11, 16, 18, 37, 61). Integrins, by virtue of their cytoskeletal and signaling protein linkages, are thus believed to form an important mechanosensing and -transducing axis capable of inside-out and outside-in signaling (12, 28, 55, 79). In cardiomyocytes, integrins have been found localized in costameres, the sites where Z bands connect to the basement membrane. The costamere is structurally integrated with cytoskeletal components and signaling complexes, further supporting the proposition that integrins are involved in mechanical signaling (14, 19, 30, 57). It has been reported that an application of mechanical stress to integrin adhesion sites causes increased cytoskeletal stiffening, second messenger signals, and phosphorylation of proteins anchored to the cytoskeleton (41, 60, 79). Thus, there is strong evidence suggesting that integrins act as conduits for the

* M. Muthuchamy and G. A. Meininger are equal contributing authors. G. A. Meininger may be contacted at meiningerg@missouri.edu.

Address for reprint requests and other correspondence: M. Muthuchamy, Dept. of Systems Biology and Translational Medicine, Texas A&M Health Science Center College of Medicine, College Station, TX 77843-1114 (e-mail: marim@tamu.edu).

transmission of mechanical force across the cell membrane and the initiation of intracellular signaling (12, 28, 55).

Cardiomyocytes have been shown to express at least four dominant integrin subtypes, which include $\alpha_1\beta_1$, $\alpha_3\beta_1$, $\alpha_5\beta_1$, and $\alpha_7\beta_1$ (50). Both $\alpha_3\beta_1$- and $\alpha_5\beta_1$-integrins recognize ECM proteins containing the RGD sequence, such as found in FN (57, 59). In addition to β_1-integrin expression, expression of β_3- and β_5-integrins has been reported in cardiomyocytes (33, 46, 66). In this study, our focus was to determine whether the adhesion properties of two major β_1-integrin subtypes, $\alpha_3\beta_1$ and $\alpha_5\beta_1$, which interact with FN, change during the contracted and relaxed states in cardiomyocytes. We hypothesized that the regulation of the interaction between integrins and ECM could form a basis for the physiological modulation of myocyte function as well as for the pathological changes in myocyte function that are correlated with the altered expression of ECM proteins and integrins. If integrin interactions with ECM are capable of rapid modifications, then it is also possible that they may ultimately be shown operative on a beat-to-beat basis.

Currently, little is known about the mechanical characteristics of integrin-ECM interactions in myocytes, and there is nothing known about how these interactions are affected by the contractile state. Technical limitations have somewhat slowed progress toward understanding adhesive interactions at the cellular and molecular levels, particularly in mechanically active cells such as cardiac myocytes. In this study, we used atomic force microscopy (AFM) to measure forces at the pico- and nano-Newton scales to evaluate the adhesion between FN and integrins and to measure cell stiffness as an index of activation during the contracted and relaxed states of cardiomyocytes.

MATERIALS AND METHODS

Adult cardiomyocyte preparation. Adult male mouse cardiomyocytes (FVB/N strain, 2–4 mo) were prepared as previously described (82). Briefly, the heart was harvested under anesthetic conditions and put into ice-cold Ca^{2+}-free physiological saline solution (PSS) containing (in mM) 133.5 NaCl, 4 KCl, 1.2 NaH_2PO_4, 1.2 $MgSO_4$, 10 HEPES, and 11 glucose (pH 7.4). 2,3-Butanedione monoxime (BDM; 10 mM) was present during the dissecting procedure. The aorta was cannulated, and the heart was mounted in a Langendorff perfusion system with Ca^{2+}-free control solution containing 1 mg/ml BSA (Amersham Life Science, Arlington Heights, IL) at 37°C. After 5 min, perfusion was continued with the same solution containing 25 μM Ca^{2+} together with collagenase type I (62.4 U/ml, Worthington) and type II (73.7 U/ml, Worthington). After ~15–20 min, the heart was removed and transferred to a petri dish containing PSS with 100 μM Ca^{2+}. The ventricles were cut into small pieces, which were then gently triturated using a fire-polished Pasteur pipette to release single cells. The cell suspension was filtered through a 250-μm mesh collector, and cells were allowed to settle. Collected cells were then resuspended in PSS containing 200 μM Ca^{2+}. After this procedure, cells were stored at room temperature and used within 6 h. A suspension of freshly dispersed cells was plated onto a laminin type I-coated (10 μg/ml) dish for at least 30 min in PSS with 1.8 mM Ca^{2+} before experiments. All experiments were carried out at 22–23°C. All procedures using mouse hearts were approved by the Texas A&M University Animal Care Committee.

AFM force mode operation for force and stiffness measurements. The force contact mode of operation was used for measurements of unbinding force (adhesion force) and was detected and quantified in the AFM probe retraction curve. Relative cortical membrane stiffness (elastic modulus) was measured from the approach curve as previously described (68, 73). AFM experiments were performed using a Bioscope system (model 3A, Digital Instruments, Santa Barbara, CA), which was mounted on an Axiovert 100 TV inverted microscope (Carl Zeiss). The Bioscope system is equipped with Nanoscope IIIa controller and Nanoscope III software (version 5.12). The AFM probes used were silicon nitride microlevers with conical tips (model MLCT-AUHW). Tip diameters were <40 nm, and the mean spring constant was ~14.4 ± 0.6 pN/nm. For each experiment, the position of the protein (e.g., FN)-labeled probe was controlled to repeatedly touch and retract (z-axis) from the cell surface. Force curves were recorded for these repeated cycles of probe approach and retraction at 0.5-Hz scan frequency and a z-axis movement of 800 nm. The AFM probe tip was selectively positioned between the nucleus and the edge of the cell.

To measure cell cortical stiffness (i.e., elastic modulus or cell resistance to shape deformation; see Fig. 2), approach force curves were used for analysis (see dark line in Fig. 2). Approach force curves were fitted with the Hertz model between *points 2* and *3* (see Fig. 2) using MATLAB software (Mathwork) and NForceR software to calculate the cortical stiffness based on tip displacement and membrane indentation (73). The retraction curve (see dotted line in Fig. 2) was used to analyze the specific adhesion forces related to bonding between the AFM tip and cell surface. During retraction, if a specific adhesion event occurred, it was detected as small sharp shift (bond rupture) in the deflection curve obtained during probe retraction from the cell surface. No adhesions were apparent as a smooth retraction curve similar in appearance to the approach curve. These deflection shifts, referred to as "snap-offs," were recorded in the force curve and represent the force required to cause bond failure between FN on the AFM probe and the cell surface (68, 73). With the application of the spring constant of the AFM probe cantilevers, all deflection shifts (snap-offs) in a retraction curve were detected, quantified, and used to compute the rupture force with NForceR software. Deflection shifts represent the rupture force between the probe and cell surface. With each group of experiments, 500 force curves were sampled from 10 randomly selected cells (obtained from 3 to 5 hearts, 50 curves/cell) for each treatment. Collectively, the adhesion force measurements obtained from all retraction curves were analyzed as force-density (normalized events that with adhesion) relationships. Smooth plots of relative density versus force or stiffness were obtained with standard kernel density estimation methods (48). The algorithm centers a smoothing window on the distribution of force values, and the predicted density [$f(x)$] is calculated as a weighted average of the density values for nearby points. The weight given to each point in the smoothing window is controlled by a Gaussian kernel (K) based on the distance between each force (or stiffness) value (x_i) and the center of the interval (x) in which x_i falls (29) as follows:

$$f(x) = \frac{1}{nh^d} \sum_{i=1}^{n} K\left(\frac{x - x_i}{h}\right) \quad (1)$$

where d is dimension. The bandwidth (h) determines the degree of smoothing of the density curve. For these analyses, h was based on the normal reference distribution (77).

From the density distributions, we recorded peak force/stiffness as well as integrated estimates of force and stiffness. The peak value (mode) represents the most frequent or maximum likelihood value obtained over 500 approach and retraction curves in each experiment. However, the peak values do not convey information about the spread of the force or stiffness measures. We therefore measured integrated values of force and stiffness as well. The integrated values correspond to the areas under the force/stiffness density distribution curves; departures from symmetry in the density distribution (e.g., rightward skew) will thus cause the integrated measures to be greater than the peak values. In probability theory, the integral of the density corresponds to the mean. Although force and stiffness are continuous variables, their density curves can only be estimated at discrete points.

We measured the center and spread of the force/stiffness distributions using standard algorithms for the mean and variance of random variables, allowing summations to approximate integration over the discrete points. *X* represents the set of plotted values for either force or stiffness having values $x_1, x_2, x_3, \ldots x_k$. For each of these values, there is a corresponding set of probabilities ($p_1, p_2, p_3, \ldots p_k$) that can be obtained from the density curve (i.e., plotted relative densities divided by *n*, the total area under the curve). The mean (i.e., integrated value) of X (μ_X) is as follows:

$$\mu_X = \sum_{i=1}^{k} x_i p_i \quad (2)$$

SEs of the peak or integrated values of force and stiffness were computed from each density curve by resampling (i.e., sampling with replacement). A bootstrap distribution of the peak or integrated value of a density curve was obtained by constructing density curves from 5,000 random resamples of the data and estimating the peak and integral for each curve. The bootstrap SE for each measure is the SD of the bootstrap distributions (13, 25).

Labeling of AFM probes. AFM probes were labeled with the ECM protein (i.e., FN) or control proteins using methods we have previously described, which were adopted from Lehenkari and Horton (34, 68). Polyethylene glycol (PEG; Sigma) was used to cross-link proteins onto silicon nitride probes at room temperature. The probe was first incubated with 10 mg/ml PEG for 5 min, washed with PBS four times, and then incubated with FN (1 mg/ml, Invitrogen, Grand Island, NY) for 1 min. The tip was again washed with PBS for four times. The spring constants were assumed to be unchanged after the protein labeling because only the very end of the cantilever was coated. In nonintegrin antibody, control adhesion experiments, anti-rat major histocompatibility complex class I (MHC) monoclonal antibody (U.S. Biological, Swampscott, MA, 1 mg/ml)-coated AFM probes were used. In nonspecific protein experiments, BSA-coated AFM probes were used.

Ligand application. To determine the specificity of FN-integrin bond, experiments were performed on cells pretreated with either mouse anti-α_3-integrin monoclonal antibody (60 nM) or anti-α_5-integrin monoclonal antibody (HMα5–1, 60 nM, BD Bioscience, San Jose, CA). α_3- and α_5-integrin subunits are known to associate only with β_1-integrin (but not the reverse) (mouse anti-β_1-integrin monoclonal antibody, 50 μM, BD Bioscience), making these antibodies specific for the $\alpha_3\beta_1$- and $\alpha_5\beta_1$-heterodimers. Anti-mouse α_{11}-integrin monoclonal antibody (60 nM, R&D Systems) was used as a control for non-FN-recognized integrin.

Fluorescence confocal microscopy. Overnight cultured cardiac myocytes were fixed with 2% paraformaldehyde for 1 h followed by several glycine-PBS washes. Cells were permeabilized with ice-cold methanol for 3 min at 4°C followed again by several rinses with PBS. Cells were then incubated with blocking solution containing 1% BSA (Vector Laboratories), 2.5% normal goat serum, and 0.1% Triton X-100 for 1 h. After the blockade, cells were incubated together with primary mouse anti-α_3-integrin and rat anti-mouse α_5-integrin (5H10–27, 1:100, BD Bioscience) or primary mouse anti-vinculin (1:100, Chemicon) and rat anti-mouse α_5-integrin (1:100, BD Bioscience) for 1 h. Samples were rinsed and then incubated with secondary antibodies of goat anti-mouse Oregon green 488 IgG and goat anti-rat red Cy5 IgG (1:200, Molecular Probes, Invitrogen) for 1 h in the dark, washed extensively, and treated with ProLong AntiFade (Molecular Probes, Invitrogen). Serial image sections through focus with a step size of 0.1–0.3 μm thickness were collected using a Leica AOBS SP2 confocal microscope (Leica Microsystems, Wetzlar, Germany).

Solutions. For normal physiological conditions, PSS with 1.8 mM Ca^{2+} was used. For tonic contractions, cells were incubated with high-K^+ Ringer solution (high-K^+ solution) containing (in mM) 150 KCl, 2 $CaCl_2$, 1.17 $MgSO_4$, 5 glucose, 1.22 NaH_2PO_4, 0.02 EDTA, 2 sodium pyruvate, and 3 MOPS (pH 7.4). High-K^+ solution was used to depolarize the cell membrane and activate Ca^{2+} entry. For relaxing conditions, cells were incubated with low-Ca^{2+} solution containing (in mM) 53.3 KCl, 6.8 $MgCl_2$, 0.025 $CaCl_2$, 10 EGTA, 20 MOPS, 5.35 ATP, 12 creatine phosphate, and 10 BDM [Sigma; pH 7.2, Ca^{2+} concentration ($[Ca^{2+}]$) of 50 nM]. Low-Ca^{2+} solution served to keep the sarcomeres in a relaxed state through the combination of BDM, low $[Ca^{2+}]$, and high [ATP] (72). All chemicals, except as specifically stated, were obtained from Sigma-Aldrich.

General data analysis. For adhesion force and stiffness measurements, the NForceR program, Matlab software (MathWorks, Natick, MA), Origin (OriginLab), StatView, and SAS were used. Adhesion force between FN and integrins on myocytes were plotted as a function of the frequency (events) of occurrence. Single-rupture forces (F) were determined using Hooke's law as follows: $F = kd$, where *d* is the height of the step change in the retraction curve representing bond rupture (see *point 5* in Fig. 2) and *k* is the spring constant. Differences between means for the effect of a given treatment were determined using ANOVA or with an independent two-tail *t*-test as appropriate. Averaged values are expressed as mean ± SE. Values of $P < 0.05$ were considered to be statistically significant.

RESULTS

Distribution of integrins on cardiomyocytes. To confirm the presence of $\alpha_3\beta_1$- and $\alpha_5\beta_1$-integrins in cardiomyocytes, the distribution of these integrins was determined by fluorescent immunocytochemistry using monoclonal antibodies against α_3- and α_5-integrin subunits. A single cardiac myocyte dual immunolabeled with α_3-integrin (Fig. 1*A*, green) and α_5-integrin (Fig. 1*A*, red) monoclonal antibodies showed that these two integrins are heavily concentrated in the costameric structures of myocytes. The overlay of the α_3- and α_5-integrin images with "zoom-in" revealed that the two integrins are distributed in costameric structures of the myocyte (Fig. 1*A*, $\alpha_3 + \alpha_5$), which is consistent with previous studies (21, 57) describing integrin distribution in cardiomyocytes. To further determine the proximity of the integrins to the cytoskeleton structure in cardiomyocytes, we examined the distribution of $\alpha_5\beta_1$-integrin and vinculin as a cytoskeletal protein. Cardiac myocytes dual immunolabeled with vinculin (Fig. 1*B*, green) and $\alpha_5\beta_1$-integrin (Fig. 1*B*, red) monoclonal antibodies showed that vinculin and $\alpha5\beta1$-integrin are concentrated in costameres and the intercalated disk of myocytes. The overlay of α_5-integrin and vinculin with zoom-in magnifications revealed that these two structures are closely localized in the vicinity of the costamere structure (Fig. 1*B*).

Analyses of the adhesion force between the FN-coated probe and a single cardiomyocyte. To measure the cell membrane stiffness and adhesion force (unbinding force) between FN and the cardiomyocyte surface, AFM probes coated with FN were applied to the membrane surface of noncontracting cardiomyocytes. A typical force curve is shown in Fig. 2. When the FN-coated probe moved to approach the cell surface (from *point 1* to *point 2*), force remained at zero level. The cantilever bent, encountered a resistance, and changed the deflection signal after contact with the surface (dark "approach" line, from *point 2* to *3*). *Point 2* represents the "reflection" point or "contact" point. Data in the region of *points 2–3* were used to fit the Hertz model to calculate cell cortical stiffness. The stiffer the cell, the less the indentation and the steeper the upslope of the force curve. As probe retraction started (dotted "retraction" line), resistance force decreased (from *point 3* to *4*). The snap-off that represents bond rupture (i.e., adhesion

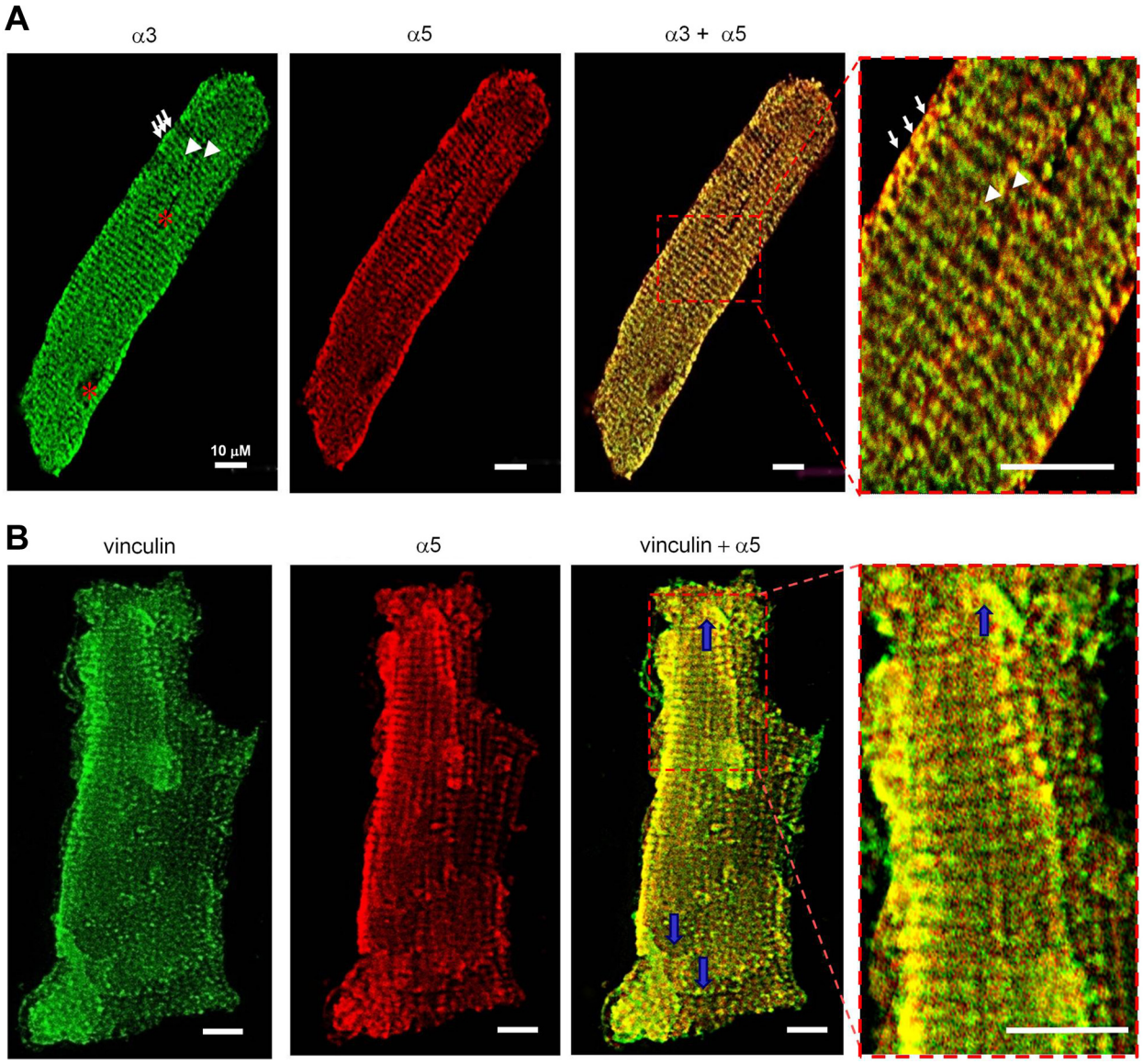

Fig. 1. Immunofluorescence localization of integrins and the cytoskeleton protein vinculin in adult mouse cardiomyocytes under high confocal magnification (×63). *A*: immunofluorescence labeling was performed on isolated cardiomyocytes using anti-α_3-integrin with an Oregon green-labeled secondary monoclonal antibody and anti-α_5-integrin with a Cy5-labeled secondary monoclonal antibody. The enlarged *inset* (*right* image) shows the overlay of anti-α_3 and anti-α_5-integrin micrographs, where the closest or colocalized areas are indicated as yellow-orange. Regions of costameric (arrows), striated (arrowheads), and nuclear (red asterisks) structures are shown. *B*: immunofluorescence staining of a single cardiomyocyte using anti-vinculin with an Oregon green-labeled secondary monoclonal antibody and anti-α_5-integrin with a Cy5-labeled secondary monoclonal antibody. The enlarged *inset* (*right* image) shows the overlay of anti-vinculin and anti-α_5-integrin micrographs, where the closest or colocalized areas are shown as yellow-orange. Integrin and vinculin exhibited costameric and intercalated disk (blue arrow) localization. Bar = 10 μm.

force) between FN and the cardiomyocyte is shown in the retraction line (dotted line *point 5*). As shown in Fig. 2, the example trace shows three adhesion events (bond rupture) that occurred when the FN-coated probe retracted. When all adhesions between the FN-coated probe and cardiomyocyte have been broken, the retraction curve again overlies the initial approach curve level (*point 6*) because net forces acting on the cantilever are zero (i.e., equivalent to force acting on the probe during the approach).

To analyze the distribution of adhesion events, the observed adhesion events plotted as histograms were fitted with Gaussian distributions to resolve integrin-FN bond adhesion force. Data analyses showed a good agreement between the raw data (histogram) and the fitted line (Fig. 3*A*, solid line). The peak bond rupture force (initial peak of the adhesion force in Fig. 3*A*) of FN-integrin was ~39.6 ± 1.3 pN (Fig. 3*A*, control, n = 10), which likely represents a FN-integrin single bond unbinding force (67, 68, 73). The bar at the *right* of Fig. 3*A* shows the probability of FN-integrin adhesion events defined as the percentage of the curves with adhesion divided by total recorded curves. Under conditions defined for these experiments, the probability of adhesion events between the FN-coated probe and cardiomyocyte was 65% (Fig. 3). We also performed control experiments in which myocytes were plated directly on the glass plate without laminin and measured adhesive force and probability. Our results showed that the adhesion (force

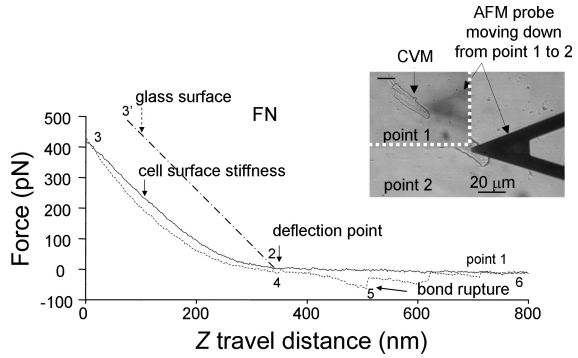

Fig. 2. Raw force curves generated using fibronectin (FN)-coated atomic force microscopy (AFM) probes on cardiomyocytes. FN-coated probes (1 mg/ml) were controlled to repeatedly (800 nm/s z-axis movement at 0.5-Hz frequency) approach (solid trace) and retract (dotted line trace) from freshly isolated cardiomyocytes. Points *1–6* represent the stages of approach and retraction (explained in detail in the RESULTS). The *insets* show the AFM probe approaching the myocyte (*top left inset*, *point 1* in the curve). Note that the image of the AFM cantilever is blurred as it is above the plane of focus. The *bottom right inset* shows the AFM probe in contact with the myocyte (*point 2* in the curve). Note that the AFM cantilever is in sharp focus. CVM, cardiomyocyte.

and probability of binding) between FN and integrins was not significantly different from the cells plated on laminin-coated plates (adhesion force: 38.6 ± 0.9 vs. 39.6 ± 1.3 and probability: 61% vs. 65%), indicating that there was no significant influence of the substrate laminin on the measured interactions with FN. We also examined the adhesion force and probability of adhesion using FN-coated microbeads (5 μm, $n = 6$) on the tip of the AFM probe. While the adhesion force between FN-integrin was not significantly different from the adhesion force measured with the conically tipped AFM probe (38.1 ± 1.0 vs. 39.6 ± 1.3 pN), the probability of adhesion was significantly greater with the microbead-tipped AFM probe due to the larger contact area of the microbead with the cardiomyocyte cell membrane (84% vs. 65%).

To determine whether adhesion or mechanical characteristics would vary in different regions of the cell body, force curve measurements were performed on three regions of the cell body. Measurement sites were selected 25% from either end of the myocyte and in the lengthwise center of the cell ($n = 4$). Results demonstrated that there were no differences in cell stiffness or adhesion characteristics at either of the two cell ends (data not shown). However, the adhesion probability and cell stiffness from the central region of the cell were 14% and 47%, respectively, lower than similar measurements made at the end of the cells (data not shown). A comparison of the FN adhesion force indicated that there were no differences among the three different regions. For all experiments reported below, data presented were collected with the probe positioned 25% from the end of the myocyte.

FN exhibits binding specificity for $\alpha_3\beta_1$- and $\alpha_5\beta_1$-integrins on cardiomyocytes. $\alpha_3\beta_1$-Integrin and $\alpha_5\beta_1$-integrin have been documented to bind FN (50). To verify their roles in adhesion events between FN and cardiomyocytes, cells were pretreated with integrin monoclonal antibodies. We used anti-α_3- or anti-α_5-integrin antibody (60 nM) to block α_3- or α_5-integrin subunits. Since α_3- and α_5-integrin subunits are known to associate only with the β_1-integrin subunit, we assumed that these antibodies provide information regarding binding specificity for $\alpha_3\beta_1$- and $\alpha_5\beta_1$-integrins (27). There were no significant changes in the initial peak adhesion force in the presence of either α_3-integrin (41.1 ± 3.2 pN, 60 nM, $n = 10$; Figs. 3*C* and 4*A*) or α_5-integrin (41.2 ± 2.2 pN, 60 nM, $n = 10$; Figs. 3*B* and 4*A*) monoclonal antibodies. However, the probability of attachment to FN was inhibited by 48% or 65% in the presence of anti-α_3- or anti-α_5-integrin monoclonal antibodies, respectively (Fig. 3, *B* and *C*). Pretreatment with antibodies also reduced the area under the

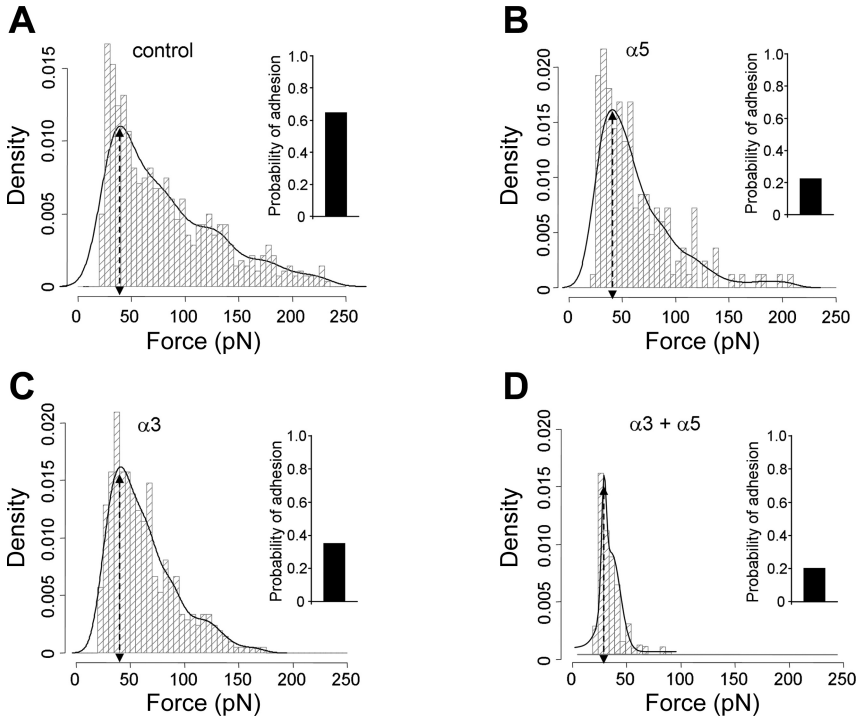

Fig. 3. Summary of adhesion force results with the FN-coated AFM probe in cardiomyocytes. *A*: analyses of force-density plots of adhesion events during FN-coated probe retraction in cardiomyocytes. The observed adhesion force and corresponding number of events in the experiments (50 curves/cell for a total of 500 curves) were plotted as histograms. Solid lines represent the results that fitted with multiple Gaussian distributions. *Insets*: integrin-FN binding probabilities (solid bars). *B–D*: force-density plots of adhesion events and integrin-FN binding probabilities (solid bars) in the presence of function-blocking antibodies against α_5-integrin (*B*; 60 nM), α_3-integrin (*C*; 60 nM), or the combination of α_3- and α_5-integrins. $n = 10$ for each group.

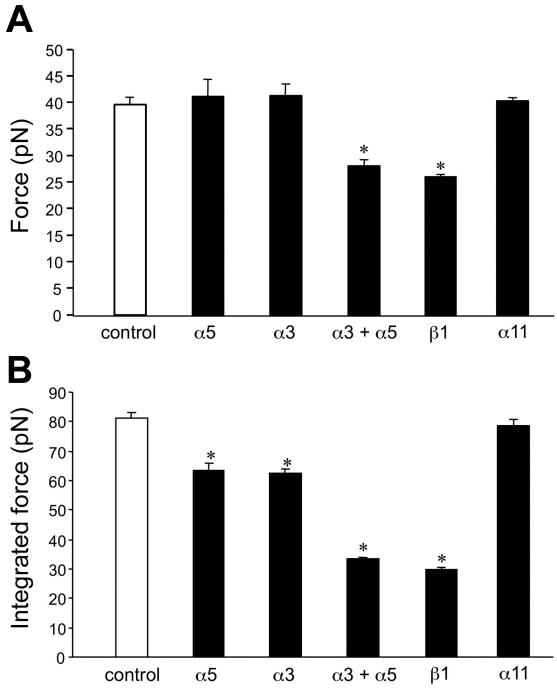

Fig. 4. Summary data of adhesion force and integrated force with the FN-coated AFM probe in cardiomyocytes. The adhesion force (*A*) represents the first peak force, and the integrated force (*B*) represents the total area under the force-density distribution curves. Calculations are presented in MATERIALS AND METHODS. Adhesion force was not changed in the presence of α_3- or α_5-integrin monoclonal antibodies alone, whereas the combination of α_3- and α_5-integrin monoclonal antibodies and β_1-integrin monoclonal antibody decreased adhesion force. Integrated force, which provides a metric reflecting the average overall adhesiveness, was decreased by α_3- or α_5-integrin monoclonal antibodies and further decreased by the combination of α_3- and α_5-integrin monoclonal antibodies and β_1-integrin monoclonal antibody (50 μM). Non-FN α_{11}-integrin (60 nM) showed no significant effects on adhesion force and integrated force. *$P < 0.05$ vs. control (FN-coated AFM probe alone). $n = 10$ for each group.

adhesion force density distribution curve (i.e., displayed less spread than with FN alone), indicating fewer total adhesion events (Fig. 3, *A–C*). The integrated force value, determined as average force from all adhesion events, was also calculated as described in MATERIALS AND METHODS. The integrated adhesion force between FN and the myocyte was 81.1 ± 2.3 pN. The integrated force was inhibited by 21% in the presence of α_3-integrin monoclonal antibody and by 23% in the presence of α_5-integrin monoclonal antibody (Fig. 4*B*). Treatment with the combination of anti-α_3- and α_5-integrin monoclonal antibodies significantly reduced the adhesion force (to 28.1 ± 1.2 pN), probability of attachment, and integrated force by 29%, 70%, and 59%, respectively, compared with FN binding alone (Figs. 3*D* and 4). In addition, treatment with β_1-integrin monoclonal antibody, to block all available αβ-integrin combinations, including $\alpha_3\beta_1$- and $\alpha_5\beta_1$-integrins, significantly reduced the adhesion force (to 25.2 ± 0.1 pN), probability of attachment, and integrated force by 36%, 75%, and 61%, respectively ($n = 10$; Fig. 4). To further determine the specificity of the adhesion force and probability between $\alpha_3\beta_1$-integrin-FN and $\alpha_5\beta_1$-integrin-FN, a non-FN α_{11}-integrin subunit monoclonal antibody was used. The results showed no significant difference in adhesion force, probability of attachment, and integrated force compared with FN alone in the presence of α_{11}-integrin monoclonal antibody ($n = 10$; Fig. 4).

Furthermore, as an antibody control, nonintegrin binding antibody, anti-rat MHC monoclonal antibody (1 mg/ml)-coated AFM tips were tested ($n = 10$). MHC class I receptor molecules were detected on almost every cell, but the probability of binding and adhesion force were significantly lower compared with FN ($n = 10$)-coated AFM probes (−85% and −29%, respectively). As a nonspecific protein control, AFM probes were coated with BSA. BSA-coated probes ($n = 10$) also exhibited a significantly lower probability of binding and adhesion force compared with FN-coated probes (−75% and −24%, respectively). Finally, uncoated AFM probes alone exhibited 65% lower probability of binding and 45% lower adhesion force than FN-coated probes.

Adhesion force and membrane stiffness of cardiomyocytes are dependent on the actin-myosin cytoskeleton. The membrane cytoskeleton is a critical junction for mechanotransduction in cardiomyocytes. Complexed with integrins at focal adhesions, mechanical forces are transmitted bidirectionally across the cell membrane. Forces transmit from the ECM to the cytoskeleton when extracellular forces act on the myocyte and from the cytoskeleton to the extracellular environment when myocytes generate contractile force. Thus, the cytoskeleton has been proposed to provide an intracellular structure for transmitting contractile forces out of the cell to the matrix as well as a pathway for transmitting external forces into the cell and nucleus (27, 42, 57). To investigate the changes in the actin-myosin cytoskeleton in cardiomyocytes, force curve measurements were performed in the presence of cytochalasin D, an F-actin-disrupting agent, or BDM, an agent that suppresses contraction by inhibiting actin-myosin interactions (23, 72). Treatment of myocytes ($n = 10$) with cytochalasin D or BDM had no effect on adhesion force (Fig. 5*A*) or adhesion probability (Fig. 5*B*). However, integrated adhesion force was significantly reduced (Fig. 5*D*) by both cytochalasin D (−32%) and BDM (−24%). Cell stiffness in control myocytes was 31.0 ± 0.5 kPa; the decrease in myocyte cell stiffness after cytochalasin D (−85%) or BDM (−70%) treatment supported the cytoskeletal effects of these agents (Fig. 5*D*).

Adhesion force and membrane stiffness of cardiomyocytes change under contracted and relaxed states. To quantify the changes in FN adhesion during contraction and relaxation of the myocyte, adhesion measurements were compared under conditions where high-K^+ solution was used to induce a tonically contracted state and low-Ca^{2+} solution with EGTA and BDM was to induce a fully relaxed state. Images of typical cardiomyocytes in these two solutions are shown as *insets* in Fig. 6, *A* and *B*. All cardiac cells that were studied were visibly observed to contract in high-K^+ solution (Fig. 6*A*, *inset*). During tonic contraction, peak adhesion force was significantly increased (1.2-fold, $P < 0.05$) from 38.4 ± 2.5 pN in relaxed cells ($n = 10$, Fig. 6*B* with *inset* cell image) compared with 47.9 ± 1.5 pN in contracted cells ($n = 10$; Fig. 6, *A* and *B*). Contraction was also associated with a 2.8-fold increase ($P < 0.05$) in adhesion probability compared with myocytes under relaxed conditions (53% in contracted vs. 19% in relaxed, $n = 10$; Fig. 6, *A* and *B*). In addition, the adhesion force density distribution curve observed in cells under the contracted state displayed significantly more adhesion events (i.e., more area under probability distribution) than occurred in cells under the relaxed state (Fig. 6, *A* and *B*). The increase in myocyte adhesiveness during contraction was also apparent as a 1.6-fold

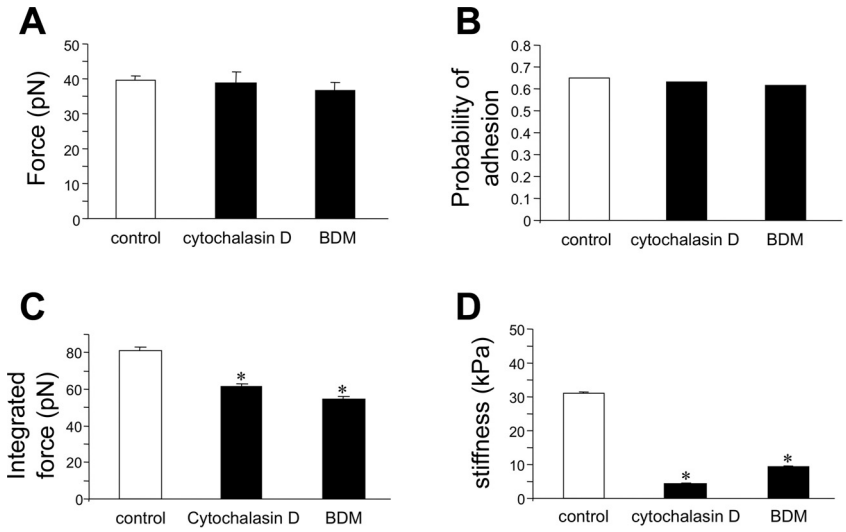

Fig. 5. Summary of results of adhesion characteristics of cardiomyocytes in the absence or presence of cytochalasin D or 2,3-butanedione monoxime (BDM). The adhesion force, probability, and cell stiffness were calculated as described in detail in MATERIALS AND METHODS from the force curves obtained from cells under normal condition or cells incubated in the presence of cytochalasin D or BDM. Adhesion force (*A*) and adhesive probability (*B*) were not changed in the presence of cytochalasin D or BDM. Integrated force (*C*) and cell stiffness (*D*) were significantly decreased in the presence of cytochalasin D or BDM. $*P < 0.05$ vs. control. $n = 10$ for each group.

higher integrated force in contracted cardiomyocytes compared with cells in the relaxed state (Fig. 7*B*).

Consistent with a state of cell contraction and relaxation, the cell stiffness or elasticity was 137.5 ± 5.3 kPa in the contracted state, which was 27.5-fold greater than in the relaxed condition (Fig. 7*C*). To control for the effect of cell shortening and force generation by actin-myosin cross-bridge cycling, myocytes were treated with a combination of high-K^+ solution plus BDM (Fig. 6*C*). With BDM (10 mM) in high-K^+ bath solution, the adhesion force and integrated force decreased by 17% and 25%, respectively (Fig. 7, *A* and *B*) compared with high-K^+ solution alone. There were no significant differences in adhesive probability without or with BDM in high-K^+ state, and the probability of binding remained significantly higher than in the relaxed state. The presence of BDM in high-K^+ solution prevented visible cell shortening (Fig. 6*C*, *inset*) and the increase in cell stiffness observed with high-K^+ solution alone. BDM decreased cell stiffness by 82% compared with high-K^+ solution alone (Fig. 7*C*). In addition, the probability, integrated force, and stiffness of high-K^+ solution + BDM-treated cells were 2.7-, 1.2-, and 5.1-fold greater than in relaxed cells, respectively (Fig. 7, *B* and *C*).

DISCUSSION

The results of this study demonstrate that FN-cardiomyocyte adhesion through α_3- and α_5-integrins varies with the contractile status of the myocyte, indicative of dynamic regulation of integrin adhesion during cell contraction.

Transmembrane integrins that link the ECM and intracellular cytoskeleton are important for mechanosensation and mechanotransduction. Integrins can act as conduits to mechanically transfer forces and initiate biochemical signals from the outside of the cell to the inside and from the inside of the cell to the outside (12, 28, 55, 79). In cardiomyocytes, costameres in general are considered as the subsarcolemmal protein assemblies that circumferentially align in register with the Z disk of peripheral myofibrils. Thus, costameres physically couple force-generating sarcomeres with the sarcolemma in cardiac muscle (9, 15, 47). The costamere structure, including integrin linkage to the Z disk of the sarcomeres via the cytoskeleton proteins talin, vinculin, desmin, FAK, and α-actinin, plays an important role in mechanotransduction (57) and is analogous to the focal adhesions found in other cell types. Cardiac myocytes normally express α_1-, α_3-, α_5-, α_6-, α_7-, α_9-, α_{10}-, and β_1-integrins; of these, the four most prevalent subtypes are $\alpha_1\beta_1$-, $\alpha_3\beta_1$-, $\alpha_5\beta_1$-, and $\alpha_7\beta_1$-integrins (49, 50). We (59) have previously shown the expression of $\alpha_5\beta_1$-integrin in the intact mouse myocardium. The data in the present study show that the presence of $\alpha_5\beta_1$-integrin in isolated cardiomyocytes qualitatively matches the expression of integrins in the intact heart tissue. The expression of $\alpha_3\beta_1$- and $\alpha_5\beta_1$-integrins and the cytoskeleton protein vinculin in the vicinity of the costameres

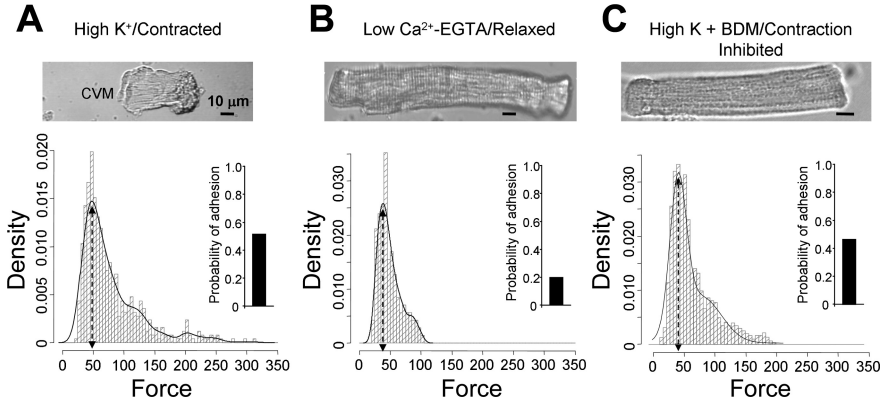

Fig. 6. Summary of results of adhesion force in contracted (high-K^+ solution), relaxed (low-Ca^{2+} solution), and high-K^+ solution + BDM-treated cardiomyocytes. *A–C*: analyses of force-density plots of adhesion events during FN-coated probe retraction in cardiomyocytes. Adhesion to FN was enhanced during contraction or contraction with BDM compared with the relaxed state. The observed adhesion force and corresponding number of events in the experiments (50 curves/cell for a total of 500 curves) were plotted as histograms in contracted cells (*A*), relaxed cells (*B*), and high-K^+ solution + BDM-treated cells (*C*). Solid lines represent the results that fitted with multiple Gaussian distributions. *Insets*: integrin-FN binding probabilities (solid bars) in contracted (*A*) and relaxed (*B*) cardiomyocytes and high-K^+ solution + BDM treated cells (*C*). *Top*: AFM images of cardiomyocytes under each condition. $n = 10$ for each group.

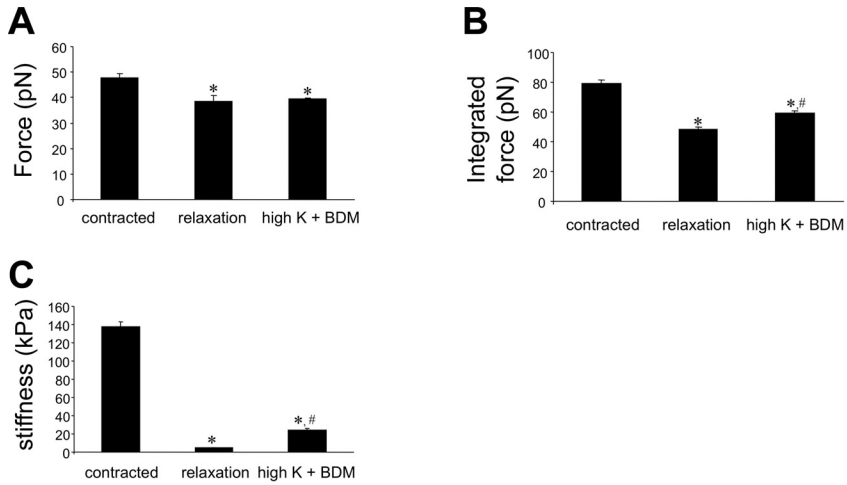

Fig. 7. Summary of results of cell adhesive and mechanical properties of cardiomyocytes in the contracted and relaxed states. The adhesion force (*A*), integrated force (*B*), and stiffness (*C*) of relaxed cells and high K^+ solution + BDM-treated cells were significantly smaller than in contracted cells. In addition, the integrated force (*B*) and stiffness (*C*) of high-K^+ solution + BDM-treated cells were significantly greater than in relaxed cells. $*P < 0.05$ vs. contracted cells; $\#P < 0.05$ vs. relaxed cells. $n = 10$ for each group.

and intercalated disk (Fig. 1) in cardiomyocytes is consistent with the importance of the ECM-integrin-cytoskeleton axis in mechanotransduction.

The ECM of heart tissue is largely composed of collagen, FN, and laminin (26, 39). FN is deposited as an insoluble complex of either a cellular form that is synthesized and secreted locally by nonmuscle cells or a circulating form that is synthesized and secreted by hepatocytes (30, 58). The presence of FN in normal rat and mouse cardiac tissues has been previously reported (10, 76), and an increase in the amount of FN deposition in the hypertrophied or injured myocardium has also been documented (6, 38 , 58, 75). However, in isolated myocytes using the collagenase digestion method as we used in this study, the basement membrane is completely disrupted and collagen and pericelluar matrix proteins, like FN, are mostly removed from the cell surface (10, 36). In this study, we sought to explore the relationship between FN adhesion and mechanosensation in normal myocytes. Our hypothesis was that transmission of an increased level of force during cell contraction and a decreased level of force during relaxation would correlate with a corresponding increase in integrin adhesion to FN during contraction and a decrease in adhesion during

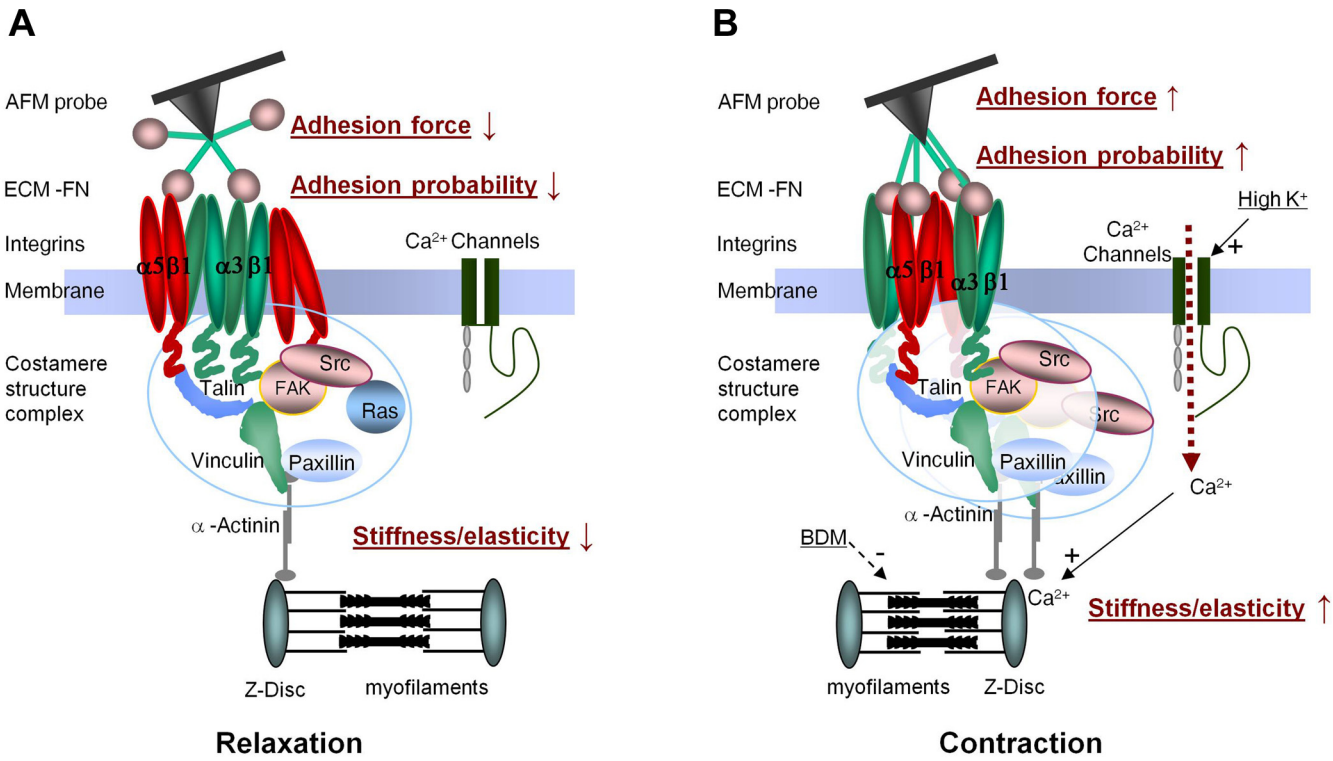

Fig. 8. Simplified schematic representation of the FN-integrin-costamere axis. *A*: during relaxation, decreased adhesion force, probability of adhesion, and cell stiffness could be related to the decreased availability of activated integrin receptors within the costamere complex. *B*: in comparison, during contraction, increased adhesion force, probability of adhesion, and stiffness could be related to the increased availability of active integrin receptors and fortification of the costamere complex. The activation of integrins could hypothetically be related to inside-out ligand-activated signaling mechanisms (e.g., Ca^{2+}) that can act to coordinate the contractile state with adhesion. Myofilaments: actin, myosin, tropomyosin, and troponin. ECM, extracellular matrix; +, activation; −, inhibition.

relaxation (Fig. 8). It was speculated that this would allow the myocyte to be mechanically and energetically more efficient at transferring force. AFM has been proven to be an unparalleled tool for the study of adhesion kinetics in cells (24, 45). It has both the spatial and temporal resolution to permit the study of adhesion at the scale of single molecules and is a proven technique for the study of adhesion in cells. In our experiments, we used AFM to measure adhesion force and adhesion probability as indicators of FN-integrin interactions and to measure cell stiffness as an indicator of the cell contractile state.

To quantify the adhesive events between FN and myocyte integrin proteins, the force that caused the bond between integrin and FN to rupture (unbinding force) was quantified. Previous work in our laboratory and by others (35, 68, 73) has provided evidence to show that the force required to disrupt adhesion between FN and $\alpha_5\beta_1$-integrin is between 35 and 80 pN. In the present study, we measured the comparable unbinding force for the interaction between FN and integrins as 39.6 $\pm$ 1.3 pN using a conically tipped FN-coated AFM probe and as 38.1 $\pm$ 1.0 pN using a microbead-tipped AFM probe. A number of factors have been shown to contribute to the measured unbinding force and probability of an adhesion event occurring, such as the sampling location on the cell surface, ligand concentration, probe spring constant, and loading rate (3, 68). To minimize contributions from these sources of variation, we held each of these variables constant for our experiments.

The data from the present study demonstrated that the probability of adhesion to FN-integrins significantly decreased but not the bond rupture force in the presence of α_3- or α_5-integrin monoclonal antibodies, whereas in the presence of both α_3- and α_5-integrin antibodies or β_1-integrin monoclonal antibody, the adhesion force was significantly reduced (Figs. 3 and 4). Non-FN α_{11}-integrin monoclonal antibody had no effects on adhesion force and adhesion probability, demonstrating the specificity of FN binding to $\alpha_3\beta_1$- and $\alpha_5\beta_1$-integrins. Presumably, α_3- or α_5-integrin monoclonal antibodies act by preventing FN on the AFM probe from interacting with these integrins on the cell surface in the manner of a competitive inhibitor; thus, the antibodies bind to the integrin and reduce the availability of these integrins to the probe, which would decrease the binding probability and binding force between FN-integrin. These results support the α_3- and α_5-integrin specificity of the binding to FN. The residual adhesion force observed in the presence of combined antibodies to α_3- and α_5-integrins (28.1 $\pm$ 1.2 pN) or to β_1-integrin (25.2 $\pm$ 0.1 pN) may be due to cell membrane force and/or membrane tether formation and/or the nonspecific binding we observed with control BSA protein on the AFM tip or tip alone. In particular, these residual forces are similar in magnitude to the membrane tether forces reported by Sun et al. (65) of 28.6 $\pm$ 10, 29.6 $\pm$ 9, and 29.6 $\pm$ 10 pN in Chinese hamster ovary cells, a malignant human brain tumor cell line, and human endothelial cells, respectively.

The data shown in Fig. 6 clearly demonstrate that the FN-integrin adhesion force and adhesion probability in contracted cells are greater than in cells under relaxed conditions. An interpretation of the increase in bond rupture force and adhesion probability observed in cardiomyocytes under the contracted state compared with cells in the relaxed state raises several possibilities. First, the increase in the probability of adhesion could have resulted from an increased number of integrins available for binding at the cell surface during contraction. Whether the increased probability is mediated by an increase in the number of receptors being expressed/inserted in the cell membrane or increased activation of receptors already present on the surface has not yet been determined. Second, the increase in measured force could result from integrin activation, leading to a more tightly bound state. Both of these types of inside-out integrin regulation have been reported to occur (27, 42). Finally, another possibility of enhanced adhesion force during contraction is that the cytoskeletal attachments to integrins at the cell surface are enhanced (43). It has been shown that the stability of the ECM-integrin-cytoskeleton axis is crucial to and required for cell contraction (70).

Furthermore, our data demonstrate that the cell stiffness or elasticity of cardiac myocytes during tonic contraction was higher than that of cells under the relaxed state (Fig. 7). This is consistent with the view that membrane depolarization caused by high extracellular K^+ would lead to Ca^{2+} entry and subsequent myofilament activation and cytoskeleton stiffening (Fig. 8). Similar to our observations, an increase in cell stiffness during contraction has been reported in rat atrial myocytes using AFM. This increase in stiffness was associated with actin-myosin formation and force generation (62). It has also been shown that changes in $[Ca^{2+}]_i$ levels and activation of cytoskeletal filaments are major components responsible for the cellular indentation stiffness (51). Thus, in addition to providing valuable insights into changes in cell adhesion, the stiffness measurements obtained from the AFM force curves can provide important temporal information related to the cell activation status.

To our knowledge, this is the first report to advance and provide support for the hypothesis that integrin adhesive properties are modulated differently in a contracted condition versus a relaxed condition in the myocyte. The mechanism we propose is one whereby the cell signaling that activates contraction or altered contractility will also activate integrins through an inside-to-out signaling pathway. The activated integrins would be evident as the altered adhesion that we examined and demonstrated in these investigations with AFM. A simplified schematic representation showing the adhesive events, probability, and cell stiffness at the contracted and relaxed states of the cardiac cell is shown in Fig. 8. In the context of our hypothesis, the subsequent alteration in integrin adhesion to the ECM could conceivably initiate a secondary round of outside-in signaling changes including the changes/activation in the costamere complex and activation of Ca^{2+} channels, as shown in Fig. 8. As an example of possible feedback from altered ECM-integrin interactions, we recently observed that FN induces a Ca^{2+} increase and an increase in force development in mouse papillary muscle fibers (unpublished observations). Rueckschloss et al. (53) demonstrated that contraction could induce an enhancement of Ca^{2+} currents by FN and RGD peptides in guinea pig cardiomyocytes. We (22, 83–85) have also previously reported that FN modulates Ca^{2+} and K^+ channels through $\alpha_5\beta_1$-integrin in vascular smooth muscle and human embryonic kidney cells heterologously expressing neuronal and smooth muscle Ca^{2+} channel isoforms. Sorting out the integrin signaling pathways and cytoskeletal changes involved in feedforward and feedback processes during cell contraction and relaxation will be an important challenge for the future.

In conclusion, our data indicate that FN interactions on cardiomyocytes involve $\alpha_3\beta_1$- and $\alpha_5\beta_1$-integrins and that adhesive interactions with these integrins are modulated by the contractile state in cardiomyocytes. We speculate that these changes in adhesion would act to match the adhesive state of the cell with the generation of contractile force thereby enhancing mechanical efficiency. Further studies will be required to clarify the mechanisms by which these adhesive changes occur and to determine if such changes in adhesion can be modulated on a beat-to-beat basis in cardiomyocytes.

ACKNOWLEDGEMENTS

The authors thank Dr. Wei Wang (Texas A&M Health Science Center) and Zhaohui Li (University of Missouri) for the skillful technical assistance.

GRANTS

This work was supported by National Institutes of Health Grants R21-EB-003888-01A1, and KO2-HL-86650 and by Texas A&M Health Science Center Research Development and Enhancement Award Program 244441-20702.

DISCLOSURES

No conflicts of interest, financial or otherwise, are declared by the author(s).

REFERENCES

1. **Ahumada GG, Saffitz JE.** Fibronectin in rat heart: a link between cardiac myocytes and collagen. *J Histochem Cytochem* 32: 383–388, 1984.
2. **Belke DD, Dillmann WH.** Altered cardiac calcium handling in diabetes. *Curr Hypertens Rep* 6: 424–429, 2004.
3. **Benoit M, Gabriel D, Gerisch G, Gaub HE.** Discrete interactions in cell adhesion measured by single-molecule force spectroscopy. *Nat Cell Biol* 2: 313–317, 2000.
4. **Brancaccio M, Hirsch E, Notte A, Selvetella G, Lembo G, Tarone G.** Integrin signalling: the tug-of-war in heart hypertrophy. *Cardiovasc Res* 70: 422–433, 2006.
5. **Brownlee M.** The pathobiology of diabetic complications: a unifying mechanism. *Diabetes* 54: 1615–1625, 2005.
6. **Casscells W, Ferrans VJ.** Growth factors in the heart. In: *The Development and Regenerative Potential of Cardiac Muscle*, edited by Oberpriller JO, Oberpriller JS, Mauro A. New York: Harvard, 1990, p. 8–21.
7. **Chen H, Huang XN, Stewart AF, Sepulveda JL.** Gene expression changes associated with fibronectin-induced cardiac myocyte hypertrophy. *Physiol Genomics* 18: 273–283, 2004.
8. **Contard F, Koteliansky V, Marotte F, Dubus I, Rappaport L, Samuel JL.** Specific alterations in the distribution of extracellular matrix components within rat myocardium during the development of pressure overload. *Lab Invest* 64: 65–75, 1991.
9. **Craig SW, Pardo JV.** Gamma actin, spectrin, and intermediate filament proteins colocalize with vinculin at costameres, myofibril-to-sarcolemma attachment sites. *Cell Motil* 3: 449–462, 1983.
10. **Dalen H, Saetersdal T, Roli J, Larsen TH.** Effect of collagenase on surface expression of immunoreactive fibronectin and laminin in freshly isolated cardiac myocytes. *J Mol Cell Cardiol* 30: 947–955, 1998.
11. **Danen EH, Yamada KM.** Fibronectin, integrins, and growth control. *J Cell Physiol* 189: 1–13, 2001.
12. **Davis MJ, Wu X, Nurkiewicz TR, Kawasaki J, Davis GE, Hill MA, Meininger GA.** Integrins and mechanotransduction of the vascular myogenic response. *Am J Physiol Heart Circ Physiol* 280: H1427–H1433, 2001.
13. **Efron B, Tibshirani R.** *An Introduction to the Bootstrap*. London: Chapman and Hall, 1993.
14. **Epstein ND, Davis JS.** Sensing stretch is fundamental. *Cell* 112: 147–150, 2003.
15. **Ervasti JM.** Costameres: the Achilles' heel of Herculean muscle. *J Biol Chem* 278: 13591–13594, 2003.
16. **Farhadian F, Contard F, Sabri A, Samuel JL, Rappaport L.** Fibronectin and basement membrane in cardiovascular organogenesis and disease pathogenesis. *Cardiovasc Res* 32: 433–442, 1996.
17. **Fredersdorf S, Thumann C, Ulucan C, Griese DP, Luchner A, Riegger GA, Kromer EP, Weil J.** Myocardial hypertrophy and enhanced left ventricular contractility in Zucker diabetic fatty rats. *Cardiovasc Pathol* 13: 11–19, 2004.
18. **Geiger B, Bershadsky A, Pankov R, Yamada KM.** Transmembrane crosstalk between the extracellular matrix and the cytoskeleton. *Nat Rev Mol Cell Biol* 2: 793–805, 2001.
19. **Glukhova M, Koteliansky V.** Integrins, cytoskeletal and extracellular matrix proteins in developing smooth muscle cells of human aorta. In: *The Vascular Smooth Muscle Cell: Molecular and Biological Responses to the Extracellular Matrix*, edited by Schwartz S, Mecham R. San Diego, CA: Academic, 1995, p. 37–79.
20. **Grimm D, Huber M, Jabusch HC, Shakibaei M, Fredersdorf S, Paul M, Riegger GA, Kromer EP.** Extracellular matrix proteins in cardiac fibroblasts derived from rat hearts with chronic pressure overload: effects of β-receptor blockade. *J Mol Cell Cardiol* 33: 487–501, 2001.
21. **Guan K, Czyz J, Furst DO, Wobus AM.** Expression and cellular distribution of $\alpha_v$integrins in $\beta_1$integrin-deficient embryonic stem cell-derived cardiac cells. *J Mol Cell Cardiol* 33: 521–532, 2001.
22. **Gui P, Wu X, Ling S, Stotz SC, Winkfein RJ, Wilson E, Davis GE, Braun AP, Zamponi GW, Davis MJ.** Integrin receptor activation triggers converging regulation of Cav1.2 calcium channels by c-Src and protein kinase A pathways. *J Biol Chem* 281: 14015–14025, 2006.
23. **Gwathmey JK, Hajjar RJ, Solaro RJ.** Contractile deactivation and uncoupling of crossbridges. Effects of 2,3-butanedione monoxime on mammalian myocardium. *Circ Res* 69: 1280–1292, 1991.
24. **Helenius J, Heisenberg CP, Gaub HE, Muller DJ.** Single-cell force spectroscopy. *J Cell Sci* 121: 1785–1791, 2008.
25. **Hesterberg T, Moore DS, Monaghan S, Clipson A, Epstein R.** Bootstrap methods and permutation tests. In: *Introduction to the Practice of Statistics*, edited by Moore DS, McCabe GP. New York: Freeman, 2005.
26. **Hynes RO.** Fibronectins. *Sci Am* 254: 42–51, 1986.
27. **Hynes RO.** Integrins: versatility, modulation, and signaling in cell adhesion. *Cell* 69: 11–25, 1992.
28. **Ingber D.** Integrins as mechanochemical transducers. *Curr Opin Cell Biol* 3: 841–848, 1991.
29. **Izenman AJ.** Recent developments in nonparametric density estimation. *J Am Stat Assoc* 86: 205–224, 1991.
30. **Jane-Lise S, Corda S, Chassagne C, Rappaport L.** The extracellular matrix and the cytoskeleton in heart hypertrophy and failure. *Heart Fail Rev* 5: 239–250, 2000.
31. **Kaur H, Chen S, Xin X, Chiu J, Khan ZA, Chakrabarti S.** Diabetes-induced extracellular matrix protein expression is mediated by transcription coactivator p300. *Diabetes* 55: 3104–3111, 2006.
32. **Knowlton AA, Connelly CM, Romo GM, Mamuya W, Apstein CS, Brecher P.** Rapid expression of fibronectin in the rabbit heart after myocardial infarction with and without reperfusion. *J Clin Invest* 89: 1060–1068, 1992.
33. **Kuppuswamy D, Kerr C, Narishige T, Kasi VS, Menick DR, Cooper GT.** Association of tyrosine-phosphorylated c-Src with the cytoskeleton of hypertrophying myocardium. *J Biol Chem* 272: 4500–4508, 1997.
34. **Lehenkari PP, Horton MA.** Single integrin molecule adhesion forces in intact cells measured by atomic force microscopy. *Biochem Biophys Res Commun* 259: 645–650, 1999.
35. **Li F, Redick SD, Erickson HP, Moy VT.** Force measurements of the α5β1 integrin-fibronectin interaction. *Biophys J* 84: 1252–1262, 2003.
36. **Lundgren E, Gullberg D, Rubin K, Borg TK, Terracio MJ, Terracio L.** In vitro studies on adult cardiac myocytes: attachment and biosynthesis of collagen type IV and laminin. *J Cell Physiol* 136: 43–53, 1988.
37. **Magnusson M, Mosher D.** Fibronectin: structure, assembly, and cardiovascular implications. *Arterioscler Thromb Vasc Biol* 18: 1363–1370, 1998.
38. **Mamuya WS, Brecher P.** Fibronectin expression in the normal and hypertrophic rat heart. *J Clin Invest* 89: 392–401, 1992.
39. **Martin GR, Timpl R.** Laminin and other basement membrane components. *Annu Rev Cell Biol* 3: 57–85, 1987.
40. **McCrossan ZA, Billeter R, White E.** Transmural changes in size, contractile and electrical properties of SHR left ventricular myocytes during compensated hypertrophy. *Cardiovasc Res* 63: 283–292, 2004.
41. **McNamee HP, Ingber DE, Schwartz MA.** Adhesion to fibronectin stimulates inositol lipid synthesis and enhances PDGF-induced inositol lipid breakdown. *J Cell Biol* 121: 673–678, 1993.
42. **Miyamoto S, Akiyama SK, Yamada KM.** Synergistic roles for receptor occupancy and aggregation in integrin transmembrane function. *Science* 267: 883–885, 1995.

43. **Miyamoto S, Teramoto H, Coso OA, Gutkind JS, Burbelo PD, Akiyama SK, Yamada KM.** Integrin function: molecular hierarchies of cytoskeletal and signaling molecules. *J Cell Biol* 131: 791–805, 1995.
44. **Moss RL, Fitzsimons DP.** Frank-Starling relationship: long on importance, short on mechanism. *Circ Res* 90: 11–13, 2002.
45. **Muller DJ, Helenius J, Alsteens D, Dufrene YF.** Force probing surfaces of living cells to molecular resolution. *Nat Chem Biol* 5: 383–390, 2009.
46. **Nagai T, Laser M, Baicu CF, Zile MR, Cooper Gt, Kuppuswamy D.** β3-Integrin-mediated focal adhesion complex formation: adult cardiocytes embedded in three-dimensional polymer matrices. *Am J Cardiol* 83: 38H–43H, 1999.
47. **Pardo JV, Siliciano JD, Craig SW.** A vinculin-containing cortical lattice in skeletal muscle: transverse lattice elements ("costameres") mark sites of attachment between myofibrils and sarcolemma. *Proc Natl Acad Sci USA* 80: 1008–1012, 1983.
48. **Parzen E.** On the estimation of a probability density and mode. *Ann Math Stat* 33: 1065–1076, 1962.
49. **Ross RS.** Molecular and mechanical synergy: cross-talk between integrins and growth factor receptors. *Cardiovasc Res* 63: 381–390, 2004.
50. **Ross RS, Borg TK.** Integrins and the myocardium. *Circ Res* 88: 1112–1119, 2001.
51. **Rotsch C, Braet F, Wisse E, Radmacher M.** AFM imaging and elasticity measurements on living rat liver macrophages. *Cell Biol Int* 21: 685–696, 1997.
52. **Roy S, Sala R, Cagliero E, Lorenzi M.** Overexpression of fibronectin induced by diabetes or high glucose: phenomenon with a memory. *Proc Natl Acad Sci USA* 87: 404–408, 1990.
53. **Rueckschloss U, Isenberg G.** Contraction augments L-type Ca^{2+} currents in adherent guinea-pig cardiomyocytes. *J Physiol* 560: 403–411, 2004.
54. **Ruwhof C, van der Laarse A.** Mechanical stress-induced cardiac hypertrophy: mechanisms and signal transduction pathways. *Cardiovasc Res* 47: 23–37, 2000.
55. **Sachs F.** Mechanical transduction by ion channels: how forces reach the channel. *Soc Gen Physiol Series* 52: 209–218, 1997.
56. **Sadoshima J, Izumo S.** The cellular and molecular response of cardiac myocytes to mechanical stress. *Annu Rev Physiol* 59: 551–571, 1997.
57. **Samarel AM.** Costameres, focal adhesions, and cardiomyocyte mechanotransduction. *Am J Physiol Heart Circ Physiol* 289: H2291–H2301, 2005.
58. **Samuel JL, Barrieux A, Dufour S, Dubus I, Contard F, Koteliansky V, Farhadian F, Marotte F, Thiery JP, Rappaport L.** Accumulation of fetal fibronectin mRNAs during the development of rat cardiac hypertrophy induced by pressure overload. *J Clin Invest* 88: 1737–1746, 1991.
59. **Sarin V, Gaffin RD, Meininger GA, Muthuchamy M.** Arginine-glycine-aspartic acid (RGD)-containing peptides inhibit the force production of mouse papillary muscle bundles via α5β1 integrin. *J Physiol* 564: 603–617, 2005.
60. **Schmidt C, Pommerenke H, Durr F, Nebe B, Rychly J.** Mechanical stressing of integrin receptors induces enhanced tyrosine phosphorylation of cytoskeletally anchored protein. *J Biol Chem* 273: 5081–5085, 1998.
61. **Schwarzbauer JE.** Fibronectin: from gene to protein. *Curr Opin Cell Biol* 3: 786–791, 1991.
62. **Shroff SG, Saner DR, Lal R.** Dynamic micromechanical properties of cultured rat atrial myocytes measured by atomic force microscopy. *Am J Physiol Cell Physiol* 269: C286–C292, 1995.
63. **Siperstein MD, Unger RH, Madison LL.** Studies of muscle capillary basement membranes in normal subjects, diabetic, and prediabetic patients. *J Clin Invest* 47: 1973–1999, 1968.
64. **Smoak IW.** Hyperglycemia-induced TGFβ and fibronectin expression in embryonic mouse heart. *Dev Dyn* 231: 179–189, 2004.
65. **Sun M, Graham JS, Hegedus B, Marga F, Zhang Y, Forgacs G, Grandbois M.** Multiple membrane tethers probed by atomic force microscopy. *Biophys J* 89: 4320–4329, 2005.
66. **Sun M, Opavsky MA, Stewart DJ, Rabinovitch M, Dawood F, Wen WH, Liu PP.** Temporal response and localization of integrins beta1 and beta3 in the heart after myocardial infarction: regulation by cytokines. *Circulation* 107: 1046–1052, 2003.
67. **Sun Z, Martinez-Lemus LA, Hill MA, Meininger GA.** Extracellular matrix-specific focal adhesions in vascular smooth muscle produce mechanically active adhesion sites. *Am J Physiol Cell Physiol* 295: C268–C278, 2008.
68. **Sun Z, Martinez-Lemus LA, Trache A, Trzeciakowski JP, Davis GE, Pohl U, Meininger GA.** Mechanical properties of the interaction between fibronectin and $\alpha_5\beta_1$-integrin on vascular smooth muscle cells studied using atomic force microscopy. *Am J Physiol Heart Circ Physiol* 289: H2526–H2535, 2005.
69. **Tagawa H, Wang N, Narishige T, Ingber DE, Zile MR, Cooper GT.** Cytoskeletal mechanics in pressure-overload cardiac hypertrophy. *Circ Res* 80: 281–289, 1997.
70. **Takagi J, Erickson HP, Springer TA.** C-terminal opening mimics "inside-out" activation of integrin α5β1. *Nat Struct Biol* 8: 412–416, 2001.
71. **Tavi P, Laine M, Weckstrom M, Ruskoaho H.** Cardiac mechanotransduction: from sensing to disease and treatment. *Trends Pharmacol Sci* 22: 254–260, 2001.
72. **Tong CW, Kolomenskii A, Lioubimov VA, Schuessler HA, Trache A, Granger HJ, Muthuchamy M.** Measurements of the cross-bridge attachment/detachment process within intact sarcomeres by surface plasmon resonance. *Biochemistry* 40: 13915–13924, 2001.
73. **Trache A, Trzeciakowski JP, Gardiner L, Sun Z, Muthuchamy M, Guo M, Yuan SY, Meininger GA.** Histamine effects on endothelial cell fibronectin interaction studied by atomic force microscopy. *Biophys J* 89: 2888–2898, 2005.
74. **Trial J, Rossen RD, Rubio J, Knowlton AA.** Inflammation and ischemia: macrophages activated by fibronectin fragments enhance the survival of injured cardiac myocytes. *Exp Biol Med (Maywood)* 229: 538–545, 2004.
75. **Ulrich MM, Janssen AM, Daemen MJ, Rappaport L, Samuel JL, Contard F, Smits JF, Cleutjens JP.** Increased expression of fibronectin isoforms after myocardial infarction in rats. *J Mol Cell Cardiol* 29: 2533–2543, 1997.
76. **Valencik ML, Zhang D, Punske B, Hu P, McDonald JA, Litwin SE.** Integrin activation in the heart: a link between electrical and contractile dysfunction? *Circ Res* 99: 1403–1410, 2006.
77. **Venables WN, Ripley BD.** *Modern Applied Statistics with S*. New York: Springer, 2002.
78. **Villarreal FJ, Dillmann WH.** Cardiac hypertrophy-induced changes in mRNA levels for TGF-β_1, fibronectin, and collagen. *Am J Physiol Heart Circ Physiol* 262: H1861–H1866, 1992.
79. **Wang N, Butler JP, Ingber DE.** Mechanotransduction across the cell surface and through the cytoskeleton. *Science* 260: 1124–1127, 1993.
80. **Weber K.** Extracellular matrix remodeling in heart failure: a role for de novo angiotensin II generation. *Circulation* 96: 4065–4082, 1997.
81. **Willems IE, Arends JW, Daemen MJ.** Tenascin and fibronectin expression in healing human myocardial scars. *J Pathol* 179: 321–325, 1996.
82. **Wolska BM, Solaro RJ.** Methood for isolation of adult mouse cardiac myocytes for studies of contraction and microfluorimetry. *Am J Physiol Heart Circ Physiol* 271: H1250–H1255, 1996.
83. **Wu X, Davis GE, Meininger GA, Wilson E, Davis MJ.** Regulation of the L-type calcium channel by α5β1 integrin requires signaling between focal adhesion proteins. *J Biol Chem* 276: 30285–30292, 2001.
84. **Wu X, Mogford JE, Platts SH, Davis GE, Meininger GA, Davis MJ.** Modulation of calcium current in arteriolar smooth muscle by αvβ3 and α5β1 integrin ligands. *J Cell Biol* 143: 241–252, 1998.
85. **Wu X, Yang Y, Gui P, Sohma Y, Meininger GA, Davis GE, Braun AP, Davis MJ.** Potentiation of large conductance, Ca^{2+}-activated K^+ (BK) channels by α5β1 integrin activation in arteriolar smooth muscle. *J Physiol* 586: 1699–1713, 2008.

Journal of Molecular and Cellular Cardiology 50 (2011) 203–213

Contents lists available at ScienceDirect

Journal of Molecular and Cellular Cardiology

journal homepage: www.elsevier.com/locate/yjmcc

Original article

Fibronectin increases the force production of mouse papillary muscles via α5β1 integrin

Xin Wu [a], Sanjukta Chakraborty [a], Cristine L. Heaps [b], Michael J. Davis [c], Gerald A. Meininger [c], Mariappan Muthuchamy [a,*]

[a] Department of Systems Biology and Translational Medicine, Texas A&M Health Science Center College of Medicine, College Station, TX 77843, USA
[b] Department of Veterinary Physiology and Pharmacology, Veterinary College of Medicine, Texas A&M University, College Station, TX 77843, USA
[c] Dalton Cardiovascular Research Center and Department of Medical Pharmacology and Physiology, University of Missouri-Columbia, Columbia, MO 65211, USA

ARTICLE INFO

Article history:
Received 3 September 2010
Received in revised form 30 September 2010
Accepted 1 October 2010
Available online 16 October 2010

Keywords:
Fibronectin
Integrin
Extracellular matrix proteins
Calcium
Force–$[Ca^{2+}]_i$ relationship
Phospholamban
Cardiac muscle

ABSTRACT

The extracellular matrix (ECM) protein–integrin–cytoskeleton axis plays a central role as a mechanotransducing protein assemblage in many cell types. However, how the process of mechanotransduction and the mechanically generated signals arising from this axis affect myofilament function in cardiac muscle are not completely understood. We hypothesize that ECM proteins can regulate cardiac function through integrin binding, and thereby alter the intracellular calcium concentration ($[Ca^{2+}]_i$) and/or modulate myofilament activation processes. Force measurements made in mouse papillary muscle demonstrated that in the presence of the soluble form of the ECM protein, fibronectin (FN), active force was increased significantly by 40% at 1 Hz, 54% at 2 Hz, 35% at 5 Hz and 16% at 9 Hz stimulation frequencies. Furthermore, increased active force in the presence of FN was associated with 12–33% increase in $[Ca^{2+}]_i$ and 20–50% increase in active force per unit Ca^{2+}. A function blocking antibody for α5 integrin prevented the effects of the FN on the changes in force and $[Ca^{2+}]_i$, whereas a function blocking α3 integrin antibody did not reverse the effects of FN. The effects of FN were reversed by an L-type Ca^{2+} channel blocker, verapamil or PKA inhibitor. Freshly isolated cardiomyocytes exhibited a 39% increase in contraction force and a 36% increase in L-type Ca^{2+} current in the presence of FN. Fibers treated with FN showed a significant increase in the phosphorylation of phospholamban; however, the phosphorylation of troponin I was unchanged. These results demonstrate that FN acts via α5β1 integrin to increase force production in myocardium and that this effect is partly mediated by increases in $[Ca^{2+}]_i$ and Ca^{2+} sensitivity, PKA activation and phosphorylation of phospholamban.

1. Introduction

Ventricular remodeling is the primary long-term adaptive mechanism in response to physiological (e.g. exercise) or pathological (e.g. diabetic cardiomyopathy) mechanical overload. In addition to hypertrophy of cardiac ventricular myocytes during mechanical overload, alterations in non-ventricular myocyte compartments, e.g. extracellular matrix (ECM), also form an essential component of the remodeling of the ventricle during diabetes mellitus and hypertension. ECM proteins communicate with intracellular molecules including cytoskeletal and Ca^{2+} signaling systems through integrins and are likely integrated with remodeling mechanisms. However, the mechanisms whereby integrin–ECM interactions are linked to mechanical signaling in cardiac muscle are poorly understood [1].

Integrins are a large family of transmembrane adhesion molecules that provide a connection between the intracellular cytoskeleton and ECM. Integrins are heterodimers composed of α and β subunits. Of the approximately 24 known integrins, cardiac myocytes express at least 4 prevalent subtypes, which include: α1β1, α3β1, α5β1 and α7β1 [2,3]. α3β1 binds to FN, collagen and laminin, whereas α5β1 binds most strongly to FN, α1β1 binds to collagen and laminin, and α7β1 binds to laminin [4]. The overlapping binding affinity between integrins and ECM proteins is likely due to common binding motifs, for example, arginine–glycine–aspartic acid (RGD) and leucine–aspartate–valine (LDV) amino acid sequences present in many ECM proteins. α1β1, α3β1 and α5β1 recognize ECM proteins that are containing RGD sequences [2,5]. In cardiac muscle, integrins localize in costameres, the sites where *Z* bands connect to basement membrane. The costamere is structurally integrated with cytoskeletal components and signaling complexes further supporting the proposition that integrins are involved in mechanical signaling [1,3,5–7]. It has been reported that application of mechanical stress to integrin adhesion sites causes increased cytoskeletal stiffening, generation of second messenger signals and tyrosine phosphorylation of proteins anchored to the cytoskeleton [8–10]. Thus, there is a strong evidence to suggest that integrins can act as a conduit for transmission of mechanical forces across the cell membrane and thereby initiating intracellular signaling.

Intracellular Ca^{2+} handling mechanisms include Ca^{2+} entry, Ca^{2+} release and Ca^{2+} reloading of the sarcoplasmic reticulum (SR). We

* Corresponding author. Tel.: +1 979 845 7816; fax: +1 979 862 4638.
E-mail address: marim@tamu.edu (M. Muthuchamy).

0022-2828/$ – see front matter © 2010 Elsevier Ltd. All rights reserved.
doi:10.1016/j.yjmcc.2010.10.003

have previously shown that at least 3 different integrins regulate voltage-gated L-type Ca^{2+} channels (Ca_L) and Ca^{2+} activated K^+ channels in native vascular smooth muscle (VSM) cells, neuronal cells, and in heterologously expressed neuronal, VSM or cardiac Ca_L in human embryonic kidney (HEK) −293 cells. Regulation of the ion channels by integrins requires signaling between focal adhesion proteins [11–17]. Numerous studies have indicated that alterations in Ca_L and $[Ca^{2+}]_i$ are primary mechanisms for the cardiac hypertrophic response [18–22]. Rueckschloss and Isenberg have reported contraction-induced enhancement of Ca_L in guinea-pig cardiomyocytes attached to coverslips coated with either FN or RGD-containing peptides [23]. We have demonstrated that RGD-containing peptides or digested fragments of collagen depress force production by mouse papillary muscle fibers [2]. Since the binding affinities between different ECM proteins and integrins are varied, we propose that the downstream mechanical signaling will also be different and will depend upon the specific ECM proteins and integrins involved.

FN is normally expressed in the heart and undergoes increased expression in hypertrophic and injured myocardium [7,24–27]. These studies address the role of FN in the structural remodeling that occurs in hypertrophic or injured hearts. However the role of soluble FN in normal heart function is poorly understood. Laser et al. have suggested that increased FN expression in feline myocardium during hypertrophy may involve focal complex formation and the activation of extracellular-regulated kinases 1/2 following α5β1 integrin binding [28]. In this study we test the hypothesis that soluble FN interacts with α5β1 integrin to augment force development by altering $[Ca^{2+}]_i$ and myofilament activation processes.

2. Materials and methods

2.1. Force measurements in intact papillary muscle fibers

Adult male mice (FVB/N strain, 15–20 weeks, 25–35 g, Harlan Houston, TX, and Charles River, USA) were anesthetized by an intraperitoneal injection of sodium pentobarbital (60 mg/kg) and hearts were excised rapidly. The hearts were placed in cold (4 °C) Krebs–Henseleit (KH) buffer containing 10 mM 2, 3-butanedione monoxime (Sigma, USA). KH buffer was composed of (in mM): 119.0 NaCl, 11.0 glucose, 4.6 KCl, 25.0 $NaHCO_3$, 1.2 KH_2PO_4, 1.2 $MgSO_4$ and 1.8 $CaCl_2$. The buffer solution was gassed with 95% O_2–5% CO_2 to maintain the pH (7.35–7.40). The right ventricular papillary muscle (2.0–3.0 mm in length, 0.3–0.4 mm in width and 0.15–0.25 mm in thickness) was isolated by dissection with a segment of the tricuspid valve at one end and a portion of the myocardial septum at the other. The muscle tapered from the ventricular wall toward the attachment to the tricuspid valve such that the shape approximated that of a triangle with length and with an oval base width. The force was normalized per cross-sectional area at the base using the approximation area = 0.75 × width × depth [29]. The papillary muscle bundles were mounted between a force transducer and a voltage-controlled motor positioner within a muscle measurement suite (Scientific Instruments, Germany). Stimulation pulse duration was 6 ms with an initial rate of 1.0 Hz. The papillary bundle was continuously superfused with KH maintained at 37 °C for force measurement. Stimulation voltage and bundle length were adjusted until maximum force was reached. The muscle was then stimulated at 1.0 Hz for 20–30 min before executing the experimental protocol. A digital phosphor oscilloscope suite (Tektronix TDS 420A with Wavestar software) measured stimulation frequency, twitching force amplitude, averaged force amplitude within preset time windows, and continuously logged the data into the computer.

The experimental protocols consisted of: (1) increasing stimulation frequency by 1.0 Hz increments (duration of 2 min or until a steady force value had been reached); (2) decreasing stimulation frequency to a randomly selected frequency (5.0 or 1.0 Hz) and superfusing with KH solution containing either 35.0 nM FN (440 kDa, Invitrogen Corporation, Grand Island, NY) or 35.0 nM bovine serum albumin (BSA. Amersham Life Science, Arlington Heights, IL) for 5 min before starting to record data; (3) in experiments with integrin-blocking monoclonal antibodies (mAb), the preparations were incubated for 5 min with α5 (HMα5-1, 60 nM) or α3 (VLA-3α, 60 nM) mAb (BD Bioscience, San Jose, CA) prior to perfusion with FN, and (4) for inhibitor studies, the papillary muscle fibers were incubated with either the cardiac selective Ca^{2+} channel blocker 2.5 μM verapamil or the cell-permeable PKA inhibitor 14–22 amide (PKA-I, 1 μM. Calbiochem, Gibbstown, NJ) for 5 min before application of FN. Chemicals, unless otherwise stated, were obtained from Sigma.

Preparation of FN: FN (5.0 mg) was reconstituted, according to the manufacturer's (Invitrogen Corporation, Grand Island, NY) manual, by adding 5 ml of sterile distilled water. The resulting solution was 1 mg/ml of FN in 100 mM CAPS, 0.15 M NaCl, and 1 mM calcium chloride, pH 11.5, and the concentration of FN in this stock solution was 2.3 μM. The FN stock solution was then filtered through Ultrafree-MC centrifugal filter to remove any particles and/or precipitates that may present in FN. Then about 100 μl to 500 μl aliquots of FN was stored at −20 °C in small plastic siliconized tubes till the use in experiments; repeated freezing and thawing of the stock solution was avoided. 300 μl of FN stock solution was added directly to 20 ml Krebs–Henseleit (KH) solution before each experiment, which yielded the desired final concentration of FN (about 35 nM); the pH was adjusted to 7.4, and used in the experiments as described earlier. Similar protocol was also done for BSA in KH solution.

2.2. Force–Ca^{2+} measurements in intact papillary muscle fibers

Right ventricular papillary muscle bundles were extracted and mounted as previously described. The muscle measurement equipment suite provided all the optics and electronics needed for measuring $[Ca^{2+}]_i$ using Fura-2 AM dye. Measurements were collected through a different data acquisition suite (National Instruments A/D board and LabVIEW software, Austin, TX) with the digital oscilloscope suite providing continuous monitoring. A mercury lamp and filter wheel provided alternating ultraviolet (UV) pulses of 340 nm and 380 nm at 250 Hz with pulse duration of 1.5 ms to illuminate the bundle. The combinations of microscope, dichroic mirror, filter and photomultiplier tube collected the Fura-2 fluorescence. A synchronized electronic integrator parsed and averaged the respective fluorescence signals associated with 340 nm and 380 nm excitation. The loading solution consisted of KH with 10 μM Fura-2 AM (Invitrogen/Molecular Probes, Eugene, OR), 4.3 mg l^{-1} N,N,N′,N′-tetrakis (2-pyridylmethyl) ethylenediamine, and 5.0 g/l cremophor. The KH to dimethyl sulfoxide volume ratio of the loading solution was 333:1. A loading duration of 1.5 h with 20 min of de-esterification gave signals of greater than 3-fold over background fluorescence. The ratio, R, of fluorescence from 340 nm excitation to fluorescence from 380 nm excitation was calculated after subtracting background fluorescence. Ca^{2+} concentration was calculated using the following equation with K_d equating to $K_d \times \beta$ after subtracting background fluorescence [30]:

$$\left[Ca^{2+}\right]_i = K_d * [(R - R_{min}) / (R_{max} - R)] * \beta$$

where β is the ratio of the 380 nm signal at zero Ca^{2+} *vs* the 380 nm signal at saturating Ca^{2+} (39.8 μM). The ratio of 340/380 fluorescence was converted to $[Ca^{2+}]_i$ using a standard method [30]. The minimum ratio (R_{min}) was determined in zero Ca^{2+} with 10 mM EGTA and the maximum ratio (R_{max}) was determined in 39.8 μM Ca^{2+}. The experimental protocols were the same as described in the earlier section except that the protocols were carried out at room temperature. Myocytes increase their ability to actively pump out the Ca^{2+} sensitive dye Fura-2 with increasing temperature. At near physiologic

temperature, the myocytes will actively eliminate enough Fura-2 such that additive noise becomes a confounder. The ratio method of Fura-2 eliminates similar multiplicative noise but does not remove the additive noise. Thus, it was not possible to load the Fura-2 into myocyte using our current protocol to conduct the force/frequency with Ca^{2+} experiments at near physiologic temperature. However, at room temperature the Fura-2 dye load into myocytes more efficiently and it is possible to measure force and Ca^{2+} simultaneously.

2.3. Analyses of the force–Ca^{2+} data

From the Ca^{2+} and force values, time-to-peak Ca^{2+} amplitude and time-to-peak force (TPF), and time from peak Ca^{2+} to peak force and the maximum rate of isometric tension development [$+dF/dt$, $(mN/mm^2)/s$)] represented contraction properties. The 50% decay time from the peak of Ca^{2+}, the 50% relaxation time from the peak of force, and the maximum rate of relaxation [$-dF/dt$, $(mN/mm^2)/s$] represented relaxation properties. The $+dF/dt$ and $-dF/dt$ were calculated using the following equation, where $F(t)$ was the measured force at a particular time t and ΔT was the 1 ms sampling period:

$$dF/dt = [F(t-\Delta T)-F(t)]/\Delta T.$$

Averaging a three data point window for each single dF/dt calculation minimized the noise. Data analyses were performed as described in our previous publications [31,32]. We analyzed the force–Ca^{2+} values at specific points during a twitch cycle. The points consisted of: (1) the resting point '*A*', (2) maximum Ca^{2+} point, '*B*', and (3) maximum force point, '*C*'. Active force, $[Ca^{2+}]_i$ and active force/delta gain of $[Ca^{2+}]_i$ were calculated at points *A*, *B* and *C*.

2.4. Adult cardiomyocyte preparation

Adult male mouse cardiomyocytes (FVB/N strain, 2–4 months) were prepared as described [3]. Briefly, the heart was harvested under anesthesia and put into ice-cold Ca^{2+} free physiological saline solution (PSS) containing (in mM): 133.5 NaCl, 4 KCl, 1.2 NaH_2PO_4, 1.2 $MgSO_4$, 10 HEPES, and 11 glucose, pH 7.4. 10 mM 2,3-butanedione monoxime (BDM) was present during the dissecting procedure. The aorta was cannulated and the heart was mounted in a Langendorff perfusion system with Ca^{2+}-free control solution containing 1 mg/ml bovine serum albumin (BSA, Amersham Life Science, Arlington Heights, IL) at 37 °C. Perfusion was continued with the same solution containing 25 μM Ca^{2+} together with collagenase type I (62.4 U/ml, Worthington, NJ) and type II (73.7 U/ml, Worthington, NJ). After about 15–20 min, the heart was removed and transferred to a Petri dish containing PSS with 100 μM Ca^{2+}. The ventricles were cut into small pieces that were then gently triturated to release single cells. The collected cells were then re-suspended in PSS containing 200 μM Ca^{2+}. A suspension of freshly dispersed cells was plated onto a dish for at least 30 min in PSS solution with 1.8 mM Ca^{2+} before beginning the experimental protocols.

2.5. Electrophysiology

Whole-cell currents were recorded using Axopatch 200B, Digidata 1322A and pCLAMP9 software (Axon/Molecular Devices, Sunnyvale, CA). All experiments were performed at 22 °C. Conventional whole-cell recordings were made as described previously [12,33]. Pipettes had resistances ranging from 1 to 5 MΩ. The extracellular solution contained (in mM): 135 TEA-Cl, 1.1 $MgCl_2$, 2 $BaCl_2$, 10 glucose, 10 HEPES, 10 4-aminopyridine, and 0.01 TTX (pH = 7.4). The intracellular solution (high Cs+) contained (in mM): 110 CsCl, 20 TEA-Cl, 10 EGTA, 10 HEPES, 2 $MgCl_2$, 4 Mg-ATP, and 1 $CaCl_2$ (pH = 7.2). These solutions provided isolation of Ca^{2+} currents (I_{Ca}) from other currents and from the Na^+–Ca^{2+} exchanger. Ba^{2+} in extracellular solution served as the charge carrier to increase the size of the inward currents elicited by depolarization, and to minimize Ca^{2+}-dependent inactivation of I_{Ca} [11,12]. I_{Ca} of cardiomyocytes was elicited by voltage ramps or by voltage steps from −60 to +40 mV in 10 mV increments every 5 s at holding potential = −50 mV.

2.6. Measurements of cell contractions

Two parallel platinum electrodes 5 mm apart were placed on each side of cardiomyocytes. The isolated myocytes were field stimulated at 1 Hz with a biphasic square pulse of 8 ms total duration. The amplitude and duration of the pulses were controlled by a SD9 Grass stimulator (Grass Technologies, MA). The stimulus amplitudes were set to 20% above threshold. Cell images were acquired through an Olympus CKX41 inverted microscope (at 400× magnification) using a Hitachi charged-coupled device color camera, and video acquisition card (PCI 1409; National Instruments). The cell contraction tracking program was written in LabView, with subroutines called from the supplemental IMAQ Vision Development Package (National Instruments, Austin, TX) [34].

2.7. Western blot analysis

Papillary fibers were stimulated at 3.0 Hz, either in the absence or presence of FN, at 37 °C for 4 min. The fibers were then flash-frozen in liquid nitrogen and stored at −80 °C until use. Lysates were prepared by homogenizing the tissue in ice-cold RIPA lysis buffer supplemented with phosphatase inhibitors and protease inhibitor cocktail (Sigma, MO), as described earlier [35]. The tissue samples were then further sonicated in protein-solubilizing buffer. The supernatant was assayed for protein concentration, mixed with an equal volume of SDS gel-loading buffer [36], and run on a 4–20% precast gradient SDS-polyacrylamide gel (Bio-Rad Laboratories). For analysis of total phospholamban (PLB) and phospho-phospholamban (p-PLB) expression, both the control and FN-treated samples in SDS gel-loading buffer were either boiled for 3 min or were heated at 37 °C for 15 min prior to loading [37]. The proteins were transferred to a nitrocellulose membrane with a Bio-Rad transblot apparatus and the transfer was verified by Ponceau-S staining. The membrane was blocked in 5% milk in Tris buffered saline (TBS) and then incubated with a primary antibody followed by incubation with the corresponding HRP-conjugated secondary antibody. The following dilutions of the primary antibodies in TBS were used: PLB (1:1000) and anti-p-PLB Ser16 (1:1000), (Upstate Biotechnology, VA), GAPDH (1:5000) (Millipore, MA), phospho-TnI Ser23/24 (1:1000) (Abcam, MA) and TnI (1:4000) (Advanced Immunochemical, CA). The immunoreactive bands were visualized using the Pierce detection system (Super Signal West Dura Extended Duration Substrate, Pierce). Membranes were stripped by incubation in Restore western blot stripping buffer (Thermo Scientific, MA) and re-probed with the corresponding total antibody or GAPDH (1:1000). Densitometry analyses on the resulting bands were performed using Quantity One multi-analyst software (Bio-Rad, CA). The ratios of p-PLB were calculated with respect to both PLB and GAPDH, and the ratio of phosphorylated cardiac troponin I (p-TnI) and total troponin I (TnI) was also calculated. Each experiment was repeated three times.

2.8. Statistical analyses

All data are expressed as means ± SEM. Statistical analyses were done using either a Student's paired *t*-test or a two-way ANOVA with Fisher's or Bonferroni/Dunn's post hoc tests. Repeated measures ANOVA were used for comparison of repeated measurements within the same group (e.g. response to increasing pacing frequency). $P<0.05$ was regarded as statistically significant.

3. Results

3.1. FN increased force development in ventricular papillary muscle

Fig. 1(A) shows that FN increased active force in a concentration-dependent manner (1 to 200 nM, $n=9$) at 5 Hz at 37 °C. A fit of the Boltzmann equation to the data in Fig. 1(A) shows that a half-maximum effect was evoked by 36.5 nM FN. Fig. 1(B) shows typical force curves before and after application of 35.0 nM FN to a papillary muscle fiber. The peak force was enhanced by 31% after FN addition (Fig. 1(B)). Application of FN led to an enhancement of normalized peak force as early as 1 min at 5 Hz. This enhancement peaked at 3–4 min (about 130 to 140% of control), remained stable for 10 min, and then declined gradually by 14–15 min (Fig. 1(C)). Active force that describes the difference between the maximum and minimum force (passive tension) developed by the ventricle fibers increased at all given stimulation rates after application of FN (Fig. 1(D)). The enhanced active force varied from 17% at 9 Hz to 55% at 2 Hz ($p<0.05$, $n=9$). Note that the fibers also demonstrated a positive force–frequency response (FFR) from 2 to 9 Hz, similar to previous reports [32]. BSA in the perfusion solution was used as a control, and had no significant effect on the time course of force generation (Fig. 1(C)).

The rates of force generation and relaxation ($+dF/dt$ and $-dF/dt$) were calculated as described in Materials and methods. FN caused a significant increased in both $+dF/dt$ and $-dF/dt$ at all the tested stimulation frequencies between 1 and 9 Hz, ($p<0.05$, $n=9$) in papillary muscle (Figs. 2(A and C)). The rate of force generation increased from 18% at 9 Hz to 105% at 2 Hz (Fig. 2(A)). Furthermore, TPF was significantly decreased in papillary fibers stimulated at all frequencies except 9 Hz after treatment with FN (Fig. 2(B)). The rate of force relaxation increased from 23% at 9 Hz to 136% at 2 Hz (Fig. 2(C)). The times to 50% relaxation from the peak force were 20%, 22% and 15% shorter at 1, 2 and 5 Hz, respectively, after application of FN (Fig. 2(D), $p<0.05$, $n=9$).

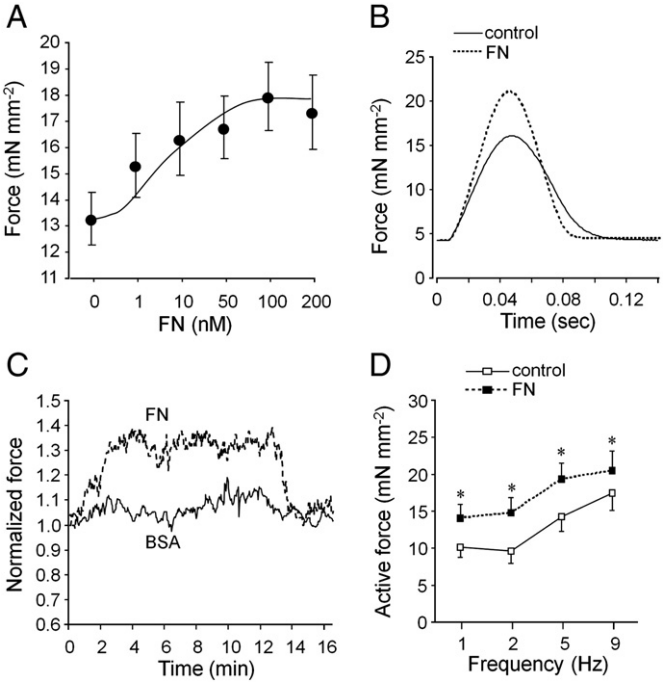

Fig. 1. Force generation in the presence of fibronectin (FN, 35 nM) in mouse right ventricular papillary muscles. (A) FN caused a concentration-dependent increase in active force generation at 5 Hz and 37 °C. Data were fit by a Boltzmann equation with half-maximal force equal to 36.5 nM FN. (B) A typical force curve showing that force increased in the presence of FN at 5 Hz. (C) A representative trace showing the effect of FN on the active force generated by a mouse papillary muscle fiber. Bovine serum albumin (BSA, 35 nM) was used as control protein. (D) Changes of peak active force in the presence of FN at stimulation rates of 1 Hz to 9 Hz. Data are presented as mean ± SEM. $n=9$. *$p<0.05$ *vs* control.

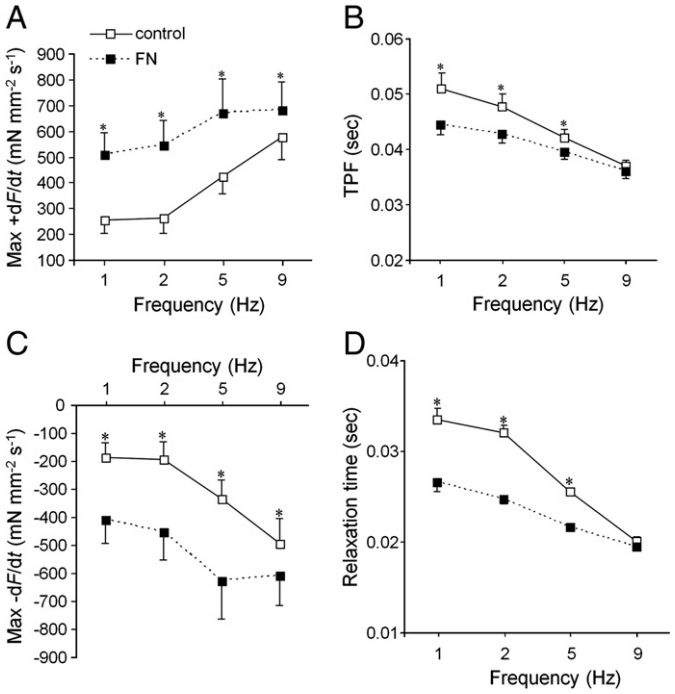

Fig. 2. FN enhanced both the contraction and relaxation parameters in papillary muscle. (A and C) The maximum rates of contraction and relaxation ($+dF/dt$ and $-dF/dt$) are enhanced in fibers treated with FN. (B and D) TPF and the time to 50% off the peak of maximum force are lower in the FN-treated fibers. Data are presented as mean ± SEM. $n=9$; TPF: time-to-peak force. *$p<0.05$ *vs* control.

3.2. Increased force generation in FN-treated ventricular papillary fibers associated with increase in both $[Ca^{2+}]_i$ and Ca^{2+} sensitivity

To further elucidate the mechanisms for the enhancement of force in the presence of FN, we measured the force and $[Ca^{2+}]_i$ simultaneously in papillary muscle fibers at room temperature. The Ca^{2+} transients and force measured at 1 Hz before and after FN incubation are shown in Figs. 3(A and B), respectively. Both force and $[Ca^{2+}]_i$ transients were increased in the presence of FN. The Ca^{2+} transients declined faster to 50% of the peak in the presence of FN at 1 Hz (175 ± 11 ms at control *vs* 144 ± 12 ms at FN, $p<0.05$; $n=9$). The relaxation time (50% from the peak) was 16% faster after application of FN. The time to peak of $[Ca^{2+}]_i$ (Fig. 3(A)) and TPF (Fig. 3(B)) were not significantly changed in the presence of FN. However, the time between peak Ca^{2+} and peak force was 9% shorter at 1 Hz in papillary fibers perfused with FN (Control: 85 ± 3 ms *vs* FN: 77 ± 4 ms, $p<0.05$; $n=9$).

Fig. 4(A) shows typical force–$[Ca^{2+}]_i$ loops for papillary fibers before and after FN application at 1 Hz. Note three distinct points labeled as '*A*', '*B*' and '*C*' on the force–$[Ca^{2+}]_i$ hysteresis loop. Point '*A*' represents the resting (basal) point, point '*B*' represents maximal $[Ca^{2+}]_i$ concentration and point '*C*' represents maximal force. At point '*A*', an increase in stimulation frequency did not significantly change the $[Ca^{2+}]_i$ and diastolic force of the fiber in either the control or FN-treated condition. Figs. 4(B and C) show the changes in the maximum active force, maximum $[Ca^{2+}]_i$, and delta gain (DG) of active force divided by the change in $[Ca^{2+}]_i$ (active force/$\Delta[Ca^{2+}]_i$) for stimulation frequencies 1.0 Hz and 2.0 Hz that occur at point '*B*' and point '*C*', respectively. The delta gain (DG) of the active force/$\Delta[Ca^{2+}]_i$ is defined as the active force divided by the difference in $[Ca^{2+}]_i$ from point '*B*' to point '*A*' or from point '*C*' to point '*A*'. Since delta gain quantifies changes in force per unit Ca^{2+}, the alteration in this parameter could represent changes in the myofilament activation

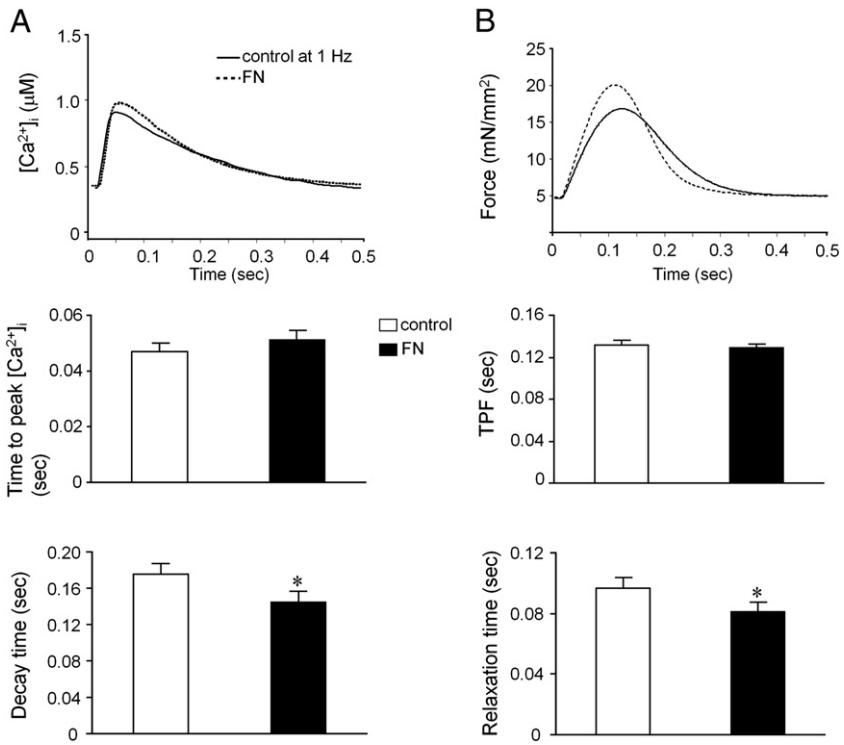

Fig. 3. Ca^{2+} transient and force during a contraction cycle before and after FN application. Raw data showing $[Ca^{2+}]_i$ transients (A) and force (B) in top panels. Force and $[Ca^{2+}]_i$ with respect to time at a stimulation rate = 1 Hz. Decay time of $[Ca^{2+}]_i$ and force relaxation time are the times representing EC_{50} values. TPF: time-to-peak force. Data are presented as mean ± SEM. $n = 9$. $^*p < 0.05$ *vs* control.

processes [2,31,32], such as an increase in Ca^{2+} sensitivity. The results demonstrate that at point '*B*' (Fig. 4(B)), the active force significantly increased by 73% and 22% at 1 Hz and 2 Hz, while the maximum Ca^{2+} was increased by 33% and 11% respectively. Furthermore, DG significantly increased by 22% at 1 Hz. At point '*C*' (Fig. 4(C)) the maximum active force was increased by 57% and 31% at 1 Hz and 2 Hz, respectively, in the presence of FN. The $[Ca^{2+}]_i$ concentration was also increased by 26% at 1 Hz and by 12% at 2 Hz after FN application. The DG at point '*C*' significantly increased by 24% and 15% at 1.0 and 2.0 Hz, respectively, in the presence of FN.

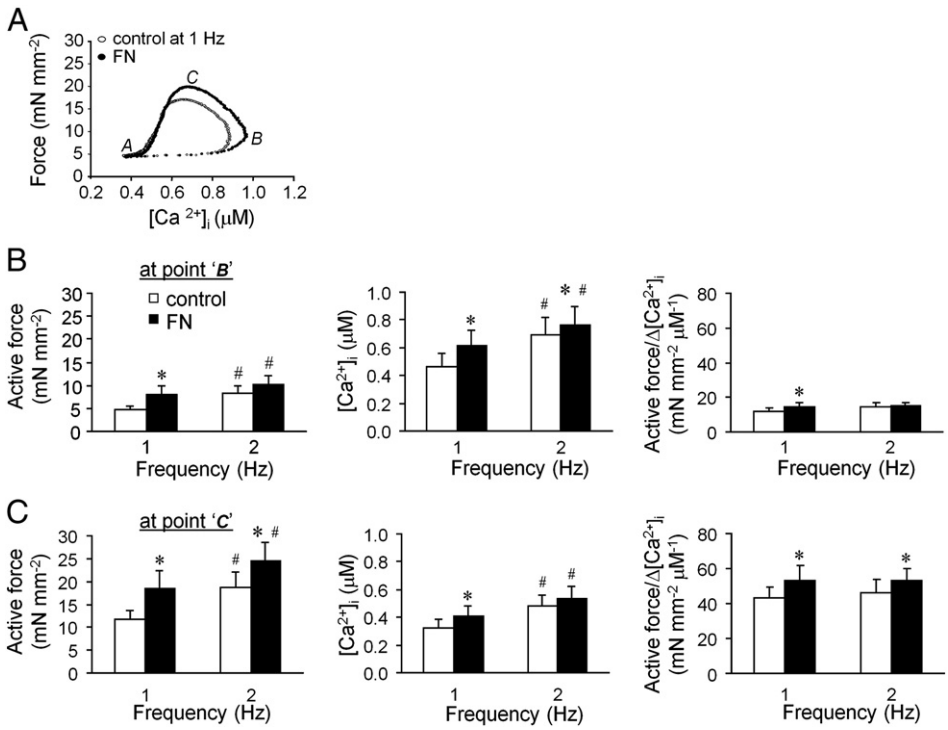

Fig. 4. Analysis of the force–$[Ca^{2+}]_i$ loop in the absence and presence of FN. (A) Representative force–Ca^{2+} loop in the absence and presence of FN at a stimulation rate = 1 Hz. '*A*' is the resting point; '*B*' is the peak $[Ca^{2+}]_i$ point; and '*C*' is the peak force point. (B and C) $[Ca^{2+}]_i$, active force, and active force/$\Delta[Ca^{2+}]_i$ in the absence and presence of FN ($n = 9$). Data are presented as mean ± SEM. $^*p < 0.05$ *vs* control of corresponding rates. $^\#p < 0.05$ *vs* 1 Hz within control or FN group.

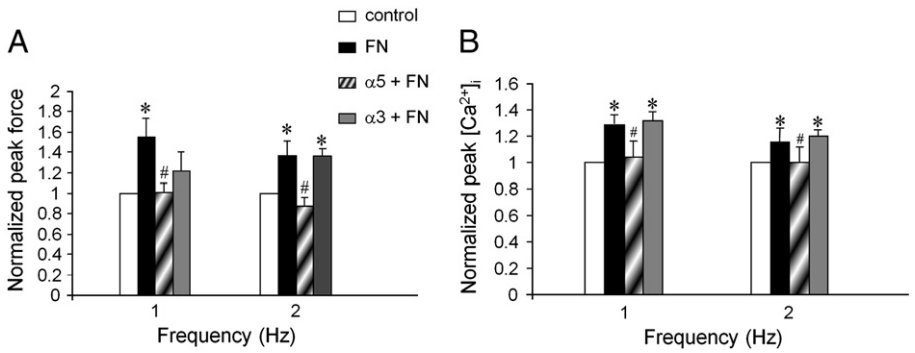

Fig. 5. The FN-enhancement in peak force and $[Ca^{2+}]_i$ was inhibited by an α5 integrin function blocking antibody. Bar graph summary of normalized force changes (A) or $[Ca^{2+}]_i$ (B) after FN ($n=9$) or after pretreatment with α3 integrin function blocking antibody (60 nM, $n=7$) or α5 integrin function blocking antibody (60 nM, $n=7$) at 1 or 2 Hz rate. $^{*}p<0.05$ *vs* control. $^{\#}p<0.05$ *vs* FN alone.

3.3. The increased force generation in FN-treated muscle fiber is mediated by α5β1 integrins

To investigate the role of integrins in the activation effect on force development in FN-treated fibers, we pretreated the papillary fiber bundles with function blocking antibodies for α3 or α5 integrin subunits and measured the force development as described in Materials and methods. α3 and α5 integrin subunits are known to associate only with β1 integrin subunit, making α3 and α5 antibodies specific for α3β1 and α5β1 heterodimer integrins, respectively. The results show that the effect of FN on force was significantly attenuated in the presence of antibodies for α5 integrins (Fig. 5(A)). The data show that the maximum force development of papillary muscle preparations was significantly reduced by 39% at 1 Hz and 36% at 2 Hz ($n=7$, $P<0.05$) in the presence of α5 blocking antibody (α5 + FN group) compared to FN-treated fibers alone. Furthermore, the peak $[Ca^{2+}]_i$ was significantly decreased by 19% at 1 Hz in fibers treated with α5 blocking antibody compared to FN-treated fibers alone ($n=7$, $p<0.05$). There were no significant differences in normalized peak force and $[Ca^{2+}]_i$ between control and α5 + FN groups. The effects of FN on force and $[Ca^{2+}]_i$ were not significantly affected in the presence of α3 integrin function blocking antibody (Fig. 5).

3.4. Enhanced force and Ca^{2+} by FN are PKA and L-type Ca^{2+} channel dependent

Phosphorylation via PKA at serine 1928 of the L-type Ca^{2+} channels and PKA-dependent phosphorylation of myofilament proteins and Ca^{2+}-handling proteins lead to positive inotropic, lusitropic, and chronotropic effects on the heart [38–41]. Since FN enhanced force development and increased $[Ca^{2+}]_i$ with shorter time to the peak of force development in papillary fibers, we propose that activation of both the L-type Ca^{2+} channel and PKA would be involved in modulating the $[Ca^{2+}]_i$ and myofilament or Ca^{2+}-handling proteins. To test this hypothesis, papillary muscle fibers were pretreated with the cell-permeable PKA inhibitor 14–22 amide (PKA-I, 1 μM) or with the Ca^{2+} channel blocker verapamil (2.5 μM) prior to perfusion with FN. Figs. 6(A and B) clearly demonstrate that the effect of FN on force development and $[Ca^{2+}]_i$ were greatly reduced in the fibers treated with PKA-I at both 1 Hz and 2 Hz. Furthermore the increase in active force per unit Ca^{2+} associated with FN treatment was significantly reduced in fibers treated with PKA-I (Table 1).

As shown in Figs. 6(C and D), verapamil significantly reduced maximum force generation by 74 and 76% at 1 and 2 Hz stimulation,

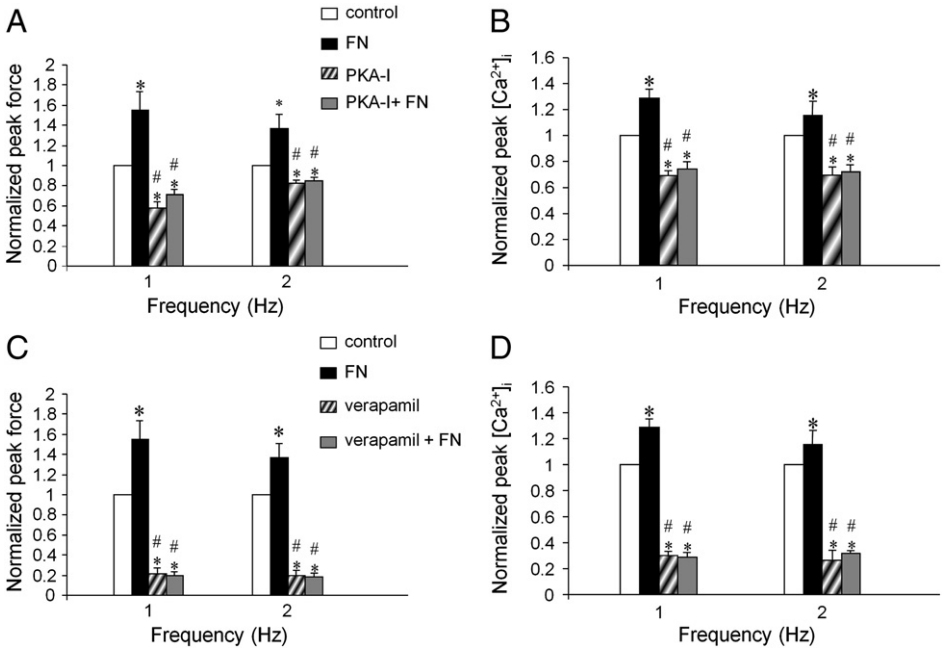

Fig. 6. FN enhanced force and $[Ca^{2+}]_i$ were blocked by PKA inhibitor (PKA-I) or L-type Ca^{2+} channel blocker verapamil. Bar graph summary of normalized peak force changes (A or C) and peak $[Ca^{2+}]_i$ (B or D) in the pretreatment of PKA-I (1 μM, $n=6$, A and B) or verapamil (2.5 μM, $n=7$. C and D) at 1 or 2 Hz rate. There are no differences before and after application of FN in the presence of PKA-I or verapamil. $^{*}p<0.05$ *vs* control. $^{\#}p<0.05$ *vs* FN alone.

Table 1
Active force per unit Ca^{2+} changes after application of FN in the presence of PKA inhibitor (PKA-I).

At 2 Hz	Control	FN ($n=9$)	PKA-I ($n=6$)	PKA-I + FN ($n=6$)
Active force/$\Delta[Ca^{2+}]_i$ at point '*B*'	12.3 ± 3	14.5 ± 2.2*	10.6 ± 1.9*	11.8 ± 1.6#
Active force/Δ $[Ca^{2+}]_i$ at point '*C*'	32.6 ± 5	53.1 ± 8.6*	28.1 ± 4.5*	30.1 ± 3.9#

Unit: mN mm^{-2} μM^{-1}. *$p<0.05$ *vs* control; #$p<0.05$ *vs* FN alone.

respectively, while the maximum $[Ca^{2+}]_i$ was inhibited by 64 and 68% at 1 and 2 Hz, respectively. There was no further increase in active force and $[Ca^{2+}]_i$ after FN application in the presence of verapamil (Figs. 6(C and D)).

3.5. FN enhanced myocyte cell shortening and I_{Ca}

To determine the effects of FN on the shortening of single cardiomyocytes, freshly isolated adult mouse cardiomyocytes were treated with 35 nM FN under 1 Hz field stimulation. Prior to stimulation, cell length was not significantly different in the presence of 35 nM FN (98.8 ± 4.6 μm in control *vs* 95.4 ± 4.7 μm after FN). Fig. 7(A) shows typical contractions (normalized to control length) in cardiomyocytes before and after FN by 1 Hz field stimulation. Pooled average data (Fig. 7(B)) revealed that the amplitude of contraction was increased by 40% in the presence of FN ($P<0.05$, $n=13$). The time to the peak of contraction and time to 50% relaxation were also shortened by 12% and 19%, respectively, after FN application (Fig. 7(C)). In addition, the rates of contraction and relaxation were increased by 59% and 70%, respectively, in the presence of FN (Fig. 7(D)).

Since force enhancement by papillary muscle was accompanied by an increase in the $[Ca^{2+}]_i$ in the presence of FN, and Ca^{2+} entry through the L-type Ca^{2+} channel is the first step leading to an $[Ca^{2+}]_i$ increase, the activity of Ca_L was examined. Whole-cell inward I_{Ca} in freshly isolated mouse cardiomyocytes was elicited by voltage steps (−60 to +40 mV in 10 mV increments, duration = 200 ms from a holding potential = −50 mV) or by voltage ramps (−50 to +40 mV, duration = 200 ms. Fig. 8(A)). Both protocols evoked inward currents that peaked at −10 mV and were blocked by the cardiac Ca^{2+} channel blocker verapamil (2.5 μM, Fig. 8(A)). Application of FN (35 nM) in the bath solution led to an enhancement of I_{Ca} (Fig. 8(A)). Furthermore, the increase in I_{ca} was detected as early as 1 min, reached a peak at 3 to 5 min, and was followed by a gradual return (data not shown). The average response of 4 cells to FN is summarized in Fig. 8(B). On average, 4 min application of 35 nM FN was associated with a 36% enhancement of I_{Ca} at −10 mV. The data in Fig. 8(B) represent the peak I_{Ca} normalized to the peak I_{Ca} recorded in the same cell just before FN application.

3.6. Phosphorylation of PLB increased in the presence of FN

To test if integrin engagement with FN led to protein phosphorylation of cardiac TnI (Ser 23/24) and phospholamban (PLB) Ser16, papillary muscles were stimulated at 3 Hz for 4 min after FN and then subjected to western blot analyses with specific antibodies. Quantitative analyses (Fig. 9(A)) from the sample preparations either by boiling or heating to 37 °C showed that the p-PLB/total PLB ratio was significantly increased in the fibers treated with FN (Boiled samples: 0.611 ± 0.049 in FN treated *vs* 0.305 ± 0.061 in control; samples heated to 37 °C: 0.691 ± 0.005 in FN treated *vs* 0.242 ± 0.069 in control. $p<0.05$). Analysis of p-PLB was also carried out with respect to GAPDH expression in the same samples. The ratio of p-PLB/GAPDH was significantly increased in FN-treated fibers (Boiled samples: 0.636 ± 0.044 in FN treated *vs* 0.358 ± 0.066 in controls; samples heated to 37 °C: 0.759 ± 0.029 in FN treated *vs* 0.297 ± 0.079 in controls. $p<0.05$). As shown in Fig. 9(B), the p-TnI/total TnI ratio did not show any significant difference between control and FN-treated fiber samples (0.706 ± 0.039 in FN treated *vs* 0.732 ± 0.0125 in controls).

4. Discussion

The main goal of this study was to determine the mechanisms whereby FN modulates cardiac muscle contractility. A significant enhancement in ventricular myocyte force was recorded in the presence of FN. The increase in force was accompanied by an increase in Ca^{2+} concentration, an increase in Ca^{2+} sensitivity as deduced from analysis of Ca^{2+}–force loops, and an enhancement in the phosphorylation of phospholamban. Electrophysiological recordings of current through the L-type Ca^{2+} channel revealed an increase in I_{Ca} in the presence of FN. The enhancement of myocyte force induced by FN was significantly reversed in the presence of a function blocking antibody against α5β1 integrin. A PKA inhibitor and a Ca^{2+} channel blocker

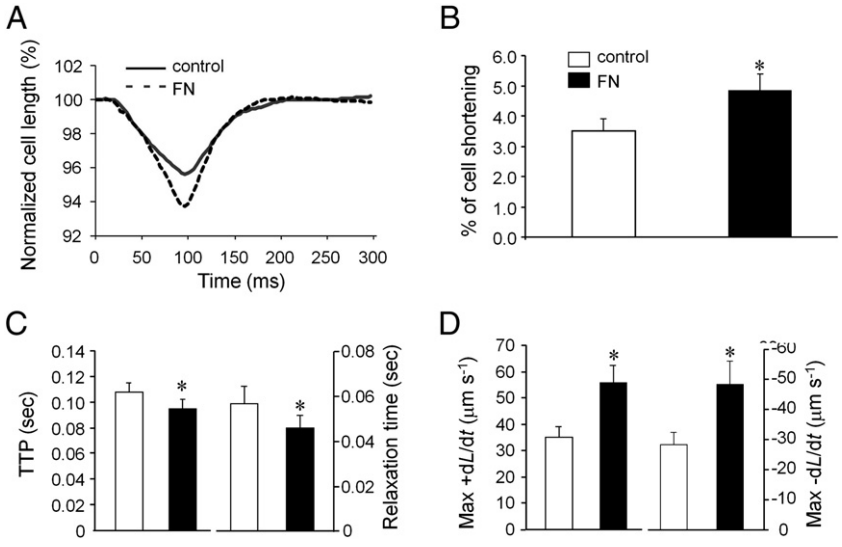

Fig. 7. The effects of FN on cell contraction. (A) Representative tracings of cell shortening triggered by 1 Hz field stimulation before and after FN application in adult cardiomyocytes. In the presence of FN (35 nM), increased fractional shortening, shorter time to peak of shortening (TTP), and shorter time to half relaxation (relaxation time) are evident (B and C) ($n=13$). (D) Pooled data showing higher rates of contraction and relaxation in the presence of FN. *$p<0.05$ *vs* control.

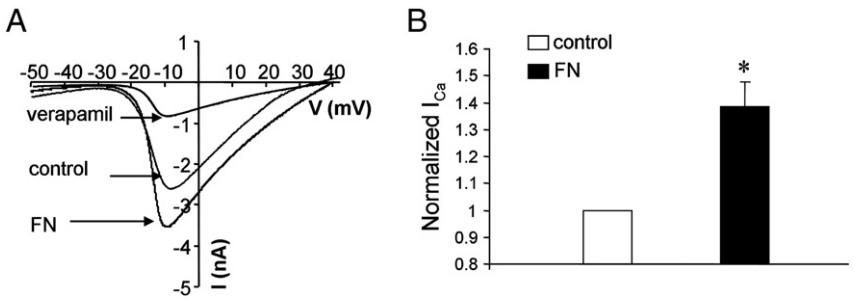

Fig. 8. The effects of FN on L-type Ca^{2+} channel (Ca_L). (A) Whole-cell inward Ca_L currents (I_{Ca})–voltage (I–V) relationships obtained from freshly isolated adult mouse cardiomyocyte using a ramp protocol (−50 to +40 mV over 200 ms). I_{Ca} was enhanced at 4 min after application of FN (35 nM). The current was substantially inhibited by 2.5 μM verapamil. (B) Bar graph represents normalized peak currents 4 min after application of FN, where current was significantly enhanced ($n=4$). Peak currents after FN were normalized to the currents at the peak of the control I–V relationship (usually at a test potential of −10 mV). *$p<0.05$ *vs* control. Pipette: 110 Cs+; bath: 2 mM Ba^{2+}; holding potential: −50 mV.

reversed the effects of FN on muscle fiber force development. These results demonstrate that FN acts via α5β1 integrin to increase ventricular myocyte force production and that the underlying mechanisms involve an increase in $[Ca^{2+}]_i$ through the L-type Ca^{2+} channel and an increase in Ca^{2+} handling by phosphorylation of phospholamban in addition to changes in myofilament activation processes such as Ca^{2+} sensitivity and crossbridge activation in the myocardium.

4.1. FN and cardiac function

In adult myocardial tissue, the increased expression of cellular FN mRNA was seen as a response to hypertrophy that accompanied by re-expression of fetal isoforms of FN [42,43]. Moreover, accumulation of FN is observed in ischemic myocardium during the early stages of acute myocardial infarction, and may play a role in the repair process and fibrotic remodeling of the ventricular wall [44,45]. During the progression of diabetes, hypertension and myocardial infarction, there is an increase in expression and deposition of insoluble FN and collagen in non-cardiovascular myocyte compartments, which have a relatively similar distribution throughout the myocardium [46]. An imbalance in the production and the degradation of ECM proteins may lead to structural alterations such as basement membrane thickening and ECM protein deposition in tissues during the development of cardiovascular diseases [22,26,42,47–59]. All of these studies imply that FN is a major component of the myocardial interstitium, may affect myocardial compliance, and modulate the contraction and/or relaxation cardiomyocytes. However, the role that FN plays in modulating cardiac muscle contraction has not been directly studied.

The FN polypeptide is composed of three repeat regions, I, II, and III [7,60]. The recognition site for α3β1 or α5β1 integrin is in FN region III, which contains RGD repeats. When FN binds to the integrin receptor, integrin clustering and assembly of multiple focal proteins occurs inside the cell initiating various signaling pathways. We previously showed that soluble RGD-containing synthetic peptide, or fragments of denatured collagen (Type I) significantly reduced force

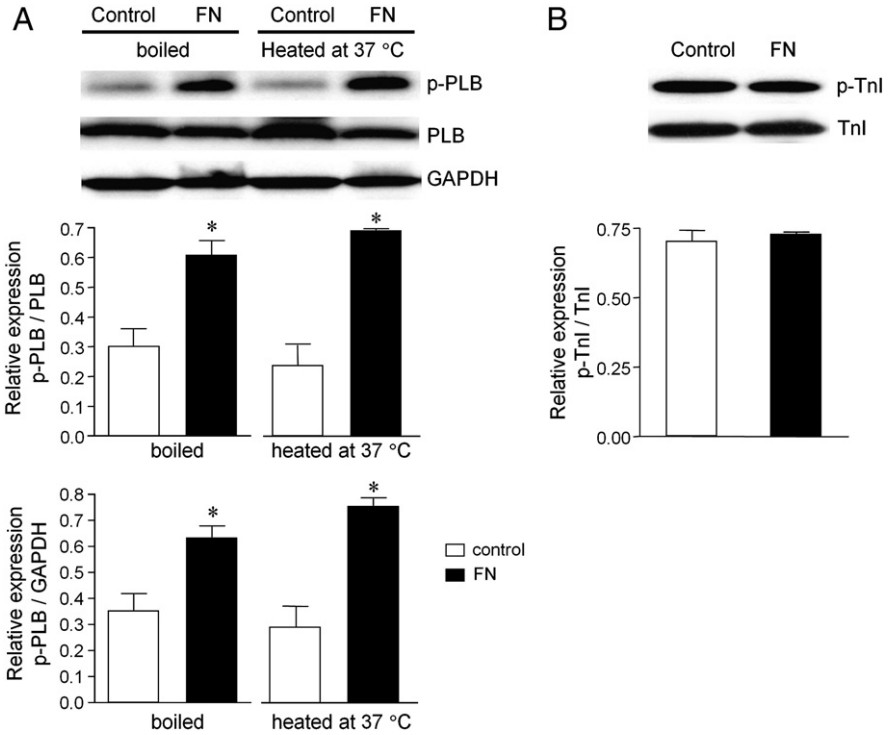

Fig. 9. Western blot analysis of p-PLB and p-TnI expression with or without FN treatment: mouse papillary muscle bundles were subjected to FN treatment (stimulated at 3 Hz) and analyzed for differential expression of p-PLB and p-TnI. (A) Top panel: representative blot showing the expression of p-PLB, PLB and GAPDH in control and FN-treated samples that were boiled or heated to 37 °C. Bottom panel: the relative expression of p-PLB/PLB and p-PLB/GAPDH were calculated and plotted. (B) Top panel: representative blot showing the expression of p-TnI and TnI in control and FN-treated samples. Bottom panel: the relative expression of p-TnI/TnI was calculated and plotted. Both A and B represent data from three independent experiments and the mean ± SEM is plotted. *$p<0.05$ *vs* control.

production in papillary muscle fibers. Integrin antibodies for α5 and β1 integrins, but not α3 integrin antibody, reversed the effect of the RGD-containing peptide. Force–$[Ca^{2+}]_i$ measurements showed that the depressed force generation in the presence of RGD peptide, acting via α5β1 integrin, was associated with reduced $[Ca^{2+}]_i$ and myofilament activation processes [2]. The data presented in this study demonstrated that soluble intact FN, acting through α5β1 integrin, enhanced force and increased $[Ca^{2+}]_i$, which might be related to activation of Ca_L and myofilament activation processes. The different downstream effects of ECM proteins through various integrins or the activation of integrins by different integrin antibodies (i.e. soluble or insoluble form) leading to specific signaling have also been reported in other studies. In VSM, soluble RGD, vitronectin, RGD-containing FN fragment, as well as insoluble vitronectin inhibited Ca^{2+} current probably through αvβ3 integrin. In contrast, insoluble FN acted through α5β1 to enhance Ca^{2+} current and Ca^{2+} entry. A peptide containing the LDV sequence (in the IIICS region of FN) enhanced contraction and Ca^{2+} current through α4β1 integrin [12–14]. Soluble α5β1 antibody had no effect on Ca^{2+} currents in VSM but increased Ca^{2+} in heterologously expressed neuronal and smooth muscle Ca_L channel isoforms in HEK-293 cells [12–14]. Rueckschloss et al. [23] have reported that soluble FN enhanced Ca^{2+} current in cardiomyocytes while soluble RGD peptide did not have any effect on Ca^{2+} current. Lamberts et al. used a specific type 1 collagenase enzyme and observed an increase in diastolic and developed tension [61]. Laminin binding to β1 integrins modulates Ca_L through signaling pathways linked to adrenergic and cholinergic receptors signaling in cat atrial myocytes [62,63]. The difference in the downstream signaling observed between RGD-containing collagen and FN could be explained by the activation of different intracellular signaling pathways. Digested/soluble collagen, upon binding to α5β1 integrin, activated protein kinase C to inhibit Ca_L and decreased Ca^{2+} to myofilaments [2]; whereas in this study we showed that binding of intact soluble FN to α5β1 integrin activated PKA and increased phosphorylation of PLB and thereby enhanced Ca^{2+} sensitivity and crossbridge kinetics. Thus, it is likely that the overlapping distribution of FN and collagen in the myocardial matrix has differential functions on cardiomyocytes whose actions might represent an equilibrium mechanism during physiological or pathological circumstances.

4.2. FN modulates cardiac contractility through Ca^{2+} signaling, Ca^{2+} sensitivity and crossbridge kinetics

The data presented in Figs. 1 and 4 clearly show an increase in force development in the FN-treated fibers. Though the active force (total force − passive force) values at 1.0 Hz are comparable both at room temperature and 37 °C (for control samples: 10.7 ± 1.2 mN/mm^2 at room temperature and 11.8 ± 1.8 mN/mm^2 at 37 °C; the values are from data shown in Figs. 1(D) and 4(C), respectively), the force values are higher in the fibers stimulated at 2.0 Hz measured at room temperature. We think that the force values are different due to the temperature at which the experiments have been performed. These data are also consistent with our previous publication [32], which showed that the maximum force at 34 °C peaks at 6–7 Hz, whereas at room temperature the force peaks at 3.0 Hz. The simultaneous force and Ca^{2+} measurements were performed at room temperature, since Fura-2 dye load into myocytes more efficiently at room temperature as we have discussed in the Materials and methods section.

The level of $[Ca^{2+}]_i$ along with the sensitivity of the myofilaments to $[Ca^{2+}]_i$, determines the level of activation of the cardiac muscle fibers. Increasing stimulation frequency caused a progressive an increase in myocyte force development, which is evident as a positive force–frequency relationship (FFR) in both control and FN-treated groups. Several studies have shown that the Ca_L channel and the Ca^{2+} handling protein sarcoplasmic reticulum Ca^{2+} ATPase (SERCA2a) have frequency-dependent characteristics that contribute to a positive FFR [64–67]. Phosphorylation of the PKA site on the Ca_L channel causes an increase in the open probability and the open time, leading to an increased influx of Ca^{2+} and enhancement of cardiac excitation–contraction due to an increase in the free cytosolic Ca^{2+} concentration [68–70]. As evident from the presented data, the increased force, $[Ca^{2+}]_i$ and I_{Ca} stimulated by FN were significantly inhibited by verapamil and PKA-I, suggesting that the FN affected force generation in cardiomyocyte through activation of Ca_L and increase in PKA activity. Ca^{2+} release and Ca^{2+} reload are also involved in the regulation of free $[Ca^{2+}]_i$, which was supported by an increase in the phosphorylation of PLB. In this study, faster declined time of Ca^{2+} transients to 50% of the peak $[Ca^{2+}]_i$ during relaxation (Fig. 3), indicating faster Ca^{2+} reload by FN. Additional experiments are warranted to directly test the SERCA2a activity.

Increases in $[Ca^{2+}]_i$, force and force/unit Ca^{2+} in the FN-treated papillary fibers at the point of the Ca^{2+} peak (Point '*B*') point to Ca^{2+}-activated thin filament activation processes, such as an increase in Ca^{2+} sensitivity, during the *A* to *B* segment of the force–Ca^{2+} loop. The *B* to *C* segment is typically attributed to strongly-bound crossbridges keeping tropomyosin in the open state to allow continued myosin attachment to actin despite decreasing $[Ca^{2+}]_i$ [32]. Increased force and force/unit Ca^{2+} at the point of maximum force ('C') suggest an increased rate of contraction and decreased time of peak Ca^{2+} to peak force; these processes may reflect an increased cooperative feedback effect and accelerated crossbridge kinetics in the presence of FN. Furthermore, despite a small increase in $[Ca^{2+}]_i$, both at *B* and *C* points, the effect of FN on the force development is relatively greater (Fig. 4), which strongly demonstrate an increase in myofilament Ca^{2+} sensitivity in the FN-treated myocardium. In addition, FN enhanced papillary muscle twitch force, cell contraction speed, and Ca^{2+} transient decay, suggesting an enhancement in Ca^{2+} dynamics, which would also augment the faster crossbridge kinetics.

4.3. Role of PKA in the downstream effects of FN–integrin adhesion

PKA activation has been shown to be involved in multiple signaling pathways downstream from integrin–ECM interactions. In migrating cells, the participation of α4β1 or α5β1 integrins in adhesion-mediated, and localized activation of PKA is one of the earliest steps in directional cell migration [71]. Several studies in myocardium have shown that PKA-dependent phosphorylation of both Ca^{2+} handling (SERCA2a, PLB, ryanodine receptor and Ca_L) and myofilament (TnI and myosin binding protein-C) proteins plays a critical role in modulating the crossbridge kinetics [72–74]; however adhesion-mediated activation of PKA in the myocardium has not been previously shown. Our results, showing reversal of the FN-stimulatory effect on force development of papillary muscle fibers by PKA-I indicate that PKA is acting downstream of the FN–integrin axis to modulate the force generation in the myocardium. The presented data (Table 1), demonstrating a significant decrease in FN-augmented force per unit Ca^{2+} in the presence of PKA-I at both points B and C in the force–Ca^{2+} loop suggest that both Ca^{2+} activation of the thin filament (*A* to *B* segment) and positive feedback by strongly-bound crossbridge mechanisms (*B* to *C* segment [31,32]), are to a large extent mediated by PKA in FN-treated myofibers. Furthermore, western blotting data showed an increase in the phosphorylation of PLB. Increased phosphorylation of PLB has been reported during catecholamine stimulation and β-adrenergic-induced acceleration of cardiac relaxation [29,75]. Taken together, our data indicate that in the presence of FN, α5β1 integrin-mediated signaling changes the characteristics of Ca^{2+}-handling protein, PLB, through PKA, which further alters the myofilament activation processes, such as Ca^{2+} sensitivity and crossbridge activation, leading to the observed enhancement of force. Cheng et al. [76] have demonstrated that the overexpression of β1A integrin subunit decreases the isoproterenol-induced Ca^{2+} current and also, decreases the levels of cAMP. A

different downstream effect of β1 integrin activation seen by Cheng et al. [76] could be due to the fact that in our study we used FN that only binds to α5β1 or α3β1; whereas, in Cheng et al. overexpression of the β1A integrin subunit that would associate primarily with α1, α3, α5 and α6 integrin subunits in cardiomyocytes showed a decrease PKA activation.

This study identifies an important role for the FN–α5β1 integrin signaling pathway in cardiac myocytes relative to myocyte contractile function. The data presented here provide the first experimental evidence that FN enhances force in mouse papillary muscle fibers through α5β1 integrins. We speculate that this increase in force by FN would probably temporarily compensate for impaired heart function from overload in the hypertrophied or damaged heart. Furthermore the augmentation of force in the presence of FN is associated with an increase in $[Ca^{2+}]_i$ and changes in the myofilament activation processes, partially due to the effects of PKA on PLB. These data, along with our previous study showing that digested collagen fragments or RGD-containing peptide decrease cardiomyocyte force [2], indicate that the dynamic adhesion events between ECM proteins and integrins, which are dramatically altered during the development of disease conditions in myocardium, play significant roles in modulating cardiac muscle dynamics. We have recently shown [3] that FN–integrin adhesion force and adhesion probability in contracted cells are greater than in cells under relaxed condition. We propose that the continuing alterations in integrin adhesion to the ECM would initiate outside in signaling changes that includes the changes/activation in the costamere complex and its associated kinases, to provide feedback responses of the contractile status of the cells. Our data presented in this study showed that FN-induces a Ca^{2+} increase and an increase in force development in mouse papillary muscle fibers as a feedback response to FN–α5β1 integrin interaction. However, further experiments are warranted to address how the pathological remodeling of ECM proteins including increase levels of FN affects the outside in signaling pathways in modulating the cardiac muscle contractility.

Acknowledgment

This work was supported by National Institutes of Health grants R21-EB-003888-01A1 and KO2HL-86650 to MM; AHA 09POST2280005 to SC.

References

[1] Epstein ND, Davis JS. Sensing stretch is fundamental. Cell Jan 24 2003;112(2):147–50.
[2] Sarin V, Gaffin RD, Meininger GA, Muthuchamy M. Arginine–glycine–aspartic acid (RGD)-containing peptides inhibit the force production of mouse papillary muscle bundles via alpha 5 beta 1 integrin. J Physiol Apr 15 2005;564(Pt 2):603–17.
[3] Wu X, Sun Z, Foskett A, Trzeciakowski JP, Meininger GA, Muthuchamy M. Cardiomyocyte contractile status is associated with differences in fibronectin and integrin interactions. Am J Physiol Heart Circ Physiol Jun 2010;298(6):H2071–81.
[4] Ross RS, Borg TK. Integrins and the myocardium. Circ Res 2001;88(11):1112–9.
[5] Samarel AM. Costameres, focal adhesions, and cardiomyocyte mechanotransduction. Am J Physiol Heart Circ Physiol Dec 2005;289(6):H2291–301.
[6] Glukhova M, Koteliansky V. Integrins, cytoskeletal and extracellular matrix proteins in developing smooth muscle cells of human aorta. In: Schwartz S, Mecham R, editors. The vascular smooth muscle cell: molecular and biological responses to the extracellular matrix. San Diego, CA: Academic Press; 1995. p. p37–79.
[7] Jane-Lise S, Corda S, Chassagne C, Rappaport L. The extracellular matrix and the cytoskeleton in heart hypertrophy and failure. Heart Fail Rev 2000 Oct;5(3):239–50.
[8] Wang N, Butler JP, Ingber DE. Mechanotransduction across the cell surface and through the cytoskeleton. Science 1993;260:1124–7.
[9] McNamee HP, Ingber DE, Schwartz MA. Adhesion to fibronectin stimulates inositol lipid synthesis and enhances PDGF-induced inositol lipid breakdown. J Cell Biol 1993 May;121(3):673–8.
[10] Schmidt C, Pommerenke H, Durr F, Nebe B, Rychly J. Mechanical stressing of integrin receptors induces enhanced tyrosine phosphorylation of cytoskeletally anchored protein. J Biol Chem 1998;273:5081–5.
[11] Wu X, Davis GE, Meininger GA, Wilson E, Davis MJ. Regulation of the L-type calcium channel by alpha 5beta 1 integrin requires signaling between focal adhesion proteins. J Biol Chem 2001;276(32):30285–92.
[12] Wu X, Mogford JE, Platts SH, Davis GE, Meininger GA, Davis MJ. Modulation of calcium current in arteriolar smooth muscle by alphav beta3 and alpha5 beta1 integrin ligands. J Cell Biol 1998;143(1):241–52.
[13] Waitkus-Edwards KR, Martinez-Lemus LA, Wu X, Trzeciakowski JP, Davis MJ, Davis GE, et al. alpha(4)beta(1) Integrin activation of L-type calcium channels in vascular smooth muscle causes arteriole vasoconstriction. Circ Res 2002;90(4):473–80.
[14] Gui P, Wu X, Ling S, Stotz SC, Winkfein RJ, Wilson E, et al. Integrin receptor activation triggers converging regulation of Cav1.2 calcium channels by c-Src and protein kinase A pathways. J Biol Chem 2006 May 19;281(20):14015–25.
[15] Gui P, Balasubramanian B, Wu X, Ling S, Stotz S, Wilson E, et al. Effect of α5β1 integrin activation on heterologously expressed cardiac L-type calcium channels (abstract). 48th Annual Meeting of Biophysical Society; 2004. Baltimore; 2004. p. **.
[16] Wu X, Yang Y, Gui P, Sohma Y, Meininger GA, Davis GE, et al. Potentiation of large conductance, Ca2+-activated K+ (BK) channels by alpha5beta1 integrin activation in arteriolar smooth muscle. J Physiol 2008 Mar 15;586(6):1699–713.
[17] Yang Y, Wu X, Gui P, Wu J, Sheng JZ, Ling S, et al. Alpha5beta1 integrin engagement increases large conductance, Ca2+-activated K+ channel current and Ca2+ sensitivity through c-src-mediated channel phosphorylation. J Biol Chem 2010 Jan 1;285(1):131–41.
[18] Passier R, Zeng H, Frey N, Naya FJ, Nicol RL, McKinsey TA, et al. CaM kinase signaling induces cardiac hypertrophy and activates the MEF2 transcription factor in vivo. J Clin Invest 2000 May;105(10):1395–406.
[19] Sei CA, Irons CE, Sprenkle AB, McDonough PM, Brown JH, Glembotski CC. The alpha-adrenergic stimulation of atrial natriuretic factor expression in cardiac myocytes requires calcium influx, protein kinase C, and calmodulin-regulated pathways. J Biol Chem 1991 Aug 25;266(24):15910–6.
[20] Clark RJ, McDonough PM, Swanson E, Trost SU, Suzuki M, Fukuda M, et al. Diabetes and the accompanying hyperglycemia impairs cardiomyocyte calcium cycling through increased nuclear O-GlcNAcylation. J Biol Chem 2003 Nov 7;278(45):44230–7.
[21] Belke DD, Swanson EA, Dillmann WH. Decreased sarcoplasmic reticulum activity and contractility in diabetic db/db mouse heart. Diabetes 2004 Dec;53(12):3201–8.
[22] Belke DD, Dillmann WH. Altered cardiac calcium handling in diabetes. Curr Hypertens Rep 2004 Dec;6(6):424–9.
[23] Rueckschloss U, Isenberg G. Contraction augments L-type Ca2+ currents in adherent guinea-pig cardiomyocytes. J Physiol 2004 Oct 15;560(Pt 2):403–11.
[24] Trial J, Rossen RD, Rubio J, Knowlton AA. Inflammation and ischemia: macrophages activated by fibronectin fragments enhance the survival of injured cardiac myocytes. Exp Biol Med (Maywood) 2004 Jun;229(6):538–45.
[25] Chen H, Huang XN, Stewart AF, Sepulveda JL. Gene expression changes associated with fibronectin-induced cardiac myocyte hypertrophy. Physiol Genomics 2004 Aug 11;18(3):273–83.
[26] Mamuya WS, Brecher P. Fibronectin expression in the normal and hypertrophic rat heart. J Clin Invest 1992 Feb;89(2):392–401.
[27] Ahumada GG, Saffitz JE. Fibronectin in rat heart: a link between cardiac myocytes and collagen. J Histochem Cytochem 1984 Apr;32(4):383–8.
[28] Laser M, Willey CD, Jiang W, Cooper GT, Menick DR, Zile MR, et al. Integrin activation and focal complex formation in cardiac hypertrophy. J Biol Chem Nov 10 2000;275(45):35624–30.
[29] Li L, Desantiago J, Chu G, Kranias EG, Bers DM. Phosphorylation of phospholamban and troponin I in beta-adrenergic-induced acceleration of cardiac relaxation. Am J Physiol Heart Circ Physiol 2000 Mar;278(3):H769–79.
[30] Grynkiewicz G, Poenie M, Tsien R. A new generation of Ca2+ indicators with greatly improved fluorescence properties. J Biol Chem 1985;260:3440–50.
[31] Gaffin RD, Tong CW, Zawieja DC, Hewett TE, Klevitsky R, Robbins J, et al. Charged residue alterations in the inner-core domain and carboxy-terminus of alpha-tropomyosin differentially affect mouse cardiac muscle contractility. J Physiol Dec 15 2004;561(Pt 3):777–91.
[32] Tong CW, Gaffin RD, Zawieja DC, Muthuchamy M. Roles of phosphorylation of myosin binding protein-C and troponin I in mouse cardiac muscle twitch dynamics. J Physiol Aug 1 2004;558(Pt 3):927–41.
[33] Hamill OP, Marty A, Neher E, Sakmann B, Sigworth FJ. Improved patch-clamp techniques for high-resolution current recording from cells and cell-free membrane patches. Pflugers Arch Aug 1981;391(2):85–100.
[34] Davis MJ. An improved, computer-based method to automatically track internal and external diameter of isolated microvessels. Microcirculation Jun 2005;12(4):361–72.
[35] Dias FA, Walker LA, Arteaga GM, Walker JS, Vijayan K, Pena JR, et al. The effect of myosin regulatory light chain phosphorylation on the frequency-dependent regulation of cardiac function. J Mol Cell Cardiol Aug 2006;41(2):330–9.
[36] Kolwicz SC, Kubo H, MacDonnell SM, Houser SR, Libonati JR. Effects of forskolin on inotropic performance and phospholamban phosphorylation in exercise-trained hypertensive myocardium. J Appl Physiol Feb 2007;102(2):628–33.
[37] Chen W, Lah M, Robinson PJ, Kemp BE. Phosphorylation of phospholamban in aortic smooth muscle cells and heart by calcium/calmodulin-dependent protein kinase II. Cell Signal Aug 1994;6(6):617–30.
[38] Striessnig J. Pharmacology, structure and function of cardiac L-type Ca(2+) channels. Cell Physiol Biochem 1999;9(4–5):242–69.
[39] Hulme JT, Westenbroek RE, Scheuer T, Catterall WA. Phosphorylation of serine 1928 in the distal C-terminal domain of cardiac CaV1.2 channels during beta1-adrenergic regulation. Proc Natl Acad Sci USA Oct 31 2006;103(44):16574–9.
[40] Kentish JC, McCloskey DT, Layland J, Palmer S, Leiden JM, Martin AF, et al. Phosphorylation of troponin I by protein kinase A accelerates relaxation and crossbridge cycle kinetics in mouse ventricular muscle. Circ Res May 25 2001;88(10):1059–65.

[41] Tong CW, Stelzer JE, Greaser ML, Powers PA, Moss RL. Acceleration of crossbridge kinetics by protein kinase A phosphorylation of cardiac myosin binding protein C modulates cardiac function. Circ Res Oct 24 2008;103(9):974–82.
[42] Samuel JL, Barrieux A, Dufour S, Dubus I, Contard F, Koteliansky V, et al. Accumulation of fetal fibronectin mRNAs during the development of rat cardiac hypertrophy induced by pressure overload. J Clin Invest 1991;88(5):1737–46.
[43] Farhadian F, Contard F, Corbier A, Barrieux A, Rappaport L, Samuel JL. Fibronectin expression during physiological and pathological cardiac growth. J Mol Cell Cardiol Apr 1995;27(4):981–90.
[44] Casscells W, Ferrans VJ. Growth factors in the heart. In: Oberpriller JO, Oberpriller JS, Mauro A, editors. The development and regenerative potential of cardiac muscle. New York: Harvard; 1990. p. 8–21.
[45] Knowlton AA, Connelly CM, Romo GM, Mamuya W, Apstein CS, Brecher P. Rapid expression of fibronectin in the rabbit heart after myocardial infarction with and without reperfusion. J Clin Invest Apr 1992;89(4):1060–8.
[46] Bouzeghrane F, Reinhardt DP, Reudelhuber TL, Thibault G. Enhanced expression of fibrillin-1, a constituent of the myocardial extracellular matrix in fibrosis. Am J Physiol Heart Circ Physiol Sep 2005;289(3):H982–91.
[47] Siperstein MD, Unger RH, Madison LL. Studies of muscle capillary basement membranes in normal subjects, diabetic, and prediabetic patients. J Clin Invest Sep 1968;47(9):1973–99.
[48] Weber K. Extracellular matrix remodeling in heart failure: a role for de novo angiotensin II generation. Circulation 1997;96(11):4065–82.
[49] Villarreal FJ, Dillmann WH. Cardiac hypertrophy-induced changes in mRNA levels for TGF-beta 1, fibronectin, and collagen. Am J Physiol 1992;262(6 pt 2): H1861–6.
[50] Contard F, Koteliansky V, Marotte F, Dubus I, Rappaport L, Samuel JL. Specific alterations in the distribution of extracellular matrix components within rat myocardium during the development of pressure overload. Lab Invest 1991;64(1):65–75.
[51] Willems IE, Arends JW, Daemen MJ. Tenascin and fibronectin expression in healing human myocardial scars. J Pathol 1996;179(3):321–5.
[52] Ulrich MM, Janssen AM, Daemen MJ, Rappaport L, Samuel JL, Contard F, et al. Increased expression of fibronectin isoforms after myocardial infarction in rats. J Mol Cell Cardiol 1997;29(9):2533–43.
[53] McCrossan ZA, Billeter R, White E. Transmural changes in size, contractile and electrical properties of SHR left ventricular myocytes during compensated hypertrophy. Cardiovasc Res Aug 1 2004;63(2):283–92.
[54] Kaur H, Chen S, Xin X, Chiu J, Khan ZA, Chakrabarti S. Diabetes-induced extracellular matrix protein expression is mediated by transcription coactivator p300. Diabetes Nov 2006;55(11):3104–11.
[55] Fredersdorf S, Thumann C, Ulucan C, Griese DP, Luchner A, Riegger GA, et al. Myocardial hypertrophy and enhanced left ventricular contractility in Zucker diabetic fatty rats. Cardiovasc Pathol Jan–Feb 2004;13(1):11–9.
[56] Grimm D, Huber M, Jabusch HC, Shakibaei M, Fredersdorf S, Paul M, et al. Extracellular matrix proteins in cardiac fibroblasts derived from rat hearts with chronic pressure overload: effects of beta-receptor blockade. J Mol Cell Cardiol Mar 2001;33(3):487–501.
[57] Brownlee M. The pathobiology of diabetic complications: a unifying mechanism. Diabetes Jun 2005;54(6):1615–25.
[58] Roy S, Sala R, Cagliero E, Lorenzi M. Overexpression of fibronectin induced by diabetes or high glucose: phenomenon with a memory. Proc Natl Acad Sci USA Jan 1990;87(1):404–8.
[59] Smoak IW. Hyperglycemia-induced TGFbeta and fibronectin expression in embryonic mouse heart. Dev Dyn Sep 2004;231(1):179–89.
[60] Dalen H, Saetersdal T, Roli J, Larsen TH. Effect of collagenase on surface expression of immunoreactive fibronectin and laminin in freshly isolated cardiac myocytes. J Mol Cell Cardiol May 1998;30(5):947–55.
[61] Lamberts RR, Willemsen MJ, Perez NG, Sipkema P, Westerhof N. Acute and specific collagen type I degradation increases diastolic and developed tension in perfused rat papillary muscle. Am J Physiol Heart Circ Physiol Mar 2004;286(3): H889–94.
[62] Wang YG, Samarel AM, Lipsius SL. Laminin binding to beta1-integrins selectively alters beta1- and beta2-adrenoceptor signalling in cat atrial myocytes. J Physiol 2000;527(Pt 1):3–9.
[63] Wang YG, Samarel AM, Lipsius SL. Laminin acts via beta 1 integrin signalling to alter cholinergic regulation of L-type Ca(2+) current in cat atrial myocytes. J Physiol 2000;526(Pt 1):57–68.
[64] Lemaire S, Piot C, Leclercq F, Leuranguer V, Nargeot J, Richard S. Heart rate as a determinant of L-type Ca2+ channel activity: mechanisms and implication in force–frequency relation. Basic Res Cardiol 1998;93(Suppl 1):51–9.
[65] Alpert NR, Leavitt BJ, Ittleman FP, Hasenfuss G, Pieske B, Mulieri LA. A mechanistic analysis of the force–frequency relation in non-failing and progressively failing human myocardium. Basic Res Cardiol 1998;93(Suppl 1):23–32.
[66] Hashimoto K, Perez NG, Kusuoka H, Baker DL, Periasamy M, Marban E. Frequency-dependent changes in calcium cycling and contractile activation in SERCA2a transgenic mice. Basic Res Cardiol Apr 2000;95(2):144–51.
[67] Miyamoto MI, del Monte F, Schmidt U, DiSalvo TS, Kang ZB, Matsui T, et al. Adenoviral gene transfer of SERCA2a improves left-ventricular function in aortic-banded rats in transition to heart failure. Proc Natl Acad Sci USA Jan 18 2000;97(2):793–8.
[68] Hescheler J, Fleischmann BK. Regulation of voltage-dependent Ca2+ channels in the early developing heart: role of beta1 integrins. Basic Res Cardiol 2002;97 (Suppl 1):I153–8.
[69] Sculptoreanu A, Rotman E, Takahashi M, Scheuer T, Catterall WA. Voltage-dependent potentiation of the activity of cardiac L-type calcium channel alpha 1 subunits due to phosphorylation by cAMP-dependent protein kinase. Proc Natl Acad Sci USA Nov 1 1993;90(21):10135–9.
[70] Sculptoreanu A, Scheuer T, Catterall WA. Voltage-dependent potentiation of L-type Ca2+ channels due to phosphorylation by cAMP-dependent protein kinase. Nature Jul 15 1993;364(6434):240–3.
[71] Lim CJ, Kain KH, Tkachenko E, Goldfinger LE, Gutierrez E, Allen MD, et al. Integrin-mediated protein kinase A activation at the leading edge of migrating cells. Mol Biol Cell Nov 2008;19(11):4930–41.
[72] Strang KT, Sweitzer NK, Greaser ML, Moss RL. Beta-adrenergic receptor stimulation increases unloaded shortening velocity of skinned single ventricular myocytes from rats. Circ Res Mar 1994;74(3):542–9.
[73] Solaro RJ, Rarick HM. Troponin and tropomyosin: proteins that switch on and tune in the activity of cardiac myofilaments. Circ Res Sep 7 1998;83(5):471–80.
[74] Winegrad S. Myosin binding protein C, a potential regulator of cardiac contractility. Circ Res Jan 7–21 2000;86(1):6–7.
[75] Kranias EG, Solaro RJ. Phosphorylation of troponin I and phospholamban during catecholamine stimulation of rabbit heart. Nature 1982 Jul 8;298(5870):182–4.
[76] Cheng Q, Ross RS, Walsh KB. Overexpression of the integrin beta(1A) subunit and the beta(1A) cytoplasmic domain modifies the beta-adrenergic regulation of the cardiac L-type Ca(2+)current. J Mol Cell Cardiol Jun 2004;36(6):809–19.

Meth Find Exp Clin Pharmacol 1994, 16(8): 583-587

Effects of Histamine on Electrophysiological Properties and Triggered Activity in Guinea Pig Papillary Muscles

Xin Wu[1], Wei-Qiu Huang[2], Qing-Quan Zhang[1] and Zhi-Ming Yu[2]

[1]Department of Physiology, Nantong Medical College, Nantong and [2]Department of Physiology, Suzhou Medical College, Suzhou, P.R. China

SUMMARY

The effects of histamine on action potentials (APs) and on early afterdepolarizations (EADs) were studied with standard microelectrode and computer in guinea pig papillary muscles. Experiments offer evidence that histamine (6.0 μmol/l) results in a significant diminution in action potential duration at 50% repolarization (APD_{50}) and 90% repolarization (APD_{90}) (data taken from no abnormal automaticity and oscillatory potential cells, 10 out of 19 preparations). Particularly, histamine can induce EADs (about 58%), oscillatory potentials and triggered activity. EADs frequently occur at low stimulation rates of 0.2-1.0 Hz and with prolongation of the action potential duration. EAD-induced triggered activity may exhibit fast spontaneous APs. Cimetidine (10 μmol/l, n = 6), an H_2-receptor antagonist, antagonizes the effects of histamine. In the presence of cimetidine no EADs are observed by perfusing histamine. An H_1-receptor antagonist, chlorpheniramine (10 μmol/l, n = 9), has no effect on the alterations of APs induced by histamine in ventricular myocardium. The results suggest that the mechanisms of histamine-induced shortness of AP duration, EADs and triggered activity may be related to the H_2 receptor-mediated enhancement of the slow inward calcium current.

Key words: Histamine - Cimetidine - Chlorpheniramine - Ventricular fibers - Microelectrode - Action potentials - Early afterdepolarizations

INTRODUCTION

Histamine has both inotropic and chronotropic effects on the human heart and additionally induces a variety of arrhythmogenic responses, including triggered arrhythmias during acute myocardial infarction, cardiac anaphylaxis, *etc.* (1). Differentiation of the roles of H_1 and H_2 receptors in the mediation of the effects of histamine in the working heart has been investigated (1-4).

Early afterdepolarizations (EADs) are a type of triggered activity that can arise from heart muscles before the action potential repolarization is completed. A triggered activity is defined as a second nonstimulated upstroke arising from the EADs and exhibiting an amplitude greater than 10 mV. EADs are believed to cause torsade de pointes (5, 6). The mechanisms of EADs and triggered activity induced by histamine have not yet been studied in ventricular cells.

The aim of the present study was to investigate the mechanisms of histamine on the alterations of action potentials (APs) and induction of EADs in guinea pig papillary muscles, with or without application of H_1- and H_2-receptor antagonists, by using computerized standard microelectrode techniques.

MATERIALS AND METHODS

Guinea pigs of either sex weighing 250-400 g were stunned. The right ventricular papillary

TABLE 1. Effects of histamine on action potentials in guinea pig papillary muscles (mean ± SD, n = 10)

	Control	Histamine (6.0 μmol/l)			Wash
		10 min	30 min	60 min	30 min
APD_{50} (ms)	181 ± 27	158 ± 20**	139 ± 18**	136 ± 24**	180 ± 26
APD_{90} (ms)	223 ± 38	187 ± 22**	168 ± 22**	165 ± 23**	219 ± 36
RP (mV)	88 ± 3	87 ± 4	88 ± 4	88 ± 3	89 ± 3
APA (mV)	121 ± 4	122 ± 3	123 ± 5	123 ± 8	121 ± 3
DP_3 (ms)	41 ± 22	28 ± 8*	28 ± 13*	25 ± 9*	39 ± 19
V_{max} (V/s)	270 ± 54	274 ± 93	272 ± 83	292 ± 101	260 ± 76

Data taken from no abnormal automaticity and oscillatory potential cells, 10 out of 19 preparations. APD_{50} and APD_{90}: action potential duration at 50% and 90% level of repolarization, respectively. RP: resting potential. APA: action potential amplitude. DP_3: duration of phase 3. V_{max}: maximum velocity of depolarization. Stimulation rate: 1.0 Hz. *$p < 0.05$; **$p < 0.01$ *vs.* control.

muscles (diameter ≤ 1.0 mm) were quickly cut and placed in a 2.5 ml bath perfused with Tyrode solution gassed with 95% O_2 + 5% CO_2 at 35 ± 0.2 °C, pH 7.4. The Tyrode solution contained the following components (in mmol/l): NaCl, 125.00; KCl, 5.00; $MgCl_2$, 1.05; $CaCl_2$, 1.80; NaH_2PO_4, 0.42; $NaHCO_3$, 24.00; glucose, 11.00. The perfusing speed was 7 ml/min. Preparations were allowed to equilibrate for 1 h before control recordings were taken and driven by square pulse (duration: 1.0 ms; intensity: 1.5 times threshold; stimulation rate: 1.0 Hz) with an electronic stimulator (SEN-7103, Nihon Koden) through bipolar stainless steel electrode. APs and EADs were recorded by glass microelectrodes filled with KCl 3.0 mol/l having resistance of 10-20 MΩ. The signals via microelectrode amplifier (MEZ-7101, Nihon Koden) were delivered to a dual-beam oscilloscope (SBR-1, Santou Electronic Co.), monitored simultaneously and transmitted into a computer which automatically analyzed the APs and EADs (real time on-line operation) or stored them on diskettes (7).

Ventricular muscle preparations were divided into 3 groups: 1) effects of histamine hydrochloride (HIS, 6.0 μmol/l; Sigma Co.) on APs of papillary muscles (n = 19); 2) effects of HIS on APs pretreated with the H_1-receptor antagonist chlorpheniramine (10 μmol/l; Long March Pharmaceutical Factory, Suzhou) for 30 min (n = 9); 3) effects of HIS on APs pretreated with the H_2-receptor antagonist cimetidine (10 μmol/l; Shanghai First Pharmaceutical Factory) for 30 min (n = 6). The APs were recorded 10, 30 and 60 min after perfusing of HIS. To study EADs induced by HIS, the preparations were driven by stimuli at various rates (0.2, 0.5, 1.0 and 2.0 Hz). Finally, the preparations were washed with Tyrode solution to observe the recovery of APs.

Measurement of duration of phase 3 (DP_3) was: $DP_3 = APD_{90} - APD_{50}$ (8).

The results were expressed as mean ± SD values. The significance of the difference between two means within the same experimental group was analyzed using Student's paired *t* test. Linear regression analysis was used for other data.

RESULTS

Effects of HIS on APs

By perfusion with Tyrode solution containing HIS for 10, 30 and 60 min, the action potential duration of 50% repolarization (APD_{50}) and 90% repolarization (APD_{90}) were greatly diminished ($p < 0.01$). DP_3 was reduced ($p < 0.05$). HIS had no significant effect on resting potential (RP), amplitude of APs (APA) and maximum velocity of depolarization (V_{max}) (data taken from no abnormal automaticity and oscillatory potential cells, 10 out of 19 preparations) (Table 1, Fig. 1.). These parameters of APs were mainly recovered within 30 min of washing with Tyrode solution. Stimulation rate was 1.0 Hz.

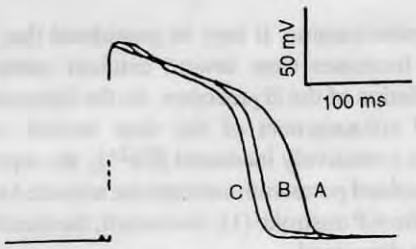

FIG. 1. The effects of histamine on duration of action potentials in guinea pig papillary muscles. A) Control; B, C) 10 and 30 min after perfusion of histamine. Stimulation rate: 1.0 Hz.

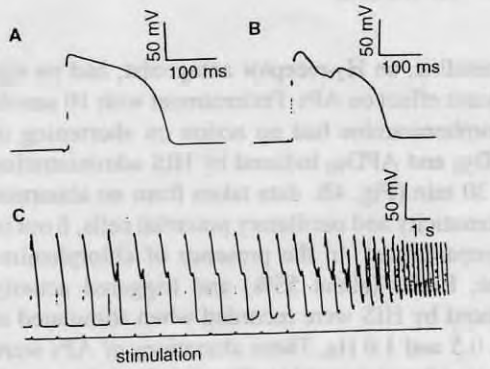

FIG. 2. Histamine-induced EADs and triggered activity in guinea pig papillary muscles. A) Normal, stimulation rate: 0.2 Hz; B) EADs and triggered activity, stimulation rate: 0.2 Hz; C) EAD-induced triggered activity in presence of histamine; after cessation of stimulation fast spontaneous action potentials were recorded. Stimulation rate: 1.0 Hz.

HIS-induced EADs and triggered activity

By perfusion with Tyrode solution by pacing at 0.2, 0.5, 1.0 and 2.0 Hz, EADs and triggered activity were not induced (Fig. 2A, n = 19). EADs and triggered activity were induced after adding HIS (incidence about 58%) stimulated at 0.2, 0.5 and 1.0 Hz, but not at 2.0 Hz. In 2 cases, EADs were not induced by pacing at 0.5 and 1.0 Hz, but were induced by pacing at 0.2 Hz. However, this phenomenon was occasionally found during perfusing of histamine. EADs occurred at phase 2 and/or phase 3 (Fig. 2B). Before and/or after formation of EADs, the duration of APs was usually prolonged. The amplitude of EADs often exceeded 10 mV, forming a triggered activity (*i.e.*, non-driven APs, Fig. 2B). However, in 2 cases, a train of triggered activities (*i.e.*, fast spontaneous APs) suddenly appeared. The duration of APs were prolonged during the occurrence of oscillatory potentials. Less negative take-off potentials resulted in EADs with decreased peak voltages.

We performed regression analysis on the relation between take-off potentials and peak voltage of the EADs for partisan fibers. Linear regression analysis was used and good inverse correlations (r = -0.962 - -0.997, p <0.01 for each regression, n = 3) were obtained. Figure 2C shows the partial course of HIS-induced EADs and triggered activity after 30 min perfusion with HIS. At first, (whole) duration of APs was lengthened (the first duration was 336 ms, the third 376 ms), and then immediately EADs rose (the first APs duration of EADs was 496 ms). More negative take-off potentials increased EADs peak voltage. Linear analysis revealed a highly significant correlation (r= -0.962, p <0.01) between the

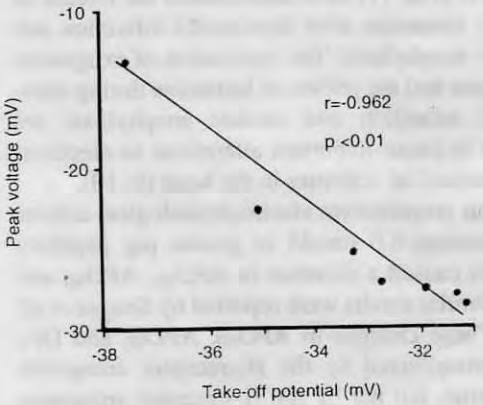

FIG. 3. Relation between EADs peak voltage and take-off potential. Results from effects of 6.0 µmol/l histamine on action potentials in guinea pig papillary muscles is shown.

EADs peak voltage and their take-off potentials (Fig. 3). After cessation of stimulation, EAD-induced fast spontaneous APs were recorded for about 15 min.

Effects of HIS on APs in the presence of antagonists

Pretreatment for 30 min with chlorpheniramine, a selective histamine H_1-receptor antagonist, or

cimetidine, an H_2-receptor antagonist, had no significant effect on APs. Pretreatment with 10 μmol/l chlorpheniramine had no action on shortening of APD_{50} and APD_{90} induced by HIS administration for 30 min (Fig. 4B. data taken from no abnormal automaticity and oscillatory potential cells, 6 out of 9 preparations). In the presence of chlorpheniramine, EADs (about 55%) and triggered activity induced by HIS were recorded when stimulated at 0.2, 0.5 and 1.0 Hz. These alterations of APs were recovered mainly within 30 min of washing with Tyrode solution. However, in contrast to chlorpheniramine, pretreatment with 10 μmol/l cimetidine completely antagonized the effects of HIS on various durations of APs, 30 min after the initiation of HIS (Fig. 4A) and induction of EADs (n = 6).

DISCUSSION

Wolff *et al.* (1) have documented the release of cardiac histamine after myocardial infarction and cardiac anaphylaxis. The application of exogenous histamine and the release of histamine during myocardial infarction and cardiac anaphylaxis are known to cause important alterations in electrical and mechanical activities in the heart (9, 10).

In our preparations, electrophysiological actions of histamine 6.0 μmol/l in guinea pig papillary muscles caused a decrease in APD_{50}, APD_{90} and DP_3. Similar results were reported by Senges *et al.* (11). These changes in APD_{50}, APD_{90} and DP_3 were antagonized by the H_2-receptor antagonist cimetidine, but not by the H_1-receptor antagonist chlorpheniramine. It may be postulated that histamine increases slow inward calcium current via stimulation of the H_2 receptor. As the histamine-induced enhancement of the slow inward current causes a relatively increased $[Ca^{2+}]_i$, the repolarizing outward potassium currents are activated sooner after the AP upstroke (1). As a result, the duration of APs is decreased.

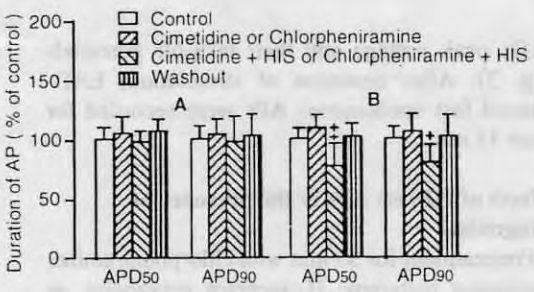

FIG. 4. Effects of histamine on duration of action potentials in the presence of cimetidine (A, n = 6) or chlorpheniramine (B, n = 6) in guinea pig papillary muscles. Stimulation rate: 1.0 Hz. $^{+}p < 0.05$; $^{++}p < 0.01$ *vs.* control.

As can be seen from our experiments, histamine induced EADs and triggered activity in guinea pig papillary muscles. EADs induced by histamine originated at phase 2 and/or phase 3. The H_2-receptor antagonist cimetidine completely antagonized the EADs induced by histamine via H_2-receptor operated calcium channels (1, 12). The H_1-receptor antagonist chlorpheniramine had no effect on the histamine-induced EADs in guinea pig papillary muscles. The specific ionic mechanisms of EAD generation are still vague. The reason for EAD generation is probably the decrease of repolarization and depolarization currents, that is, a delay or decrease in outward currents or an increase in inward currents. For the generation of EADs, a net inward current is required (5, 6, 13).

Because histamine-induced EADs occurred at phase 2 and/or phase 3 and were blocked by cimetidine, they may be associated with the histamine-induced increase of slow inward calcium current. Also, during perfusion of histamine we found that EADs were frequently induced by pacing at 0.2, 0.5 and 1.0 Hz, especially at 0.2 Hz. Thus, EADs are more likely to occur at low stimulation rates. On one hand, the slow driving rates presumably act by reducing the Na^+/K^+ pump (Ip). On the other hand, at low stimulation rates, sufficient diastolic time exists for extrusion of $[Ca^{2+}]_i$ to normal resting levels, which leads to the decreased calcium-activated potassium current and then results in slowness of repolarization and increase in the duration of APs (1, 6). Lengthening the duration of APs induced by histamine causes the amplitude of transient inward calcium currents, carried through L-type calcium channels, to increase greatly. The depolarizations of EADs depend on the charge carried by the transient inward current, a Ca^{2+} current carried through L-type Ca^{2+} channel (1, 14, 15).

According to our experiments, EADs and triggered activity induced by histamine may be the elec-

trophysiological basis of oscillatory contraction which was reported by Senges *et al.*, and may play an important role in the occurrence of torsade de pointes, where the heart rate remains slow in patients with myocardial infarction, *etc.*

The results suggest that the mechanisms of histamine-induced shortness of AP duration, EADs and triggered activity may be related to the H_2 receptor-mediated enhancement of the slow inward calcium current.

ACKNOWLEDGEMENTS

This project was supported by the Public Health Department of Jiangsu Province, No. H9313.

REFERENCES

1. Wolff, A.A., Levi, R. *Histamine and cardiac arrhythmias.* Circ Res 1986, 58: 1-16.
2. Felix, S.B., Baumann, G., Helmus, S., Sattelberger, U. *The role of histamine in cardiac anaphylaxis: Characterization of histaminergic H_1 and H_2 receptor effects.* Basic Res Cardiol 1988, 83: 531-39.
3. Levi, R.C., Alloatti, G. *Histamine modulates calcium current in guinea pig ventricular myocytes.* J Pharmacol Exp Ther 1988, 246: 377-83.
4. Levi, R., Capurro, N., Lee, C.H. *Pharmacological characterization of cardiac histamine receptors: Sensitivity to H_1- and H_2-receptor agonists and antagonists.* Eur J Pharmacol 1975, 30: 328-35.
5. Davidenko, J.M., Cohen, L., Goodrow, R., Antzelevitch, C. *Quinidine-induced action potential prolongation, early afterdepolarizations, and triggered activity in canine Purkinje fibres. Effects of stimulation rate, potassium and magnesium.* Circulation 1989, 79: 674-86.
6. El-Sherif, N. *Early afterdepolarizations and arrhythmogenesis. Experimental and clinical aspects.* Arch Mal Coeur Vaiss 1991, 84: 227-34.
7. Pan, H., Shen, W.Q., Yu, Z.M., Xu, B. *Frequency- and voltage-dependent effects of changrolin on maximal upstroke velocity of action potentials in guinea pig papillary muscles.* Acta Pharmacol Sin 1990, 11: 317-21.
8. Guo, S.R., Zhou, E.F. *Effects of methylflavonolamine hydrochloride on action potentials of isolated guinea pig papillary muscles.* Acta Pharmacol Sin 1990, 11: 232-5.
9. Cameron, J.S., Gaide, M.S., Goad, P.L. et al. *Enhanced adverse electrophysiologic effects of histamine after myocardial infarction in guinea pigs.* J Pharmacol Exp Ther 1985, 232 (2): 480-4.
10. Heller, L.J., Regal, J.F. *Relationship between alterations in atrial and ventricular histamine content and cardiac function during cardiac anaphylaxis of isolated guinea pig hearts.* Int Arch Allergy Appl Immunol 1990, 91: 285-90.
11. Senges, J., Katus, H., Kubler, W. *Action of anaphylaxis and histamine on isolated mammalian ventricles: Contractile hyperactivation and changes of membrane potentials.* J Pharmacol Exp Ther 1976, 198: 668-79.
12. Wu, X., Huang, W.Q., Yu, Z.M. *Ion channels and ion currents of action potentials in ventricular muscles.* Acta Acad Med Nantong 1993, 13 (1): 40-3.
13. Chen, X-J., Liu, T-F., Liu, K-O. *Effects of lemakalim and thalium on early afterdepolarization in mouse atrial fibres.* Meth Find Exp Clin Pharmacol 1992, 14: 489-92.
14. January, C.T., Riddle, J.M., Salata, J.J. *A model for early afterdepolarizations: Induction with the Ca^{2+} channel agonist Bay K 8644.* Circ Res 1988, 62: 563-71.
15. January, C.T., Riddle, J.M. *Early afterdepolarizations. Mechanism of induction and block: A role for L-type Ca^{2+} current.* Circ Res 1989, 64: 977-90.

Address for correspondence: Dr. Xin Wu, Department of Physiology, Nantong Medical College, Nantong, Jiangsu 226001, People's Republic of China.

Modulation of Calcium Current in Arteriolar Smooth Muscle by $\alpha_v\beta_3$ and $\alpha_5\beta_1$ Integrin Ligands

Xin Wu,* Jon E. Mogford,* Steven H. Platts,* George E. Davis,‡ Gerald A. Meininger,* and Michael J. Davis*

*Microcirculation Research Institute and Departments of Medical Physiology, ‡Pathology and Laboratory Medicine, Texas A & M University Health Science Center, College Station, Texas 77843-1114

Abstract. Vasoactive effects of soluble matrix proteins and integrin-binding peptides on arterioles are mediated by $\alpha_v\beta_3$ and $\alpha_5\beta_1$ integrins. To examine the underlying mechanisms, we measured L-type Ca^{2+} channel current in arteriolar smooth muscle cells in response to integrin ligands. Whole-cell, inward Ba^{2+} currents were inhibited after application of soluble cyclic RGD peptide, vitronectin (VN), fibronectin (FN), either of two anti–β_3 integrin antibodies, or monovalent β_3 antibody. With VN or β_3 antibody coated onto microbeads and presented as an insoluble ligand, current was also inhibited. In contrast, beads coated with FN or α_5 antibody produced significant enhancement of current after bead attachment. Soluble α_5 antibody had no effect on current but blocked the increase in current evoked by FN-coated beads and enhanced current when applied in combination with an appropriate IgG. The data suggest that $\alpha_v\beta_3$ and $\alpha_5\beta_1$ integrins are differentially linked through intracellular signaling pathways to the L-type Ca^{2+} channel and thereby alter control of Ca^{2+} influx in vascular smooth muscle. This would account for the vasoactive effects of integrin ligands on arterioles and provide a potential mechanism for wound recognition during tissue injury.

Key words: voltage-gated Ca^{2+} channel • vascular smooth muscle • wound repair • extracellular matrix • integrin-mediated signaling

Integrins are heterodimeric receptors (α, β) that mediate cell–extracellular matrix (ECM)[1] and cell–cell adhesion events. The cytoskeleton is mechanically linked to the ECM by integrins so that cytoskeletal stiffening increases in direct proportion to applied stress (Wang et al., 1993). Integrins can therefore serve as mechanochemical transducers (Ingber, 1991). Integrins can also function as signaling receptors that transduce biochemical signals both into and out of cells (Clark and Brugge, 1995; Sjaastad and Nelson, 1997). Intracellular signals known to be linked to integrins include pH, Ca^{2+}, protein kinase C activation, and protein tyrosine phosphorylation (Schwartz et al., 1991*a*; Schwartz, 1993).

Integrin signaling pathways are generally believed to be initiated by integrin clustering through interactions with insoluble ECM ligands (Clark and Brugge, 1995). These signals are initiated by cell interactions with ECM-coated substrates or with beads coated with ECM proteins or antiintegrin antibodies (Miyamoto et al., 1995*b*; Plopper et al., 1995). When soluble ECM protein or antibody is added, minimal or no signaling is thought to occur, but if soluble antibody is followed by a cross-linking antibody, signaling pathways are activated (Yamada and Geiger, 1997). A widely studied recognition site on ECM proteins, including vitronectin (VN) and fibronectin (FN) (Schwarzbauer, 1991), is the tripeptide Arg-Gly-Asp (RGD), which is recognized by a common subset of integrins, including $\alpha_v\beta_3$, $\alpha_5\beta_1$, $\alpha_v\beta_5$, and $\alpha_{IIb}\beta_3$. RGD peptides are known to disrupt integrin-dependent cell adhesive events (Akiyama, 1996) as well as produce inhibitory effects on major cellular processes such as platelet aggregation and angiogenesis (Weiss et al., 1997). For this reason, RGD peptides are potential therapeutic agents for thrombotic diseases and cancer. One important, unresolved issue is whether RGD peptides act solely by disrupting cell–ECM contacts or whether they provide direct signals to cells by binding to unoccupied integrins. Recent data from our laboratories suggest that soluble RGD peptides may provide vasoactive signals to cells in the vascular wall (Mogford et al., 1996, 1997; D'Angelo et al., 1997). Thus, RGD peptides

Address all correspondence to Michael J. Davis, Department of Medical Physiology, 336 Reynolds Medical Building, Texas A & M University Health Science Center, College Station, TX 77843-1114. Tel.: (409) 845-7816. Fax: (409) 847-8635. E-mail: mjd@tamu.edu

1. *Abbreviations used in this paper*: ECM, extracellular matrix; F11, β_3 integrin monoclonal antibody; FAK, focal adhesion kinase; FN, fibronectin; HMα5-1, α_5 integrin monoclonal antibody; I_{Ba}, whole-cell Ba^{2+} current; MHC, anti–rat IgG monoclonal antibody; PSS, physiological saline solution; SMC, smooth muscle cell(s); VN, vitronectin.

may be capable of directly stimulating integrin-dependent intracellular signaling pathways.

In rat cremaster muscle arterioles, integrin-binding RGD peptides and fragments of denatured collagen type I cause dilation through an interaction with the $\alpha_v\beta_3$ integrin on vascular smooth muscle (Mogford et al., 1996). Dilation is associated with a decrease in intracellular Ca^{2+} concentration ($[Ca^{2+}]_i$) (D'Angelo et al., 1997) and can be prevented by a function-blocking antibody specific for the β_3 integrin (Mogford et al., 1996). In addition to these prolonged effects, RGD peptides also cause a transient, endothelium-independent constriction of arterioles, mediated by the $\alpha_5\beta_1$ integrin (Mogford et al., 1997). In rat afferent arterioles, RGD peptide causes a sustained constriction that is associated with an increase in smooth muscle cell $[Ca^{2+}]_i$ (Yip and Marsh, 1997). The signaling mechanisms downstream from integrin-ligand binding are poorly understood, particularly in vascular smooth muscle cells (SMCs). We hypothesized that the L-type, voltage-gated calcium channel was involved in the vasoactive responses of arterioles since this channel is known to be a major pathway for calcium entry into vascular SMCs. To test this hypothesis, we isolated single SMCs from rat cremaster arterioles and selectively measured whole-cell calcium current before and after application of integrin ligands in both soluble and insoluble form.

Materials and Methods

Cell Isolation Techniques

Male Sprague-Dawley rats (120–200 g) were anesthetized with intraperitoneal injection of pentobarbital sodium (120 mg/kg). All animal handling procedures followed institutional guidelines. The two cremaster muscles were excised and pinned flat for vessel dissection in a 4°C silastic-coated Plexiglas chamber containing Ca^{2+}-free saline solution. The composition was (in mM) 147 NaCl, 8.6 KCl, 1.17 $MgSO_4$, 1.2 NaH_2PO_4, 5.0 D-glucose, 2.0 pyruvate, 0.02 EDTA, and 3 MOPS (pH adjusted to 7.4 with NaOH), with BSA (0.1 mg/ml; Amersham Life Science, Arlington Heights, IL) added to maintain cell integrity. Dissected segments of first- and second-order arterioles were transferred to a tube of low-Ca^{2+} saline solution containing (in mM) 144 NaCl, 5.6 KCl, 0.1 $CaCl_2$, 1.0 $MgCl_2$, 0.42 Na_2HPO_4, 0.44 NaH_2PO_4, 10 Hepes, 4.17 $NaHCO_3$, and 1 mg/ml BSA (pH adjusted to 7.4 with NaOH) at room temperature for 10 min. After allowing the vessels to settle to the bottom of the tube, the solution was decanted and replaced with low-Ca^{2+} saline containing 26 U/ml papain (Sigma Chemical Co., St. Louis, MO) and 1 mg/ml dithioerythritol (Sigma Chemical Co.). The vessels were incubated for 30 min at 37°C with occasional agitation, after which vessel fragments were transferred to low-Ca^{2+} saline solution containing 1.95 collagenase (FALGPA U/ml; Sigma Chemical Co.), 1 mg/ml soybean trypsin inhibitor (Sigma Chemical Co.), and 75 U/ml elastase (Calbiochem, La Jolla, CA) for 15 min at 37°C. After further digestion, the remaining fragments were rinsed two times with low-Ca^{2+} saline solution and gently triturated using a fire-polished Pasteur pipette to release single cells.

Patch Clamp Techniques

Perforated, whole-cell recordings were made as described previously (Rae and Fernandez, 1991). Micropipettes were pulled from 1.5-mm glass tubing (Corning No. 8161; Warner Instruments, Hamden, CT) on a programmable puller and fire polished. Pipette resistances ranged from 1 to 3 MΩ. The pipettes were dipped for 2–3 s in Cs^+ pipette solution (high Cs^+) containing (in mM) 110 CsCl, 20 TEA chloride, 10 EGTA, 2 $MgCl_2$, 10 Hepes, and 1 $CaCl_2$ (pH adjusted to 7.2 with CsOH) and then backfilled with the same solution containing 240 μg/ml amphotericin B. An EPC-7 amplifier (HEKA, Darmstadt-Eberstadt, Germany) was used to record current, and hydraulic manipulators (model M0-102; Narishige, Tokyo, Japan) were used for fine control of the micropipettes. Analog to digital conversions were made using a TL-1 DMA interface (Axon Instruments, Foster City, CA) and stored on a Pentium computer for subsequent analysis. Data were sampled at 5–10 kHz and filtered at 1–2 kHz using an eight-pole Bessel filter. Series resistance varied from 2 to 6 MΩ. Current records were analyzed using pClamp (version 6.0.3; Axon Instruments). Currents through the L-type calcium channel were elicited by voltage ramps (from −100 mV to +80 mV, duration = 200 ms) or by voltage steps (from −80 to +60 mV in 10 mV increments, duration = 300 ms). All experiments were performed at 22°C.

A suspension of freshly dispersed cells was plated onto a thin glass coverslip in a recording chamber on the stage of an inverted microscope. The coverslip was not usually treated, but in some experiments it was coated with FN (120 kD, 20 μg/ml) before addition of cells (Schwartz, 1993). Current recordings were made from individual cells between 30 min and 3 h after plating. Cells harvested using the digestion procedure were elongated with tapered ends in physiological saline solution (PSS), refractile under interference contrast optics, and contractile in solutions containing 140 mM K^+ or 20 mM Ba^{2+}. At the beginning of each experiment, the recording chamber was suffused with PSS from a gravity-fed reservoir at a rate of 1.5 ml/min. PSS had the following composition (in mM): 136 NaCl, 5.9 KCl, 10 Hepes, 1.16 NaH_2PO_4, 1.2 $MgCl_2$, 1.8 $CaCl_2$, 18 D-glucose, 0.02 EGTA, and 2 pyruvate (pH adjusted to 7.4 with NaOH). To record whole-cell current through the calcium channel, Ba^{2+} (20 mM) was used as the charge carrier in place of K^+ and Na^+ in the bath solution. This procedure is known to increase the size of the inward currents elicited by depolarization, and to minimize calcium-dependent inactivation of these currents (Griffith et al., 1994). The Ba^{2+} bath solution (20 Ba^{2+}) contained (in mM) 20 $BaCl_2$, 124 choline chloride, 10 Hepes, and 15 D-glucose (pH adjusted to 7.4 with TEA-OH).

Both ramp and step voltage protocols elicited inward, whole-cell Ba^{2+} currents (I_{Ba}) that peaked at +30 mV (range = 3.0–10.4 pA/pF); typically, these currents were stable for more than 30 min. Since current–voltage (I-V) relations for the ramp and step protocols were nearly identical, the average of five voltage ramps was used to measure I_{Ba} in most experiments. The activation portion of the I-V curve (from −60 to +30 mV) increased smoothly to a single maximum with no secondary "hump" in its voltage dependence, which is the pattern consistent with activation of only a single type Ca^{2+} channel (L-type) in this tissue (Nelson et al., 1990; Cox et al., 1992). As noted previously (Hill et al., 1996), the entire I-V relation was shifted about 30 mV to the right in 20 mM Ba^{2+} solution. This behavior is typical for voltage-gated calcium channels because of the fact that the equilibrium potential for the permeable ion shifts to the right with increasing extracellular ion concentration. When physiological Ca^{2+} is used as the charge carrier, the peak of the I-V curve occurs between −10 mV and 0 mV, and the activation threshold occurs at approximately −50 mV, as demonstrated in other SMC preparations (Aaronson et al., 1988).

Ligand Application

VN, FN (120 kD), lyophilized cyclic GPenGRGDSPCA (cRGD, with Pen indicating penicillamine), and the control GRGESP peptide (RGE) were obtained from GIBCO-BRL (Gaithersburg, MD). The anti–β_3 integrin function-blocking antibodies (F11; anti–rat monoclonal), 2C9.G2 (monoclonal), and the anti–α_5 integrin function-blocking antibody (HMα5-1; anti–rat monoclonal raised in Armenian hamster) were obtained from PharMingen (San Diego, CA). Anti–rat MHC class I monoclonal antibody (MHC; clone R4-8B1) was obtained from Seikagaku Inc. (Tokyo, Japan). Anti–Armenian hamster monoclonal IgG was obtained from Sigma Chemical Co. Monovalent antibodies were made by digesting F11 (in stock solution) with papain, followed by subsequent extraction of Fc fragments using a column of anti–mouse Fc coupled to Sephadex. The resulting Fab digest displayed a prominent band at 50 kD with no evidence of intact F11 at 150 kD.

For application to single cells, each agent was added to 20 Ba^{2+} solution and ejected from a picospritzer pipette (General Valve Corp., Fairfield, NJ) positioned ~50 μm away from a cell (Fig. 1 *A*).

Application of Protein-coated Beads

Streptavidin-coated microspheres (3.2 μm in diameter) were obtained from Bangs Laboratories (Fishers, IN). Before each experiment, the beads were coated with protein using a biotinylation procedure. Biotinylated FN, F11, VN, HMα5-1, and MHC were prepared using a method similar to that described previously (Hnatowich et al., 1987; Larson et al., 1992). The molar ratio of NHS-LC-Biotin (Pierce Chemical Co., Rockford, IL) to protein (10 μg/ml) was 20:1. To remove unreacted biotin, ul-

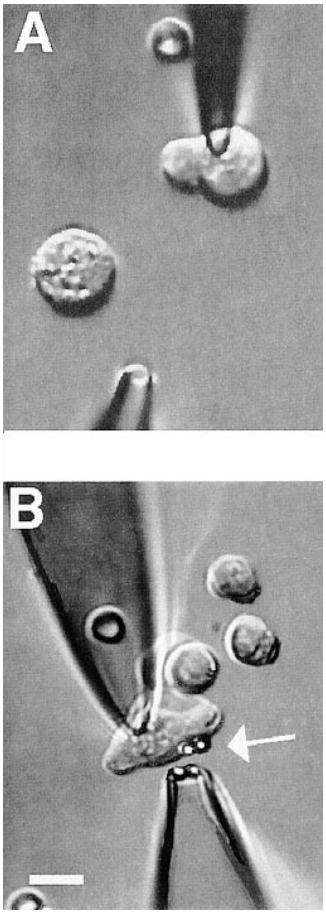

Figure 1. Methods for application of integrin ligands to smooth muscle cells. The images show voltage-clamped SMCs during application of (*A*) soluble integrin ligand from a picospritzer pipette or (*B*) protein-coated beads using gentle aspiration from a pipette. In both panels, the pipette at the top is a recording pipette used to hold the cell at −80 mV. Cells are contracted because of the solutions used. In *A*, the lower pipette is connected to a picospritzer for rapid application of solutions to the area surrounding the cell. In *B*, a red blood cell can be seen on the chamber bottom (underneath, not inside, the patch pipette). The pipette at the bottom is a large-tip pipette containing FN-coated beads. Two beads become attached to the cell (*white arrow*), and two remain in the pipette. Both panels: bath solution is 20 Ba^{2+}; patch pipette solution is high Cs^{+}; second pipette solution: 20 Ba^{2+}. Bar, 10 μm.

trafree-MC filters were used (Millipore Corp., Bedford, MA). Nonspecific sites on the beads were blocked by incubation with 0.1% heat-denatured BSA in PSS. A dilute suspension of beads in Ba^{2+} bath solution was then used to backfill micropipettes for application to single cells. These pipettes were positioned 5–10 μm away from the cells and fashioned so that their tip diameters were approximately twice the diameter of the beads; gentle pressure from a glass syringe (<2 cm H_2O) was used to eject the beads (Fig. 1 *B*).

Data Analysis

Whole-cell recordings were made from cells with capacitances varying from 4 to 16 pF. We used data only from cells in which stable gigaseals were maintained. In most analyses, the raw current value was normalized to cell capacitance (an index of cell size) and expressed as current density (pA/pF). Statistical comparisons were performed with repeated-measures analysis of variance followed by post hoc tests, or with an independent two-tail *t* test, as appropriate. Averaged values are expressed as mean ± SEM. Values of $P < 0.05$ were considered to be statistically significant.

Results

Effect of cRGD on I_{Ba}

The effect of soluble cRGD peptide (100 μM for 1 min) on inward Ba^{2+} current is shown in Fig. 2. This dose of peptide was reported to produce near-maximal dilation of isolated cremaster arterioles (Mogford et al., 1996). Currents from single arteriolar myocytes were elicited every 15 s by a depolarizing pulse to +30 mV (300-ms duration) from a holding potential of −80 mV. The time course of the response from a representative cell is shown on the left side

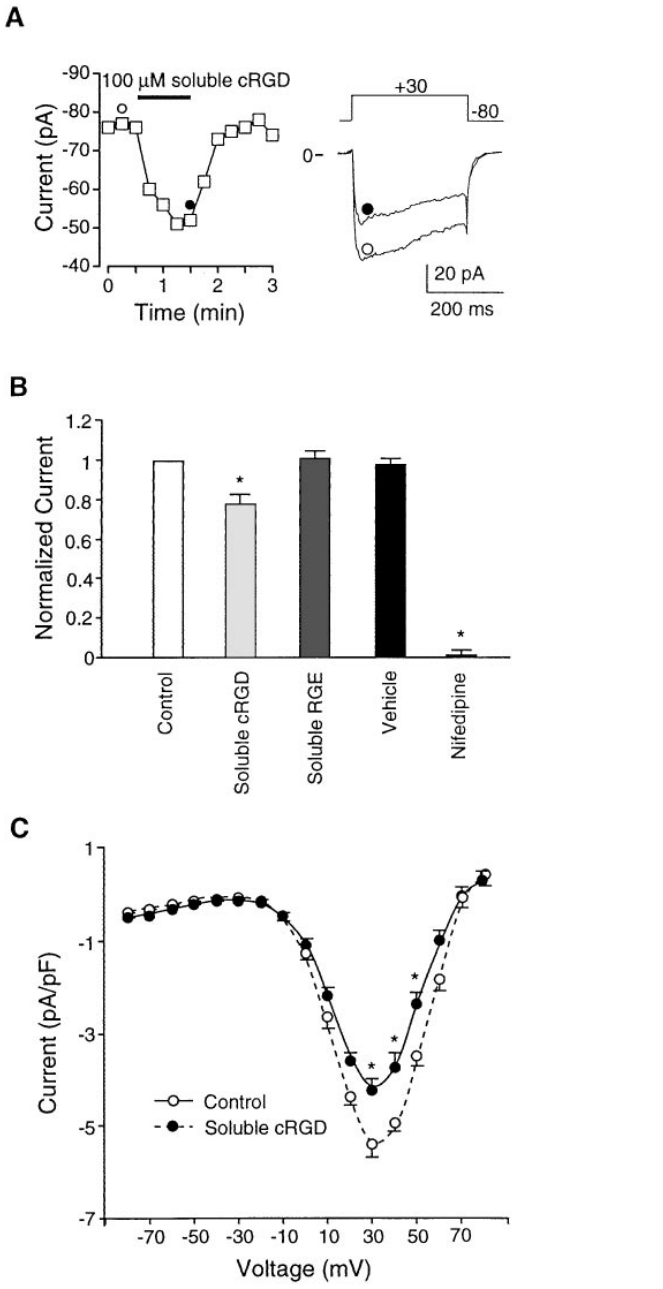

Figure 2. Effects of soluble cRGD on I_{Ba}. (*A*) Time course of changes in I_{Ba} (measurements made at 15-s intervals) for a single arteriolar SMC in response to application of soluble cRGD peptide (100 μM). Test potential was +30 mV in each case. Individual traces at right are leak-subtracted current traces at the time points indicated by the symbols. Cell capacitance was 12 pF. (*B*) Bar graph summarizing data for effects of soluble cRGD ($n = 9$), soluble RGE ($n = 4$), vehicle ($n = 4$), and nifedipine (1 μM, $n = 7$). For each cell, the data represent peak currents 1 min after application, as normalized to the current at the peak of the control I-V relationship (usually +20 or +30 mV). (*C*) Summary I-V curves for Ba^{2+} current before or 60 s after application of soluble cRGD (100 μM). Data from nine cells. All panels: bath solution is 20 Ba^{2+}; pipette solution is high Cs^{+}; HP = −80 mV. *$P < 0.05$ vs. control.

of Fig. 2 *A*, and individual current traces at the indicated time points are shown on the right side. Before peptide application, peak current ranged from −76 pA to −77 pA. Within 15 s after application of soluble cRGD peptide (100 μM) from a picospritzer pipette, current was inhibited (to −60 pA) and maximal inhibition (to −51 pA) was achieved 45 s after cRGD application. Nearly complete recovery from inhibition (to −75 pA) was observed within 30 s after peptide washout.

The average response of nine cells to soluble RGD peptide is summarized in Fig. 2 *B*, where the data for each cell have been normalized to the peak Ba^{2+} current recorded just before peptide application. On average, 100 μM cRGD produced 22% inhibition of I_{Ba} at +30 mV (measurements taken immediately before peptide washout). Also illustrated in the bar graph are the effects of vehicle, RGE peptide (which does not interact with integrin receptors), and nifedipine, a dihydropyridine calcium channel blocker. Neither vehicle nor RGE peptide (80 μM; $n = 4$) had a significant effect on I_{Ba}. Nifedipine (1 mM; $n = 7$) produced nearly 100% inhibition of current at this dose, which is consistent with the behavior of an L-type Ca^{2+} channel. A comparison of current–voltage relationships recorded before and during cRGD application (Fig. 2 *C*) indicates that inhibition of I_{Ba} occurred across the entire range of voltages associated with activation of the L-type Ca^{2+} channel. Thus, there appeared to be no significant effect of RGD peptide on the threshold or reversal potential of the current.

Effect of Vitronectin on I_{Ba}

VN is known to interact with several integrins, including $\alpha_v\beta_3$ (the VN receptor). Fig. 3 *A* illustrates the effect of soluble VN on I_{Ba}. Before application, peak current in this representative cell was stable between −86 and −87 pA. Within 15 s after ejection of soluble VN (0.04 μM) from the picospritzer pipette, I_{Ba} decreased to −69 pA, with a further inhibition to −49 pA at 60 s after application. Recovery of current was complete within 60 s after VN washout. The bar graph in Fig. 3 *A* summarizes results from seven cells. On average, this concentration of soluble VN inhibited current by 39 ± 5%. Although not illustrated in this figure, inhibition of I_{Ba} by VN was sustained during longer periods of application (48 ± 7% inhibition at 4 min).

Fig. 3 *B* shows the effect of VN-coated beads on I_{Ba}. The top trace shows the time course of changes in current before (time = 0 min) and after attachment of four beads to a representative cell. Note that both peak and steady-state currents were inhibited within 1 min of bead attachment, remained inhibited for ~5 min, and then gradually returned toward control levels even though the beads appeared to remain attached. Data from six cells are summarized in the lower portion of Fig. 3 *B*. On average, a 20% inhibition of I_{Ba} was observed in response to bead attachment. As a control for nonspecific mechanical effects associated with bead application, the response to uncoated beads was also tested (*open circles*); no significant changes in I_{Ba} were noted with uncoated beads ($n = 5$) or with BSA-coated beads ($n = 4$).

Inhibition of I_{Ba} after attachment of VN-coated beads

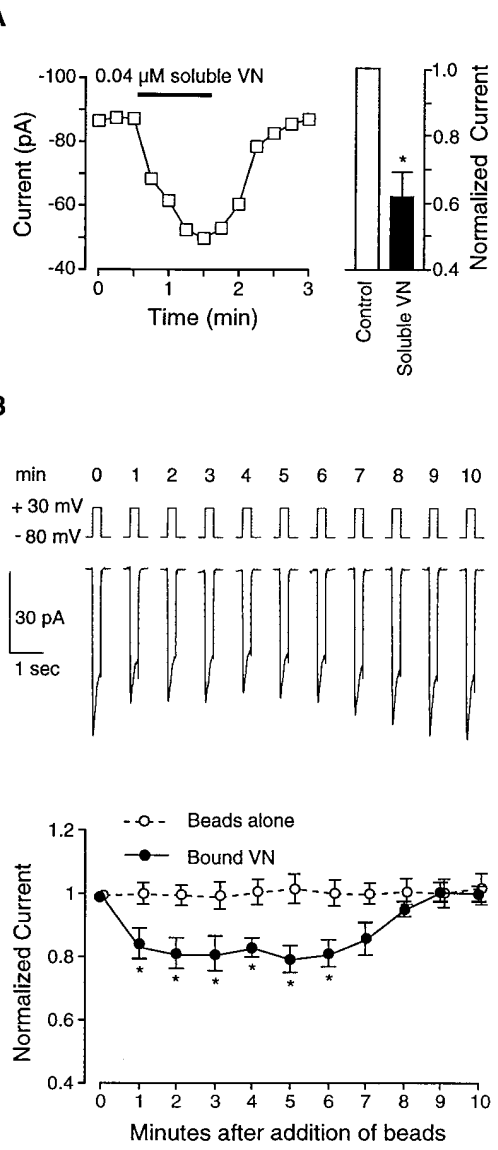

Figure 3. Effects of VN on I_{Ba}. (*A*) Graph at left shows time course of changes in I_{Ba} for a single cell before and during application of soluble VN (0.04 μM). Test potential was +30 mV in each case, and measurements were made at 15-s intervals. Cell capacitance was 15 pF. Bar graph at right shows summary data ($n = 7$) for I_{Ba} 60 s after application of soluble VN compared with control current (just before VN application). Currents were normalized to the current at the peak of the control I-V relationship. (*B*) Top traces show time course of changes in I_{Ba} (note compressed time scale for each trace compared with traces in Fig. 2 *A*) for a single cell before and after application of four VN-coated beads (at $t = 0$ min). Lower graph shows summary time course of I_{Ba} changes in response to VN-coated beads (*filled circles*; 2–5 beads/cell; $n = 6$) or uncoated beads (*open circles*; $n = 5$). All values were normalized to the peak value of I_{Ba} at $t = 0$ min. Both panels: bath solution is 20 Ba^{2+}; pipette solution is high Cs^+; HP = −80 mV. *$P < 0.05$ vs. control.

was proportional to the number of beads that attached to a given cell, a process over which we had only partial control. Regression analysis of the percent inhibition of I_{Ba} as a function of the number of attached beads gave a correlation coefficient of 0.86 ($\Delta I_{Ba} = -0.8$ pA − 5.2 × No. of

beads). For the purpose of determining the average responses of cells to coated beads in this and subsequent protocols, data were therefore pooled from cells to which between two and five beads attached.

Effect of β_3 Antibody on I_{Ba}

To test the hypothesis that the effects of cRGD and VN were mediated through the $\alpha_v\beta_3$ receptor, a function-blocking, monoclonal antibody to the rat β_3 integrin (F11) was applied to the cells. F11 is known to block the dilatory effects of cRGD peptide on isolated arterioles (Mogford et al., 1996). β_3 integrins are known to associate with two different α subunits (Hemler, 1990), but only one of those, α_v, has been identified in vascular smooth muscle (Yip and Marsh, 1997). Fig. 4 *A* shows the time course of changes in I_{Ba} after application of soluble F11 (0.03 μM) to a representative cell. In this cell, soluble F11 inhibited current from −70 pA to −45 pA by 1 min after application. Data from nine cells are summarized in the bar graph of Fig. 4 *A* and show that this dose of soluble F11 inhibited I_{Ba} by an average of 33 ± 5%. We also tested the effect of a second β_3 integrin antibody, 2C9.G2, which is reported to block adhesion (Schultz and Armant, 1995). After 60 s of application, soluble 2C9.G2 (0.03 μM) inhibited I_{Ba} by 22 ± 4.5% (n = 8). In addition, we made Fab fragments of F11 to test the effect of a monovalent integrin ligand on Ca^{2+} current. After dilution to 0.03 μM in PSS, Fab fragments caused a 29 ± 5% inhibition of I_{Ba} 1 min after application (n = 7). As a control for nonspecific effects of antibody, a nonintegrin binding antibody (anti–rat MHC, 0.2 μM) was also tested; MHC had no significant effect on current (n = 4), as shown in the right portion of Fig. 4 *A*.

When F11-coated beads were applied to cells, I_{Ba} was inhibited (Fig. 4 *B*, *closed circles*). I_{Ba} was reduced to 61% of control at 1.5 min after F11 bead attachment. The inhibition lasted ~5 min, after which current gradually and spontaneously returned toward control values, even though the beads remained attached. As a control for nonspecific effects of antibody-coated beads, we tested the responses of cells to MHC-coated beads, which had no significant effect on I_{Ba} (Fig. 4 *B*, *open circles*).

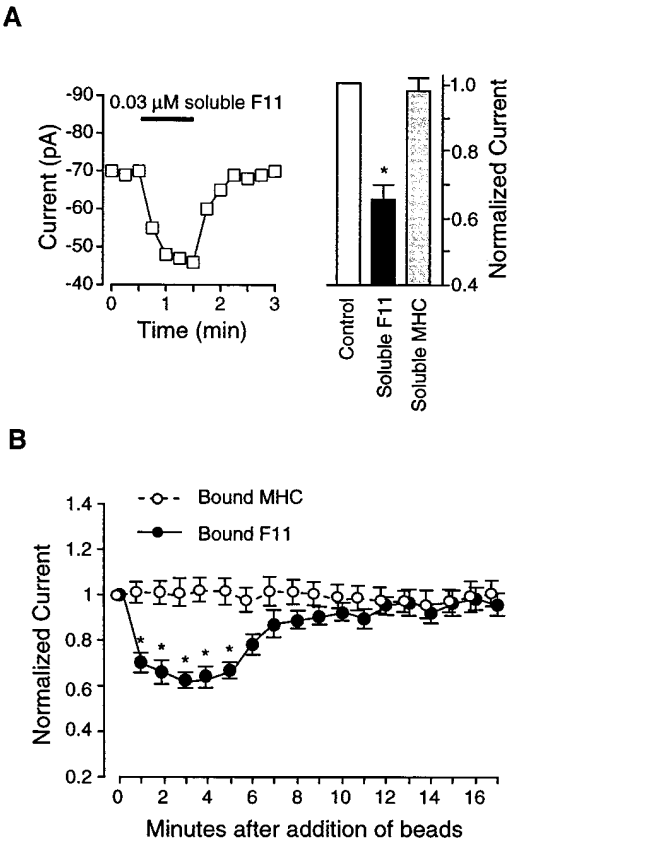

Figure 4. Effects of the β_3 antibody, F11, on I_{Ba}. (*A*) Graph at left shows time course of changes in I_{Ba} for a single cell before and during application of soluble F11 (0.03 μM). Test potential was +30 mV in each case, and measurements were made at 15-s intervals. Cell capacitance was 15 pF. Bar graph at right shows summary data for I_{Ba} 60 s after application of soluble F11 (n = 9) or soluble MHC (0.2 μM; n = 4), compared with control current. Currents were normalized to the current at the peak of the control I-V relationship. (*B*) Summary time course of I_{Ba} changes in response to F11-coated beads (*filled circles*; n = 6) or MHC-coated beads (*open circles*; n = 9). All values were normalized to the peak value of I_{Ba} at t = 0 min. Both panels: bath solution is 20 Ba^{2+}; pipette solution is high Cs^+; HP = −80 mV. *$P < 0.05$ vs. control.

Effect of Fibronectin on I_{Ba}

Next, we examined the effect of FN on current. FN is known to interact with both $\alpha_v\beta_3$ and $\alpha_5\beta_1$ receptors present in this cell type, as well as with a number of other integrins (Hynes, 1992). Fig. 5 *A* shows the time course of changes in I_{Ba} in response to soluble FN (0.1 μM). In this cell, soluble FN inhibited I_{Ba} from −80 pA to −56 pA within 60 s after application. The response of seven cells to soluble FN is summarized by the bar graph in Fig. 5 *A*. On average, this concentration of soluble FN reduced I_{Ba} to 75% of control at 1 min. The inhibition was maintained for at least 10 min, when current was still reduced to 80 ± 5% (n = 5; data not shown).

To test the effect of insoluble FN on I_{Ba}, FN-coated beads were applied to single cells. The top trace in Fig. 5 *B* shows the response of a representative cell to attachment of three FN-coated beads. Interestingly, FN-coated beads had the opposite effect on current compared with VN-coated beads or F11-coated beads. Attachment of FN-coated beads led to an enhancement of I_{Ba} as early as 1 min after bead attachment. This enhancement peaked at 2 min (~135% of control), remained stable for 10 min, and then declined gradually by 16 min, even though the beads remained attached. For reference, the time course of changes in I_{Ba} in response to BSA-coated beads (which had no significant effect on current) is shown.

Effect of α_5 Antibody on I_{Ba}

The fact that insoluble VN and insoluble FN had opposite effects on current suggests that an integrin other than $\alpha_v\beta_3$ might mediate the enhancement of I_{Ba} in response to FN-coated beads. Experiments by Mogford et al. (1997) also suggest a role for the $\alpha_5\beta_1$ receptor in vasoactive responses of arterioles because RGD peptide-mediated dilation was converted to constriction after blockade of β_3 integrins:

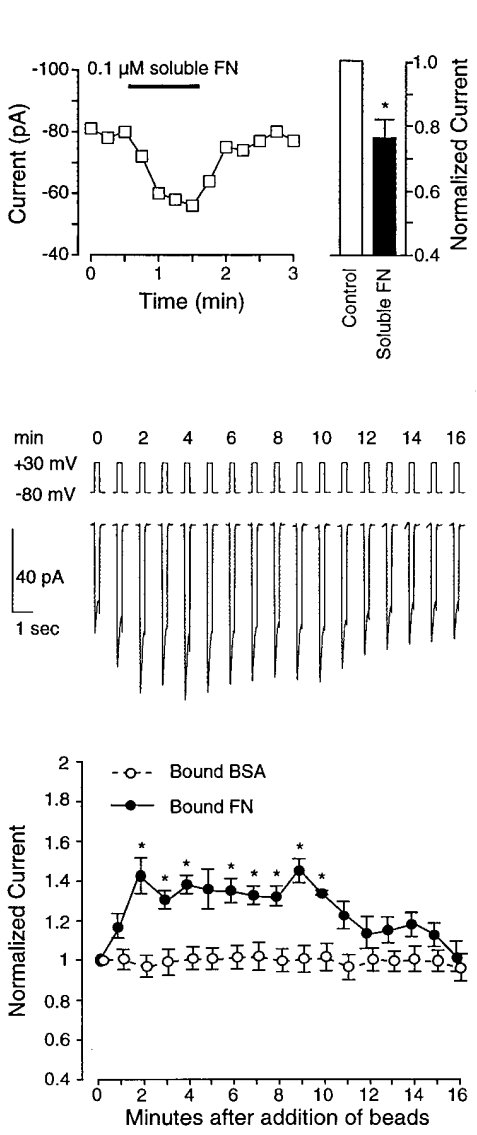

Figure 5. Effects of FN on I_{Ba}. (*A*) Graph at left shows time course of changes in I_{Ba} for a single cell before and during application of soluble FN (0.1 μM). Test potential was +30 mV in each case, and measurements were made at 15-s intervals. Cell capacitance was 12 pF. Bar graph at right shows summary data ($n = 7$ cells) for I_{Ba} 60 s after application of soluble FN, compared with control current (just before FN application). Currents were normalized to the current at the peak of the control I-V relationship. (*B*) Top traces show time course of changes in I_{Ba} for a single cell before and after application of three FN-coated beads (at $t = 0$ min). Lower graph shows summary time course of I_{Ba} changes in response to FN-coated beads (*filled circles; n* = 9) or BSA-coated beads (*open circles*; $n = 4$). All values were normalized to the peak value of I_{Ba} at $t = 0$ min. Both panels: bath solution is 20 Ba^{2+}; pipette solution is high Cs^+; HP = −80 mV. *$P <$ 0.05 vs. control.

the steady-state portion of that constriction was mediated by endothelin and blocked by α_5 antibody, but the initial transient constriction was an endothelium-independent response.

To test for the involvement of the $\alpha_5\beta_1$ integrin in our preparation, we used the anti–rat α_5 antibody, HMα5-1. The α_5 subunit is known to associate only with β_1, making this antibody specific for the $\alpha_5\beta_1$ heterodimer (Hynes, 1992). Fig. 6 *A* shows the effect of applying soluble HMα5-1 to a representative cell: no significant change in I_{Ba} was observed. The bar graph in Fig. 6 *A* summarizes the response of nine cells to application of soluble HMα5-1, which on average produced less than a 2% change in I_{Ba}.

However, when beads coated with HMα5-1 were applied to cells, a large and significant increase in I_{Ba} was consistently observed, as summarized in Fig. 6 *B* (*left*). Within the first minute after attachment of α_5-coated beads, I_{Ba} had increased to 158% of control. I_{Ba} peaked at 170% of control ~3 min after bead application and then progressively declined toward control; however, I_{Ba} did not completely recover even by 17 min after α_5-coated bead attachment. Individual current recordings before and after HMα5-1 application are shown in Fig. 6 *B* (*right*). The two sets of tracings represent currents evoked from a holding potential of −80 mV (*top*) or −40 mV (*bottom*) before and after attachment of HMα5-1–coated beads. As is evident from these recordings, the current stimulated by HMα5-1 was completely inhibited by nifedipine (1 μM), which is consistent with the conclusion that it flowed through L-type calcium channels. Although there is no selective blocker of T-type calcium channels, the possibility that some current might be contributed by T-type channels is ruled out by the fact that the time course of the current recordings evoked from the two different holding potentials are virtually identical.

Fig. 6 *C* compares the current–voltage relationships for control current and current stimulated by bound HMα5-1. There appeared to be no significant effect on either the threshold or reversal potential of the current.

Effect of Antibody Pretreatment on I_{Ba} Response to Coated Beads

To test the idea that clustering of receptors was required to initiate signaling through the $\alpha_5\beta_1$ integrin, soluble α_5 antibody was first applied to cells, and then anti–hamster IgG was subsequently added. As shown in Fig. 7 *A*, there was no response to either agent alone, but when both agents were applied in combination, a significant enhancement in current was noted. The time course of this enhancement was approximately the same as that seen in response to insoluble α_5 antibody (compare to Fig. 6 *B*).

If the response of arteriolar smooth muscle cells to FN-coated beads involves interaction of insoluble FN with both $\alpha_v\beta_3$ and $\alpha_5\beta_1$ integrins, we predicted that pretreatment with antibody specific to one integrin would result in changes in current characteristic of selective activation of the other integrin. To test this hypothesis, cells were treated with either F11 to block β_3 or HMα5-1 to block α_5 before application of FN-coated beads. Fig. 7, *B–D*, shows the results of these experiments.

In Fig. 7 *B*, application of soluble F11 caused a 30% inhibition of I_{Ba}, an effect which is comparable to that observed previously (compare to Fig. 4 *A*). From this new baseline, application of FN-coated beads increased current from 70% of control to 116% of control. Although interpretation of this response is complicated by the shift in

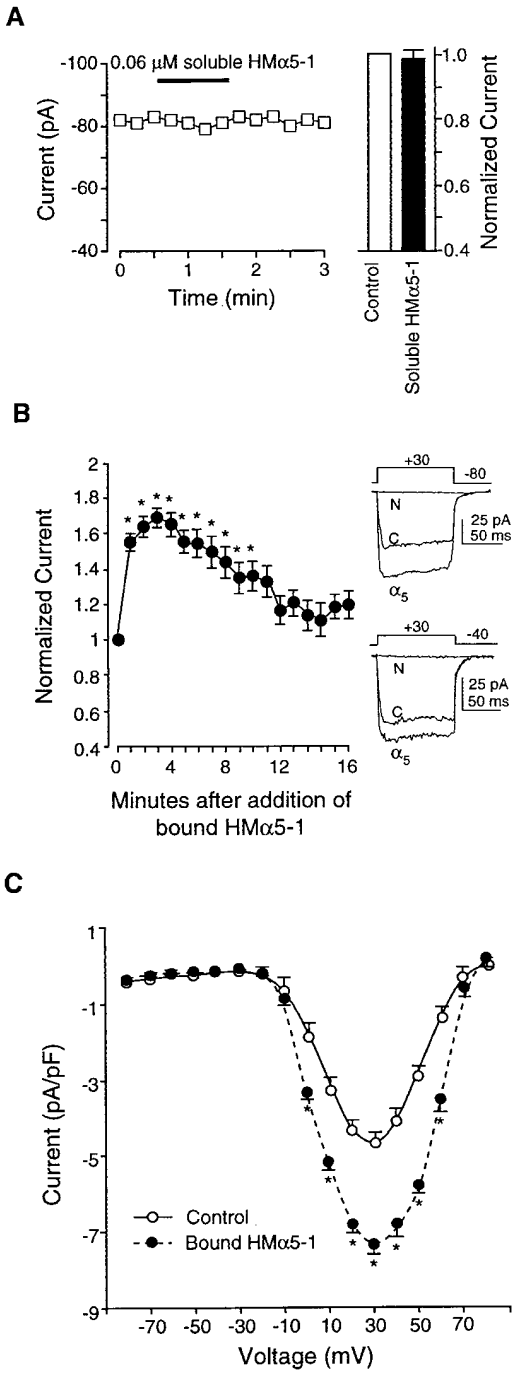

Figure 6. Effects of the α_5 antibody, HMα5-1, on I_{Ba}. (*A*) Left trace shows time course of changes in I_{Ba} for a single cell before and during application of soluble HMα5-1 (0.06 μM). Test potential was +30 mV in each case, and measurements were made at 15-s intervals. Cell capacitance was 8 pF. Bar graph at right shows summary data for I_{Ba} 60 s after application of soluble HMα5-1 (n = 9), compared with control current. Currents were normalized to the current at the peak of the control I-V relationship. (*B*) Left graph shows time course of average I_{Ba} changes in response to HMα5-1–coated beads (n = 5). HMα5-1–coated beads caused a biphasic change in I_{Ba} with a large, significant increase lasting about 4 min, followed by a slow return toward control while the beads remained attached. All values were normalized to the peak value of I_{Ba} at t = 0 min. Right traces show current traces evoked by a depolarizing pulse to +30 mV from a holding potential of −80 mV (*top*) or −40 mV (*bottom*). *C*, control; *α5*, HMα5-1-coated beads attached; *N*, HMα5-1–coated beads attached in the presence of nifedipine (1 μM). (*C*) I-V curve for currents before (*control*) or 4 min after attachment of HMα5-1–coated beads. All panels: bath solution is 20 Ba^{2+}; pipette solution is high Cs^+; $*P <$ 0.05 vs. control.

baseline, the absolute change in I_{Ba} appeared to be larger than that observed in response to FN-coated beads alone (average increase = 35%; Fig. 5 *B*) and nearly as large as that produced by insoluble HMα5-1 (Fig. 6 *B*).

In Fig. 7 *C*, application of soluble HMα5-1 again produced no change in I_{Ba}, but subsequent application of FN-coated beads caused a significant inhibition of current, which is the opposite response observed to FN-coated beads alone (Fig. 5). This observation is consistent with the hypothesis that insoluble FN activates both β_3 and α_5 integrins in these cells. Importantly, it also indicates that soluble HMα5-1 was indeed interacting with the $\alpha_5\beta_1$ receptor even though no change in I_{Ba} was noted in response to soluble HMα5-1 alone. Interestingly, simultaneous application of F11 and HMα5-1 resulted in a 34 ± 8% decrease in current (n = 5), and little change in current was noted after subsequent application of FN-coated beads (Fig. 7 *D*).

Discussion

To investigate the mechanisms underlying the vasoactive effects of ECM proteins and integrin-specific peptides on rat skeletal muscle arterioles (Mogford et al., 1996, 1997), we measured the response of L-type Ca^{2+} channel current in arteriolar myocytes to integrin ligands. Soluble $\alpha_v\beta_3$ ligands (cRGD, VN, FN, bivalent or monovalent β_3 antibodies) caused significant inhibition of calcium current, as did beads coated with VN or β_3 antibody. In contrast, beads coated with $\alpha_5\beta_1$ ligands (FN or α_5 antibody) caused significant enhancement of current. Soluble α_5 antibody alone had no effect on current but blocked the increase in current evoked by FN-coated beads and enhanced current when applied in combination with an appropriate IgG. This is the first electrophysiological evidence for regulation of a Ca^{2+} channel by integrin–ligand interactions and demonstrates that $\alpha_v\beta_3$ and $\alpha_5\beta_1$ integrins in smooth muscle are differentially linked through intracellular signaling pathways to the L-type calcium channel.

The implications of our findings are threefold: (*a*) part of the resting current through L-type Ca^{2+} channels in vascular smooth muscle, and therefore blood vessel tone, is dependent on integrin-matrix interactions; (*b*) bidirectional regulation of Ca^{2+} influx in this cell type can be achieved through preferential ligation of $\alpha_v\beta_3$ or $\alpha_5\beta_1$ integrins; (*c*) soluble integrin ligands can initiate signaling through the $\alpha_v\beta_3$ receptor. Since ECM protein denaturation and fragmentation can provide soluble integrin-specific signals to cells (Davis, 1992), this mechanism is likely to be important in the microvascular response to injury (Mogford et al., 1996). Inhibition of smooth muscle cell Ca^{2+} current could account for integrin-mediated vasodilation of arterioles (Mogford et al., 1996).

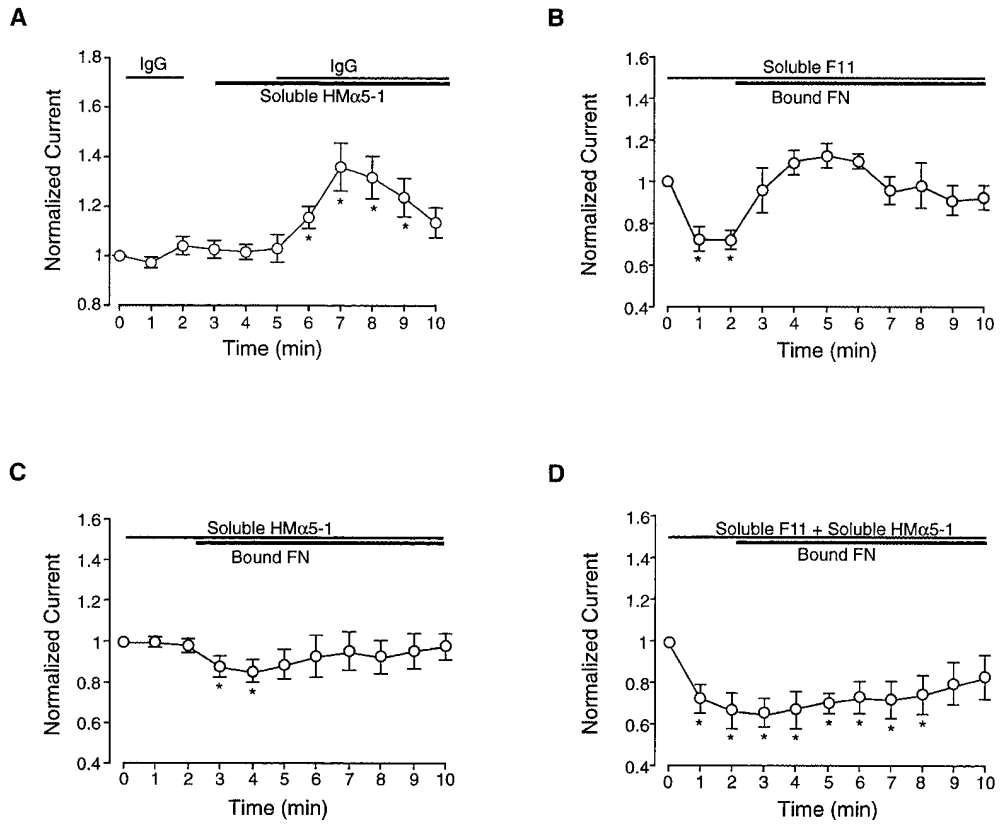

Figure 7. Effects of antibody pretreatment on response to coated beads. (*A*) Enhancement in current ($n = 5$) is observed during application of soluble HMα5-1 in combination with anti–Armenian hamster IgG. Neither IgG or soluble HMα5-1 alone altered current, but when both were added in combination, current was enhanced over approximately the same time course as with bound HMα5-1. (*B*) Time course of change in I_{Ba} when FN-coated beads were applied to cells in the presence of soluble F11 (0.03 μM; $n = 7$). Currents are normalized to the value of I_{Ba} at $t = 0$ min. Soluble F11 failed to inhibit the enhancement in I_{Ba} after bead attachment, although it inhibited current alone, as in Fig. 4 *A*. In fact, the magnitude of the change in current after FN bead attachment was greater than in the absence of F11 (Fig. 5 *B*) and similar to that observed in response to HMα5-1–coated beads (Fig. 6 *B*). (*C*) Time course of change in I_{Ba} when FN-coated beads were applied to cells after application of soluble HMα5-1 (0.06 μM; $n = 12$). Soluble HMα5-1 alone had no effect on current but blocked the rise in current after FN bead attachment; in fact, a slight but significant decrease in current was observed. (*D*) Time course of change in I_{Ba} when FN-coated beads were applied to cells after pretreatment with soluble HMα5-1 (0.06 μM) and soluble F11 (0.03 μM) in combination. An initial decrease in current was observed (presumably due to the effect of F11), and very little change in current was seen after application of insoluble FN. All panels: bath solution is 20 Ba^{2+}; pipette solution is high Cs^+; HP = −80 mV. *$P < 0.05$ vs. control.

Integrin Signaling in Response to Tissue Injury

Local vasodilation is one of the initial responses to tissue injury, resulting in an increase in blood flow to the affected area. This response is mediated primarily by arterioles, which are the strategic control point for local regulation of pressure and flow in every tissue. Increased flow contributes to injury repair by enhancing delivery of inflammatory cells to the injured site. Classic mediators of injury-induced arteriolar dilation include reactive oxygen species (Wei et al., 1981), tachykinins, and histamine (Treede et al., 1990). Recently, Mogford et al. (1996) described an additional mechanism by which RGD-containing peptides induce vasodilation by interacting with the $\alpha_v\beta_3$ integrin on smooth muscle cells of rat skeletal muscle arterioles. Involvement of the $\alpha_v\beta_3$ integrin was implicated by the findings that (*a*) cRGD and GRGDSP peptide were more potent vasodilators than GRGDNP peptide (enhancement of RGD potency by cyclization implicates the involvement of α_v integrins [Pierschbacher and Ruoslahti, 1987]) and (*b*) dilations were attenuated in the presence of a function-blocking β_3 monoclonal antibody (Mogford et al., 1996). In addition to synthetic peptides, fragments of denatured collagen type I were potent vasodilators of arterioles (Mogford et al., 1996). While RGD sequences are not exposed in native collagen, cryptic RGD sites become exposed after collagen denaturation and proteolysis, allowing for their interaction with RGD-binding integrins. Exposure of cryptic RGD sites has been proposed to be a potential wound recognition signal during tissue injury (Davis, 1992). Thus, a certain proportion of the $\alpha_v\beta_3$ receptors may normally be unoccupied on vascular smooth muscle, and after tissue injury, generation of RGD peptide signals that bind the receptor result in decreased Ca^{2+} current, arteriolar dilation, and increased blood flow to the injured tissue.

Arteriolar dilations to RGD-containing peptides and proteins are mediated by direct effects on vascular smooth muscle integrins rather than on endothelial cell integrins (Mogford et al., 1996). However, none of the downstream signaling mechanisms in smooth muscle have been identified, except that dilation to soluble cyclo-RGD peptide is preceded by a significant decrease in smooth muscle $[Ca^{2+}]_i$ (D'Angelo et al., 1997). Our finding that cRGD caused an inhibition of current through the L-type Ca^{2+} channel in the same cell type (Fig. 2) is consistent with data from intact vessels. In isolated arterioles (Mogford et al., 1996; D'Angelo et al., 1997), dilation was the result of inhibition of myogenic tone, which in resistance vessels

(Nelson et al., 1990; Hill and Meininger, 1994) is dependent on basal influx of Ca^{2+} through L-type Ca^{2+} channels and can be antagonized by dihydropyridines (Hill and Meininger, 1994). We confirmed that the dihydropyridine nifedipine completely blocked current in our cells (Figs. 2 *B* and 6 *B*). Mogford et al. (1996) found that cRGD peptide also inhibited phenylephrine- and KCl-induced vascular tone, but the primary actions of both agents are known to be mediated by Ca^{2+} influx through voltage-gated Ca^{2+} channels as well (Nelson et al., 1988).

Integrin-mediated $[Ca^{2+}]_i$ Signaling

Integrin-mediated $[Ca^{2+}]_i$ signaling has been demonstrated in a number of cell types, including endothelium (Schwartz and Denninghoff, 1994) and vascular smooth muscle (McNamee et al., 1993). Integrins including $\alpha_{IIb}\beta_3$, $\alpha_v\beta_6$, $\alpha_v\beta_5$, $\alpha_5\beta_1$, and $\alpha_v\beta_3$ (Hynes, 1992) are known to be involved in $[Ca^{2+}]_i$ signaling responses; these integrins also recognize the RGD sequence common to many ECM (FN, osteopontin, and collagens) and plasma proteins (FN, VN, and fibrinogen). Thus, our finding that Ca^{2+} channel current (and by direct extension Ca^{2+} influx [Ganitkevich and Isenberg, 1991]) is modulated after $\alpha_v\beta_3$ and $\alpha_5\beta_1$ receptor ligation is consistent with previous reports in the literature.

Changes in $[Ca^{2+}]_i$ initiated by integrin ligation involve a number of mechanisms that result in Ca^{2+} release from intracellular stores and/or Ca^{2+} influx (McNamee et al., 1993; Somogyi et al., 1994; Sjaastad et al., 1996). In endothelial cells, α_v integrins mediate a rise in $[Ca^{2+}]_i$ after adhesion to FN (Schwartz and Denninghoff, 1994). The mechanism underlying this response was not determined, but $[Ca^{2+}]_i$ increases did not occur in the absence of extracellular Ca^{2+}. Likewise, both Ca^{2+} release and Ca^{2+} influx contributed to the $[Ca^{2+}]_i$ rise after adhesion of MDCK cells to RGD-coated beads (Sjaastad et al., 1996), but the influx component was more important for feedback regulation of integrin-mediated adhesion. No mechanism for integrin-mediated Ca^{2+} influx in nonexcitable cells has been identified, although a role for a 50-kD integrin-associated protein, not yet characterized electrophysiologically, has been postulated (Brown, 1993; Schwartz et al., 1993).

Our data represent the first electrophysiological evidence that integrin ligation can modulate a plasma membrane Ca^{2+} channel. To make these measurements, Ba^{2+} was used instead of Ca^{2+} to carry current through the L-type Ca^{2+} channel because (*a*) Ba^{2+} is more permeable than Ca^{2+} through this channel, resulting in larger current; (*b*) Ba^{2+} blocks the large, outward K^+ current that normally masks Ca^{2+} current in these cells; and (*c*) Ba^{2+} currents do not exhibit the rapid inactivation observed when Ca^{2+} is used (Griffith et al., 1994). Nifedipine, a dihydropyridine that is a selective antagonist of L-type calcium channels (as opposed to other types of voltage-gated calcium channels [Birnbaumer et al., 1994]) at concentrations less than 10^{-5} M, produced essentially a complete block of basal Ca^{2+} current (Fig. 2 *B*) as well as inhibited the enhanced current in response to insoluble α_5-antibody (Fig. 6 *B*).

Although we have not directly measured $[Ca^{2+}]_i$ in our preparation, it is highly likely that any treatment causing a significant change in I_{Ba} would lead to a similar directional change in $[Ca^{2+}]_i$; this relationship has been clearly demonstrated for visceral (Ganitkevich and Isenberg, 1991) and vascular (Fleischmann et al., 1994) smooth muscle. The previously reported decrease in arteriolar smooth muscle $[Ca^{2+}]_i$ in response to soluble RGD peptide (D'Angelo et al., 1997) is consistent with inhibition of I_{Ba} by soluble RGD peptide (Fig. 2). In another vascular bed, RGD peptide caused a constriction that was associated with an increase in SMC $[Ca^{2+}]_i$ (Yip and Marsh, 1997).

The direct effect of cRGD, VN, FN, and F11 on Ca^{2+} channel current in isolated SMCs provides strong support for the concept that interaction of $\alpha_v\beta_3$ with soluble ligands transduces an intracellular signal in this cell type. It remains to be determined if $\alpha_v\beta_3$ expressed in other cell types, such as endothelium, delivers a similar or different signal. However, endothelial cells (with one exception [Bossu et al., 1989]) lack voltage-gated calcium channels and, in some ways, use opposite mechanisms of controlling calcium entry than smooth muscle. Therefore, it is not surprising that ligation of β_3 integrins might lead to increases in endothelial cell $[Ca^{2+}]_i$ (Schwartz and Denninghoff, 1994) but opposite changes in SMC $[Ca^{2+}]_i$.

Effects of Soluble and Insoluble Integrin Ligands on Ba^{2+} Current

A number of possible explanations may account for the differences between the effects of soluble and insoluble integrin ligands on Ca^{2+} channel current. An obvious possibility is that inhibition of current by soluble FN may be mediated by competitive antagonism of existing integrin–matrix interactions, as suggested for other systems (Poole and Watson, 1995). This would require constitutive phosphorylation of the channel through an integrin-dependent pathway. Indeed, the L-type calcium channel in vascular smooth muscle has been shown to require tyrosine phosphorylation for normal function (Wijetunge et al., 1992; Wijetunge and Hughes, 1996), but whether integrins regulate this pathway is not known. If they do, then disruption of existing integrin–matrix interactions by soluble ligands would produce inhibition of current while clustering of receptors by insoluble ligands (Altieri et al., 1990; Schwartz, 1993), including antibodies (Miyamoto et al., 1995*a*), would produce enhancement of current. In our system, soluble ligands of the $\alpha_v\beta_3$ receptor did produce inhibition of current; however, insoluble β_3 ligands (VN and F11) also produced inhibition of current (Figs. 3 and 4). Thus, it seems likely that these effects resulted from activation of a signaling pathway rather than competition for existing β_3–matrix interactions. Likewise, since insoluble α_5 caused enhancement of current, the competition hypothesis would predict that soluble α_5 should reduce current, which it did not.

A more tenable explanation for our results is the possibility that $\alpha_v\beta_3$ and $\alpha_5\beta_1$ integrins provide distinct and opposing signals to regulate calcium current. As illustrated in Fig. 8 *A*, we propose that selective ligands of the $\alpha_v\beta_3$ receptor (F11, 2C9.G2, VN) cause inhibition of current, selective ligands of the $\alpha_5\beta_1$ receptor (HMα5-1) cause enhancement of current, and ligands for both receptors (FN)

cause an intermediate response. Our hypothesis requires that several conditions be met: (*a*) β_1 and β_3 integrins must signal through different mechanisms in smooth muscle cells. This is supported by the different responses of current to selective ligands of the two respective integrins (Fig. 4 *B* vs. Fig. 6 *B*). In endothelial cells as well (Leavesley et al., 1993), β_1 and β_3 integrins play different roles in regulating Ca^{2+} entry (Leavesley et al., 1993). Our hypothesis also requires that (*b*) the $\alpha_5\beta_1$ integrin can only be activated by insoluble ligands. This is consistent with the observation that soluble α_5 antibody had no effect on current (Fig. 6 *A*), yet was an effective blocker of the response to insoluble FN (Fig. 7 *C*). Experiments by other groups have also shown that soluble α_5 antibody failed to increase pH_i unless it was cross-linked with a secondary antibody to induce integrin clustering (Schwartz et al., 1991*b*). Our hypothesis requires that (*c*) the $\alpha_v\beta_3$ integrin must be capable of signaling when ligands are supplied in either a soluble or insoluble form. In support of this is the observation that six different soluble β_3 ligands (cRGD, VN, FN, bivalent F11, monovalent F11, and 2C9.G2 antibody) all caused inhibition of I_{Ba}, as did two different insoluble β_3 ligands (VN and F11). According to our hypothesis, (*d*) soluble signals must be transmitted only through the $\alpha_v\beta_3$ integrin and not the $\alpha_5\beta_1$ integrin. This is supported by the observation that soluble FN (a proposed ligand only for $\alpha_v\beta_3$) inhibited current, while insoluble FN (a known ligand for both $\alpha_v\beta_3$ and $\alpha_5\beta_1$) enhanced current. Finally, our hypothesis predicts that (*e*) selective ligands of the $\alpha_5\beta_1$ receptor should produce a larger enhancement in current than a common ligand for both integrins (Fig. 8 *B*). Accordingly, the magnitude of the increased current was nearly twofold greater when cells were presented with α_5 antibody–coated beads compared with FN-coated beads (compare Figs. 5 and 6). Collectively, our data are consistent with the hypothesis that $\alpha_v\beta_3$ ligation leads to inhibition of the Ca^{2+} channel, whereas $\alpha_5\beta_1$ ligation leads to stimulation of the Ca^{2+} channel. Further work will be needed to thoroughly test this hypothesis and to determine if other integrins in vascular smooth muscle are also linked to this channel.

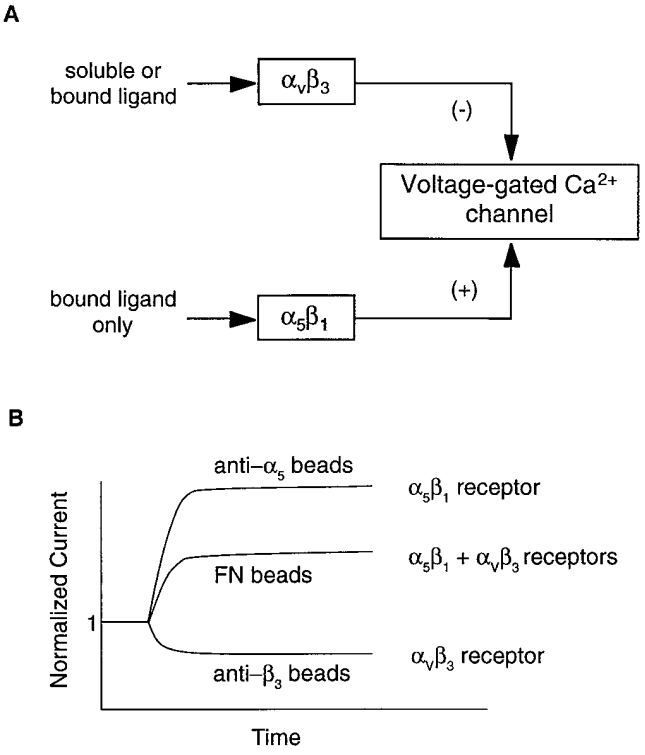

Figure 8. Diagram of hypothesized interactions between $\alpha_v\beta_3$ and $\alpha_5\beta_1$ integrins and the voltage-gated Ca^{2+} channel in vascular smooth muscle. See Discussion for details.

Mechanisms of Calcium Current Modulation

The mechanisms by which $\alpha_v\beta_3$ and $\alpha_5\beta_1$ ligands modulate this calcium channel are not yet clear, but the possibility that the ligands exert a direct effect on the channel seems unlikely for several reasons: (*a*) selective antibodies for β_3 and α_5 integrins modulate Ca^{2+} current, suggesting that regulation occurs in a signaling pathway upstream from the channel rather than at the channel itself; (*b*) there is no reported RGD binding sequence in the structure of α_{1c}, the L-type subunit found in vascular smooth muscle (Koch et al., 1990); and (*c*) antagonists such as dihydropyridines inhibit Ca^{2+} channels within seconds, and divalent cations block within a fraction of a second (Dolphin, 1995; Hughes, 1995), while inhibition of current by soluble $\alpha_v\beta_3$ ligands (Figs. 2–5) required ~60 s to achieve >90% of its maximal effect.

In terms of mechanisms, a more likely possibility is that modulation of current after integrin ligation involves clustering of integrin receptors, recruitment of cytoskeletal proteins, and tyrosine phosphorylation of cytoplasmic signaling molecules, such as FAK, Src, or paxillin, as they are brought into close proximity (Clark and Brugge, 1995). One difference between the effects of soluble and insoluble ligands in our experiments is that soluble ligands had sustained effects on current (soluble FN inhibited current for at least 10 min), while insoluble ligands elicited changes in current that lasted between 6 and 14 min followed by spontaneous recovery. The latter observation would be consistent with a phosphorylation-dependent signaling step that is subject to negative feedback control. This could occur at the level of the receptor, at the channel, or at an intermediate step. In this regard, the affinity of the $\alpha_5\beta_1$ integrin for ligand has been shown to be controlled by the Ca^{2+}-dependent phosphatase CaMKII (Bouvard et al., 1998), such that inhibition of CaMKII preserves the high affinity state of $\alpha_5\beta_1$. A link between integrin signaling and CaMKII has also been demonstrated in vascular smooth muscle (Bilato et al., 1997). Activation of CaMKII after Ca^{2+} influx through L-type channels could reduce $\alpha_5\beta_1$ affinity and reverse the enhancement of current stimulated by $\alpha_5\beta_1$ ligation. However, other possibilities for initiating signals downstream from integrin ligation may also exist, including pathways involving phospholipase C and protein kinase C (Somogyi et al., 1994).

It is likely that $\alpha_v\beta_3$ and $\alpha_5\beta_1$ integrins associate directly with one of the L-type Ca^{2+} channel subunits (e.g., α_{1c}) or with another protein that controls gating or modulates channel activity. A number of cytoplasmic signaling molecules are potential candidates to interact with the calcium

channel. Data from recent experiments on the L-type Ca^{2+} channel in visceral smooth muscle (Hu et al., 1998) have shown that PDGF, which activates a receptor tyrosine kinase, enhances L-type Ca^{2+} current and this effect is blocked after dialysis of the cells with anti-FAK or anti-Src antibodies. Furthermore, α_{1c} coprecipitates with c-Src in that tissue and has a potential tyrosine phosphorylation site (Koch et al., 1990). Dialysis of SMCs with c-Src (Wijetunge and Hughes, 1995) or with a peptide that activates c-Src (Wijetunge and Hughes, 1996) results in enhancement of Ca^{2+} current. Taken together, these results and our own preliminary data showing that tyrosine kinase inhibitors reverse the enhancement of current in response to insoluble FN (Wu, X., G.A. Meininger, G.E. Davis, J.E. Mogford, S.H. Platts, and M.J. Davis. 1997. *Microcirculation.* 4:136a) suggest that the pore-containing subunit of the L-type Ca^{2+} channel may be tyrosine phosphorylated by c-Src, which in turn is regulated by integrin ligation. Additional experiments will be needed to directly test this idea.

The authors thank Judy A. Davidson for technical assistance and Drs. Cindy Meininger and Emily Wilson for advice on various aspects of the experimental design.

This study was supported by National Institutes of Health grants HL-46502 to M.J. Davis and HL-33324 and HL-55050 to G.A. Meininger. Address for reprint requests: M.J. Davis, Dept. of Medical Physiology, 346 Reynolds Medical Building, Texas A & M University Health Science Center, College Station, TX 77843-1114.

Received for publication 9 January 1998 and in revised form 26 August 1998.

References

Aaronson, P.I., T.B. Bolton, R.J. Lang, and I. MacKenzie. 1988. Calcium currents in single isolated smooth muscle cells from the rabbit ear artery in normal-calcium and high-barium solutions. *J. Physiol.* 405:57–75.

Akiyama, S.K. 1996. Integrins in cell adhesion and signaling. *Hum. Cell.* 9:181–186.

Altieri, D.C., W.L. Wiltse, and T.S. Edgington. 1990. Signal transduction initiated by extracellular nucleotides regulates the high affinity ligand recognition of the adhesive receptor CD11b/CD18. *J. Immunol.* 145:662–670.

Bilato, C., K.A. Curto, R.E. Monticone, R.R. Pauly, A.J. White, and M.T. Crow. 1997. The inhibition of vascular smooth muscle cell migration by peptide and antibody antagonists of the $\alpha_v\beta_3$ integrin complex is reversed by activated calcium/calmodulin-dependent protein kinase II. *J. Clin. Invest.* 100: 693–704.

Birnbaumer, L., K.P. Campbell, W.A. Catterall, M.M. Harpold, F. Hofmann, W.A. Horne, Y. Mori, A. Schwartz, T.P. Snutch, T. Tanabe, and R.W. Tsien. 1994. The naming of voltage-gated calcium channels. *Neuron.* 13:505–506.

Bossu, J.L., A. Feltz, J.L. Rodeau, and F. Tanzi. 1989. Voltage-dependent transient calcium currents in freshly dissociated capillary endothelial cells. *FEBS Lett.* 255:377–380.

Bouvard, D., A. Molla, and M.R. Block. 1998. Calcium/calmodulin-dependent protein kinase II controls $\alpha_5\beta_1$ integrin–mediated inside-out signaling. *J. Cell Sci.* 111:657–665.

Brown, E.J. 1993. Signal transduction from leukocyte integrins. *In* Cell Adhesion Molecules. M.E. Hemler and E. Mihich, editors. Plenum Press, New York. 105–125.

Clark, E.A., and J.S. Brugge. 1995. Integrins and signal transduction pathways: the road taken. *Science.* 268:233–239.

Cox, R.H., D. Katzka, and M. Morad. 1992. Characteristics of calcium currents in rabbit portal vein myocytes. *Am. J. Physiol.* 263:H453–H463.

D'Angelo, G., J.E. Mogford, G.E. Davis, M.J. Davis, and G.A. Meininger. 1997. Integrin-mediated reduction in vascular smooth muscle $[Ca^{2+}]_i$ induced by RGD-containing peptide. *Am. J. Physiol.* 272:H2065–H2070.

Davis, G.E. 1992. Affinity of integrins for damaged extracellular matrix: $\alpha_v\beta_3$ binds to denatured collagen type I through RGD sites. *Biochem. Biophys. Res. Commun.* 182:1025–1031.

Dolphin, A.C. 1995. Voltage-dependent calcium channels and their modulation by neurotransmitters and G proteins. *Exp. Physiol.* 80:1–36.

Fleischmann, B.K., R.K. Murray, and M.I. Kotlikoff. 1994. Voltage window for sustained elevation of cytosolic calcium in smooth muscle cells. *Proc. Natl. Acad. Sci. USA.* 91:11914–11918.

Ganitkevich, V.Y., and G. Isenberg. 1991. Depolarization-mediated intracellular calcium transients in isolated smooth muscle cells of guinea-pig urinary bladder. *J. Physiol.* 435:187–205.

Griffith, W.H., L. Taylor, and M.J. Davis. 1994. Whole-cell and single-channel calcium currents in guinea pig basal forebrain neurons. *J. Neurophysiol.* 71: 2359–2376.

Hemler, M.E. 1990. VLA proteins in the integrin family: structures, functions, and their role on leukocytes. *Annu. Rev. Immunol.* 8:365–400.

Hill, M.A., and G.A. Meininger. 1994. Calcium entry and myogenic phenomena in skeletal muscle arterioles. *Am. J. Physiol.* 267:H1085–H1092.

Hill, M.A., M.J. Davis, J.B. Song, and H. Zou. 1996. Calcium dependence of indolactam-mediated contractions in resistance vessels. *J. Pharmacol. Exp. Ther.* 276:867–874.

Hnatowich, D.J., F. Virzi, and M. Ruschowski. 1987. Investigations of avidin and biotin for imaging applications. *J. Nucl. Med.* 28:1294–1302.

Hu, X.-Q., N. Singh, D. Mukhopadhyay, and H.I. Akbarali. 1998. Modulation of voltage-dependent Ca^{2+} channels in rabbit colonic smooth muscle cells by c-Src and focal adhesion kinase. *J. Biol. Chem.* 273:5337–5342.

Hughes, A.D. 1995. Calcium channels in vascular smooth muscle cells. *J. Vasc. Res.* 32:353–370.

Hynes, R.O. 1992. Integrins: versatility, modulation, and signaling in cell adhesion. *Cell.* 69:11–25.

Ingber, D. 1991. Integrins as mechanochemical transducers. *Curr. Opin. Cell Biol.* 3:841–848.

Koch, W.J., P.T. Ellinor, and A. Schwartz. 1990. cDNA cloning of a dihydropyridine-sensitive calcium channel from rat aorta. Evidence for the existence of alternatively spliced forms. *J. Biol. Chem.* 265:17786–17791.

Larson, R.C., G.G. Ignotz, and W.B. Currie. 1992. Effect of fibronectin on early embryo development in cows. *J. Reprod. Fert.* 96:289–297.

Leavesley, D.I., M.A. Schwartz, M. Rosenfeld, and D.A. Cheresh. 1993. Integrin β_1- and β_3-mediated endothelial cell migration is triggered through distinct signaling mechanisms. *J. Cell Biol.* 121:163–170.

McNamee, H.P., D.E. Ingber, and M.A. Schwartz. 1993. Adhesion to fibronectin stimulates inositol lipid synthesis and enhances PDGF-induced inositol lipid breakdown. *J. Cell Biol.* 121:673–678.

Miyamoto, S., S.K. Akiyama, and K.M. Yamada. 1995*a*. Synergistic roles for receptor occupancy and aggregation in integrin transmembrane function. *Science.* 267:883–885.

Miyamoto, S., H. Teramoto, O.A. Coso, J.S. Gutkind, P.D. Burbelo, S.K. Akiyama, and K.M. Yamada. 1995*b*. Integrin function: molecular hierarchies of cytoskeletal and signaling molecules. *J. Cell Biol.* 131:791–805.

Mogford, J.E., G.E. Davis, S.H. Platts, and G.A. Meininger. 1996. Vascular smooth muscle $\alpha_v\beta_3$ integrin mediates arteriolar vasodilation in response to RGD peptides. *Circ. Res.* 79:821–826.

Mogford, J.E., G.E. Davis, and G.A. Meininger. 1997. RGDN peptide interaction with endothelial $\alpha_5\beta_1$ integrin causes sustained endothelin-dependent vasoconstriction of rat skeletal muscle arterioles. *J. Clin. Invest.* 100:1647–1653.

Nelson, M.T., N.B. Standen, J.E. Brayden, and J.F. Worley III. 1988. Noradrenaline contracts arteries by activating voltage-dependent calcium channels. *Nature.* 336:382–385.

Nelson, M.T., J.B. Patlak, J.F. Worley, and N.B. Standen. 1990. Calcium channels, potassium channels, and voltage dependence of arterial smooth muscle tone. *Am. J. Physiol.* 259:C3–C18.

Pierschbacher, M.D., and E. Ruoslahti. 1987. Influence of stereochemistry of the sequence Arg-Gly-Asp-Xaa on binding specificity in cell adhesion. *J. Biol. Chem.* 262:17294–17298.

Plopper, G.E., H.P. McNamee, L.E. Dike, K. Bojanowski, and D.E. Ingber. 1995. Convergence of integrin and growth factor receptor signaling pathways within the focal adhesion complex. *Mol. Biol. Cell.* 6:1349–1365.

Poole, A.W., and S.P. Watson. 1995. Regulation of cytosolic calcium by collagen in single human platelets. *Br. J. Pharmacol.* 115:101–106.

Rae, J.L., and J. Fernandez. 1991. Perforated patch recordings in physiology. *NIPS (News Physiol. Sci.).* 6:273–277.

Schultz, J.F., and D.R. Armant. 1995. β_1- and β_3-class integrins mediate fibronectin binding activity at the surface of developing mouse peri-implantation blastocysts. *J. Biol. Chem.* 270:11522–11531.

Schwartz, M.A. 1993. Spreading of human endothelial cells on fibronectin or vitronectin triggers elevation of intracellular-free calcium. *J. Cell Biol.* 120: 1003–1010.

Schwartz, M.A., and K. Denninghoff. 1994. α_v integrins mediate the rise in intracellular calcium in endothelial cells on fibronectin even though they play a minor role in adhesion. *J. Biol. Chem.* 269:11133–11137.

Schwartz, M.A., D.E. Ingber, M. Lawrence, T.A. Springer, and C. Lechene. 1991*a*. Multiple integrins share the ability to induce elevation of intracellular pH. *Exp. Cell Res.* 195:533–535.

Schwartz, M.A., C. Lechene, and D.E. Ingber. 1991*b*. Insoluble fibronectin activates the Na/H antiporter by clustering and immobilizing integrin $\alpha_5\beta_1$, independent of cell shape. *Proc. Natl. Acad. Sci. USA.* 88:7849–7853.

Schwartz, M.A., E.J. Brown, and B. Fazeli. 1993. A 50 kDa integrin-associated protein is required for integrin-regulated calcium entry in endothelial cells. *J. Biol. Chem.* 268:19931–19934.

Schwarzbauer, J.E. 1991. Fibronectin: from gene to protein. *Curr. Opin. Cell Biol.* 3:786–791.

Sjaastad, M.D., and W.J. Nelson. 1997. Integrin-mediated calcium signaling and

regulation of cell adhesion by intracellular calcium. *BioEssays.* 19:47–55.
Sjaastad, M.D., R.S. Lewis, and W.J. Nelson. 1996. Mechanisms of integrin-mediated calcium signaling in MDCK cells: regulation of adhesion by IP_3- and store-independent calcium influx. *Mol. Biol. Cell.* 7:1025–1041.
Somogyi, L., Z. Lasic, S. Vukicevic, and H. Banfic. 1994. Collagen type IV stimulates an increase in intracellular Ca^{2+} in pancreatic acinar cells via activation of phospholipase C. *Biochem. J.* 299:603–611.
Treede, R.D., R.A. Meyer, K.D. Davis, and J.N. Campbell. 1990. Intradermal injections of bradykinin or histamine cause a flare-like vasodilation in monkey: evidence from laser Doppler studies. *Neurosci. Lett.* 115:201–206.
Wang, N., J.P. Butler, and D.E. Ingber. 1993. Mechanotransduction across the cell surface and through the cytoskeleton. *Science.* 260:1124–1127.
Wei, E.P., H.A. Kontos, W.D. Dietrich, J.T. Povlishock, and E.F. Ellis. 1981. Inhibition by free radical scavengers and by cyclooxygenase inhibitors of pial arteriolar abnormalities from concussive brain injury in cats. *Circ. Res.* 48: 95–103.
Weiss, D.J., O.A. Evanson, and R.E. Wells. 1997. Evaluation of arginine-glycine-aspartate-containing peptides as inhibitors of equine platelet function. *Am. J. Vet. Res.* 58:457–460.
Wijetunge, S., and A.D. Hughes. 1995. $pp60^{c\text{-}src}$ increases voltage-operated calcium channel currents in vascular smooth muscle cells. *Biochem. Biophys. Res. Commun.* 217:1039–1044.
Wijetunge, S., and A.D. Hughes. 1996. Activation of endogenous c-Src or a related tyrosine kinase by intracellular (PY)EEI peptide increases voltage-operated calcium channel currents in rabbit ear artery cells. *FEBS Lett.* 399: 63–66.
Wijetunge, S., C. Aalkjaer, M. Schachter, and A.D. Hughes. 1992. Tyrosine kinase inhibitors block calcium channel currents in vascular smooth muscle cells. *Biochem. Biophys. Res. Commun.* 189:1620–1623.
Yamada, K.M., and B. Geiger. 1997. Molecular interactions in cell adhesion complexes. *Curr. Opin. Cell Biol.* 9:76–85.
Yip, K.P., and D.J. Marsh. 1997. An Arg-Gly-Asp peptide stimulates constriction in rat afferent arteriole. *Am. J. Physiol.* 273:F768–F776.

Potentiation of large conductance, Ca^{2+}-activated K^+ (BK) channels by $\alpha5\beta1$ integrin activation in arteriolar smooth muscle

Xin Wu[2], Yan Yang[1], Peichun Gui[1], Yoshiro Sohma[3], Gerald A. Meininger[1], George E. Davis[1], Andrew P. Braun[4] and Michael J. Davis[1]

[1]*Department of Medical Pharmacology & Physiology and Dalton Cardiovascular Research Center, University of Missouri School of Medicine, Columbia, MO 65212, USA*

[2]*Department of Systems Biology & Translational Medicine, Texas A&M Health Science Center, College Station, TX 77843, USA*

[3]*Department of Physiology, Osaka Medical College, Takatsuki, Osaka 569–8686, Japan*

[4]*Smooth Muscle Research Group, University of Calgary School of Medicine, Calgary, Alberta, Canada T2N 4 N1*

Injury/degradation of the extracellular matrix (ECM) is associated with vascular wall remodelling and impaired reactivity, a process in which altered ECM–integrin interactions play key roles. Previously, we found that peptides containing the RGD integrin-binding sequence produce sustained vasodilatation of rat skeletal muscle arterioles. Here, we tested the hypothesis that RGD ligands work through $\alpha5\beta1$ integrin to modulate the activity of large conductance, Ca^{2+}-activated K^+ (BK) channels in arteriolar smooth muscle. K^+ currents were recorded in single arteriolar myocytes using whole-cell and single-channel patch clamp methods. Activation of $\alpha5\beta1$ integrin by an appropriate, insoluble $\alpha5\beta1$ antibody resulted in a 30–50% increase in the amplitude of iberiotoxin (IBTX)-sensitive, whole-cell K^+ current. Current potentiation occurred 1–8 min after bead–antibody application to the cell surface. Similarly, the endogenous $\alpha5\beta1$ integrin ligand fibronectin (FN) potentiated IBTX-sensitive K^+ current by 26%. Current potentiation was blocked by the c-*Src* inhibitor PP2 but not by PP3 (0.1–1 μM). In cell-attached patches, number of open channels $\times$ open probability (NP_o) of a 230–250 pS K^+ channel was significantly increased after FN application locally to the external surface of cell-attached patches through the recording pipette. In excised, inside-out patches, the same method of FN application led to large, significant increases in NP_o and caused a leftward shift in the NP_o–voltage relationship at constant $[Ca^{2+}]$. PP2 (but not PP3) nearly abolished the effect of FN on channel activity, suggesting that signalling between the integrin and channel involved an increase in Ca^{2+}sensitivity of the channel via a membrane-delimited pathway. The effects of $\alpha5\beta1$ integrin activation on both whole-cell and single-channel BK currents could be reproduced in HEK 293 cells expressing the BK channel α-subunit. This is the first demonstration at the single-channel level that integrin signalling can regulate an ion channel. Our results show that $\alpha5\beta1$ integrin activation potentiates BK channel activity in vascular smooth muscle through both Ca^{2+}- and c-*Src*-dependent mechanisms. This mechanism is likely to play a role in the arteriolar dilatation and impaired vascular reactivity associated with ECM degradation.

(Received 6 December 2007; accepted after revision 23 January 2008; first published online 24 January 2008)
Corresponding author M. J. Davis: Department of Medical Pharmacology & Physiology, University of Missouri School of Medicine, 1 Hospital Dr, Rm M451, Columbia, MO 65212, USA. Email: davismj@health.missouri.edu

Integrins are heterodimeric transmembrane receptors (α, β) that mediate cell adhesion to the extracellular matrix (ECM). Integrin subunits have extracellular domains that bind ECM proteins and short cytoplasmic tails that lack intrinsic kinase activity but associate with a complex of focal adhesion proteins, including numerous tyrosine kinases. The complete activation of integrin-linked signalling pathways, including recruitment and tyrosine phosphorylation of downstream protein targets, requires both integrin receptor occupation and clustering through interactions with insoluble ECM ligands (Yamada *et al.* 1985; Clark & Brugge, 1995).

Our previous work has shown that peptides containing the RGD (Arg-Gly-Asp) sequence, which interact

 DOI: 10.1113/jphysiol.2007.149500

with $\alpha v\beta 3$, $\alpha 5\beta 1$ and other integrins, produce acute constriction of isolated skeletal muscle arterioles. Constriction is followed by a sustained, dose-dependent vasodilatation (Mogford *et al.* 1996, 1997). The constriction is partly explained by signalling between $\alpha 5\beta 1$ integrin and the L-type Ca^{2+} channel in arteriolar smooth muscle (Wu *et al.* 1998, 2001), through a tyrosine kinase cascade in which focal adhesion kinase and c-*Src* play critical roles (Wu *et al.* 2001; Gui *et al.* 2006). However, the mechanism of the secondary, sustained vasodilatation remains unexplained; the observation that it is blocked by K^+ channel antagonists (Platts *et al.* 1998) suggests the involvement of one or more K^+ channels.

Studies show that at least two of the major K^+ channels in vascular smooth muscle (VSM) are regulated by protein tyrosine phosphorylation downstream from growth factor and/or integrin receptor signalling (Davis *et al.* 2001, 2002). hERG K^+ channels, which may contribute to the resting potential of visceral smooth muscle (Akbarali *et al.* 1999), are known to be activated in some cell types (Hofmann *et al.* 2001) following adhesion to the endogenous $\alpha 5\beta 1$ integrin ligand fibronectin (FN). Likewise, Ca^{2+}-activated K^+ channels in erythroleukaemia cells are activated following cell contact with insoluble FN, which is known to engage and aggregate several $\beta 1$ and $\beta 3$ integrins. The downstream effect of integrin activation in that system is an increase in whole-cell, Ca^{2+}-activated K^+ current leading to membrane hyperpolarization (Arcangeli *et al.* 1991, 1993; Becchetti *et al.* 1992). These observations support a possible signalling mechanism between $\beta 1/\beta 3$ integrins and Ca^{2+}-activated K^+ channels.

Large-conductance Ca^{2+}-activated K^+ (BK) channels are highly expressed in VSM and function, at least in part, to counteract depolarizing stimuli that activate Ca^{2+} channels (Brayden & Nelson, 1992). The BK channel is composed of a pore-forming α-subunit and accessory β-subunit (Toro *et al.* 1998) and is activated both by depolarization and by increases in local Ca^{2+} concentration (Nelson & Quayle, 1995; Jackson & Blair, 1998). BK channels are known to undergo protein phosphorylation by intracellular kinases, including c-*Src*, resulting in shifts in the apparent Ca^{2+} sensitivity of the channel (Toro *et al.* 1998; Brenner *et al.* 2000; Cox & Aldrich, 2000; Ling *et al.* 2000; Braun & Sy, 2001; Swayze & Braun, 2001; Alioua *et al.* 2002). For these reasons, we hypothesized that the BK channel may be a downstream target of integrin activation in VSM and may mediate part of the arteriolar vasodilatation produced by integrin ligands. The purpose of the present study was to determine if BK channels in arteriolar smooth muscle cells are regulated by $\alpha 5\beta 1$ integrin signalling.

Methods

Arteriolar smooth muscle cell isolation

Arteriolar myocytes from first- and second-order vessels were isolated according to the method of Wu *et al.* (Wu *et al.* 2001), with slight modifications. Male Sprague–Dawley rats (120–200 g) were anaesthetized with pentobarbital sodium (120 mg kg^{-1}, I.P.). All animal handling procedures followed institutional guidelines and were approved by animal care committees at the University of Missouri and Texas A&M University. Cremaster muscles were excised and pinned flat for vessel dissection at 4°C in Ca^{2+}-free physiological saline solution (PSS) containing (mM): 147 NaCl, 8.6 KCl, 1.17 $MgSO_4$, 1.2 NaH_2PO_4, 5.0 D-glucose, 2.0 pyruvate, 0.02 EDTA, 3 mM Mops, plus 0.1 mg ml^{-1} bovine serum albumin (BSA, Amersham Life Science, Arlington Heights, IL, USA). The animal was then killed with an overdose of pentobarbital (300 mg kg^{-1}, I.C.). Dissected segments of arterioles were transferred to a 1 ml tube of low-Ca^{2+} PSS containing (mM): 144 NaCl, 5.6 KCl, 0.1 $CaCl_2$, 1.0 $MgCl_2$, 0.42 Na_2HPO_4, 0.44 NaH_2PO_4, 10 Hepes, 4.17 $NaHCO_3$, and 1 mg ml^{-1} BSA at room temperature for 10 min. The solution was decanted and replaced with a similar solution containing 26 U ml^{-1} papain (Sigma, St Louis, MO, USA) and 1 mg ml^{-1} dithioerythritol. The vessels were incubated for 30 min at 37°C with occasional agitation, then transferred to a new tube containing low-Ca^{2+} PSS containing 1.95 U ml^{-1} collagenase (FALGPA, Sigma), 1 mg ml^{-1} soybean trypsin inhibitor (Sigma) and 75 U ml^{-1} elastase (Calbiochem, La Jolla, CA, USA), and incubated for 15 min at 37°C. After further digestion, the remaining fragments were gently rinsed 2–3 times with low-Ca^{2+} PSS without BSA and gently triturated using a fire-polished Pasteur pipette to release single cells. Spindle-shaped arteriolar myocytes were used within 4 h of isolation.

Electrophysiological recordings

Patch clamp techniques were employed using an EPC-9 amplifier (HEKA, Germany) to measure membrane current in the whole-cell, cell-attached and inside-out patch configurations (Hamill *et al.* 1981). The amplifier was controlled by a Dell XPS computer running Pulse + Pulsefit software through an ITC-16 interface (Instrutech, Port Washington, NY, USA). Igor Pro (WaveMetrics, Oswego, OR, USA) and Sigma Plot 9.0 (SPSS Inc., Ashburn, VA, USA) were used for data analysis. Micropipettes were pulled from borosilicate glass capillaries (Corning 8161; ID, 1.2 mm; OD, 1.5 mm; WPI, Sarasota, FL, USA) using a Sutter P-97 electrode puller (Sutter Instruments, Foster City, CA, USA).

For whole-cell recordings, pipette resistances ranged from 2.5 to 5.0 MΩ when filled with pipette solution.

Whole-cell K^+ currents were evoked by voltage steps delivered from a typical holding potential (V_h) of −60 mV to potentials ranging from −80 to +80 mV, in 10 mV increments, with a typical duration of 200 ms. Currents were sampled at 10 kHz and filtered at 3 or 5 kHz. BK currents were identified as the IBTX-sensitive component of total K^+ current.

For single-channel recordings, pipettes were 3–5 MΩ and were usually coated with beeswax to reduce noise from stray capacitance. Recordings were filtered at 1 kHz to further reduce noise. BK channels were identified from current–voltage (I–V) relationships obtained at different V_h values from −80 to +80 mV or with voltage ramps from −100 mV to +100 mV (1 s duration). All experiments were performed at room temperature.

Solutions

For whole-cell recordings, two sets of bath and pipette solutions were used. The 136 mM Na^+ bath solution contained (mM): 136 NaCl, 5.9 KCl, 1.8 $CaCl_2$, 1.2 $MgCl_2$, 18 glucose, 1.16 NaH_2PO_4, 10 Hepes, 0.02 EGTA and 2 sodium pyruvate (pH 7.4). The 140 mM Na^+ bath solution contained (mM): 140 NaCl, 5.4 KCl, 2 $CaCl_2$, 1 $MgCl_2$, 10 glucose, 10 Hepes, 2 sodium pyruvate (pH 7.4). The 115 mM K^+ pipette solution contained (mM): 6 NaCl, 115 KCl, 10 Hepes, 1.15 $NaPO_4$, 1.15 NaH_2PO_4, 1.18 $MgCl_2$, 11 glucose, 2 EGTA (pH 7.2); $CaCl_2$ was added to bring free $[Ca^{2+}] = 100$ nM. The 140 mM K^+ pipette solution contained (in mM): 140 KCl, 8 NaCl, 1–2 EGTA, 3 Mg-ATP, 10 Hepes (pH 7.2); $CaCl_2$ was added to bring free $[Ca^{2+}]$ to 600 nM. 4-aminopyridine (4-AP; 1 mM) and glibenclamide (500 nM) were added to the bath solution as indicated to block K_v and K_{ATP} channels, respectively. The addition of other reagents to the bath and/or pipette solutions for specific protocols is stated in the figure legends.

Chemicals

Paxilline was obtained from Transduction Laboratories (Lexington, KY, USA) and Alomone Laboratories (Jerusalem, Israel). Iberiotoxin (IBTX) was obtained from Alomone Laboratories and Sigma. Anti-rat $\alpha5$ integrin monoclonal antibody (HMα5-1), used for protocols on rat VSM cells, was obtained from Pharmingen (San Diego, CA, USA). Anti-rat MHC class I monoclonal antibody (major histocompatability complex; MHC) was obtained from Seikagaku Inc. (Tokyo, Japan). Anti-human $\alpha5\beta1$ integrin monoclonal antibody (JBS5), used for protocols on HEK cells, was obtained from Chemicon (Temecula, CA, USA). Soluble purified fibronectin (FN) fragment (120 kDa), RGD (Arg-Gly-Asp) peptide, PP2 and PP3 were obtained from Chemicon. The BK channel blocker tetraethylammonium chloride (TEA), the small-conductance Ca^{2+}-activated K^+ channel (SK) blocker apamin, the intermediate-conductance Ca^{2+}-activated K^+ channel (IK) blocker TRAM-34 and all other chemicals, except as specifically stated, were obtained from Sigma-Aldrich.

Application of reagents

Anti-$\alpha5$ integrin antibody was coated onto 3.2-μm-diameter streptavidin-coated microspheres (Bangs Laboratories, Fishers, IN, USA) using a biotinylation procedure and applied to individual cells using pressure ejection from a picospritzer micropipette, as previously described (Wu *et al.* 1998, 2001). Soluble RGD and FN were prepared as stock solutions by dissolving the lyophilized compounds in bath or pipette solution, followed by gentle mixing. IBTX, PP2 and PP3 were added to the bath solution.

m*Slo* expression in HEK 293 cells

HEK 293 cells (tsA-201 line) were maintained at 37°C in a 5% CO_2 incubator in Dulbecco's modified Eagle's medium (DMEM) containing L-glutamine, 4.5 g l^{-1} D-glucose and 10% (v/v) fetal bovine serum (Invitrogen, Carlsbad, CA, USA). Transient transfection of cells at 50–60% confluency was carried out in 35 mm tissue culture dishes using the lipofection technique. LipofectAMINE (6–8 μl) was mixed with 0.5 μg of total plasmid cDNA (0.2 μg GFP + 0.3 μg m*Slo*, or 0.2 μg GFP + 0.2 μg m*Slo* + 0.1 μg BK channel $\beta1$-subunit) in 1 ml of serum-free DMEM and placed on cells for 5–6 h at 37°C in a humidified incubator containing 5% CO_2. The cDNA-containing medium was then aspirated and replaced with 10% serum-containing medium. The following day, cells were detached using 0.025% trypsin–0.5 mM EDTA in phosphate-buffered saline and replated onto sterile glass coverslips coated with 0.0001% poly L-lysine in 35 mm culture dishes. Whole-cell current recordings were typically performed on days 2–4 following transfection.

Data analysis

For most whole-cell analyses, raw current values were normalized to cell capacitance and expressed as current density (pA pF^{-1}). For single-channel analysis, amplitude histograms were constructed from continuous recordings at constant V_h and fitted with Gaussian curves to determine average current amplitude. NP_o (number of open channels × open probability) was computed using the method and program previously described (Sohma *et al.* 1996). Summary data are expressed as mean ± S.E.M. Statistical significance was determined using t tests, paired

t tests, or ANOVA, as indicated for specific protocols. Significance levels of $P < 0.05$ were considered significant.

Results

Activation of $\alpha5\beta1$ integrin leads to potentiation of whole-cell BK current

In the whole-cell patch clamp configuration, voltage-dependent K^+ currents in single arteriolar myocytes were activated by depolarizing voltage steps (Fig. 1*A*). Based on previous experience with rat cremaster arteriolar myocytes (Wu *et al.* 2001), whole-cell K^+ currents were likely to be composed primarily of a combination of K_v and BK currents, because addition of 20 mM TEA to the bath or equimolar replacement of KCl with CsCl in pipette solution (140 mM) resulted in almost complete elimination of outward current ($n = 5$, data not shown). With 100 nM Ca^{2+} in the recording pipette and in the presence of 4-AP and glibenclamide externally, the majority of outward current was sensitive to the highly selective BK channel antagonist IBTX (100 nM), as shown by the representative traces (Fig. 1*A*, inset). Summary *I–V* curves from six cells in the absence and presence of IBTX

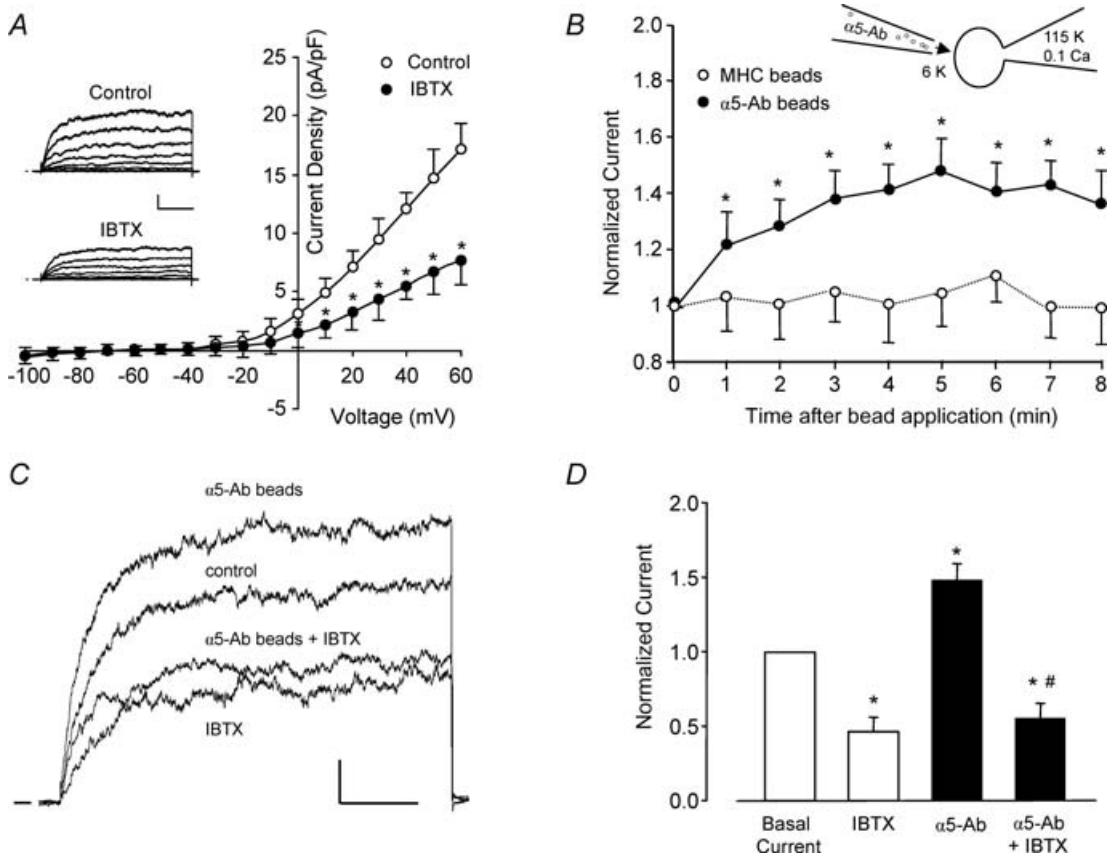

Figure 1. An outward, IBTX-sensitive K^+ current is enhanced by $\alpha5\beta1$ integrin activation
A, average outward current (expressed as current density, pA pF^{-1}) from freshly isolated rat cremaster muscle arteriolar myocytes is plotted as a function of voltage (test pulse), with or without 100 nM IBTX present in the bath ($n = 6$). Inset, representative whole-cell current traces from a single myocyte under control conditions and with 100 nM IBTX in the bath. Calibration bar: 100 pA, 50 ms. $V_h = -60$ mV. *B*, time course of K^+ current enhancement following $\alpha5\beta1$ integrin activation by beads coated with anti-rat $\alpha5$ integrin antibody (HMα5-1); beads were applied from a picospritzer pipette (~5 beads $cell^{-1}$). Beads coated with anti-rat MHC Class I Ab were used as a control to test for a mechanical artifact (○, $n = 7$). Inset shows the recording configuration for panels *B–D*, with the bath solution containing 6 mM K^+ and pipette solution containing 115 mM K^+ and 0.1 μM Ca^{2+}. *C*, sample recordings of whole-cell K^+ current from two arteriolar myocytes in the absence and presence of $\alpha5\beta1$ integrin activation and IBTX (100 nM). Holding potential = −60 mV, test potential = +50 mV, duration = 200 ms. $\alpha5\beta1$ integrin was activated by $\alpha5\beta1$ integrin Ab bound to beads (3 beads for this cell). In a second cell, the potentiation of current in response to integrin activation was blocked in the presence of IBTX (100 nM). Calibration bar: 100 pA, 50 ms. *D*, summary of effects of insoluble $\alpha5$-Ab on BK current in VSM in the absence ($n = 5$) or presence of IBTX ($n = 6$). Bath solution, 136 Na^+ + 4-AP (1 mM) + glibenclamide (500 nM); pipette, 115 K^+ (0.1 μM [Ca^{2+}]). *$P < 0.05$ *versus* control (basal current); #$P < 0.05$ *versus* $\alpha5$-integrin Ab.

are shown in Fig. 1*A*. IBTX inhibited, on average, ∼54% of whole-cell K^+ current, suggesting that this fraction of total K^+ current was contributed by BK channels. When a pipette solution containing a higher free $[Ca^{2+}]_i$ was used (600 nM), IBTX inhibited a larger fraction of the total K^+ current, ∼70% (not shown).

The application of microbeads coated with $\alpha5$ integrin antibody (HMα5-1-Ab) has been shown previously to activate $\alpha5\beta1$ integrin on rat cremaster arteriolar myocytes (Wu *et al.* 2001) and other cells (Yamada *et al.* 1985) through ligation and clustering of the integrin receptor. Under conditions optimal for recording K^+ current, the application of $\alpha5$-Ab-coated beads to individual myocytes resulted in potentiation of macroscopic outward current by ∼1.5-fold. The time course of K^+ current activation in response to +50 mV voltage clamp steps applied once per minute is shown in Fig. 1*B*. The full response was reached within 4–5 min. Current potentiation was not due to a non-specific mechanical effect because, in another group of cells, beads coated with a control Ab (rat MHC) had no significant effect. Sample recordings from two cells are shown in Fig. 1*C*, ∼5 min after $\alpha5$-Ab bead application, where K^+ currents were evoked by repeated voltage steps to +50 mV. In the first cell, current was potentiated by ∼30% after decoration of the cell with $\alpha5$-Ab-coated beads. In a second cell exhibiting approximately the same amount of K^+ current under control conditions (not shown), IBTX (100 nM) reduced basal current by ∼45%; the subsequent application of $\alpha5$ beads in the continued presence of IBTX failed to potentiate K^+ current. Figure 1*D* summarizes the effect of $\alpha5$-Ab bead application in the presence and absence of IBTX. On average, $\alpha5$-Ab bead application produced 48% potentiation of K^+ current and IBTX inhibited ∼54% of basal K^+ current. In the presence of IBTX, no significant potentiation of current occurred in response to $\alpha5$-Ab bead application.

Next, we tested other methods of activating $\alpha5\beta1$ integrin. In previous studies examining the effects of $\alpha5\beta1$ integrin ligands on L-type Ca^{2+} current, $\alpha5$-Ab-coated beads were found to cause a greater effect than the endogenous $\alpha5\beta1$ integrin ligand, FN (Wu *et al.* 1998). As shown in the recordings in Fig. 2*A*, exposure of a VSM cell to soluble FN (10 μg ml^{-1}; 120 kDa FN fragment), either via the bath or from a picospritzer pipette, potentiated whole-cell K^+ current by up to ∼80% at +80 mV (middle trace; time, 5 min; $[Ca^{2+}]_i \approx 600$ nM). Subsequent application of IBTX reduced current below control levels, as shown in the lower set of traces. It was not possible to test the effects of both IBTX and FN on each cell before and after reagent application because neither reagent could be completely washed out. The *I–V* relationship for the same cell is shown in Fig. 2*B*. The actions of FN and other $\alpha5\beta1$ integrin ligands are summarized in Fig. 2*C*. On average, FN potentiated macroscopic K^+ current by 26% ($[Ca^{2+}]_i \approx 100$ nM). Soluble $\alpha5\beta1$ Ab, which presumably ligates but does not crosslink and cluster $\alpha5\beta1$ integrins (Yamada *et al.* 1985), did not produce significant potentiation of K^+ current. RGD peptide potentiated current by 22%. Although the peptide was applied in soluble form, it may have interacted with both $\alpha5\beta1$ and $\alpha v\beta3$ integrins, the latter of which has been linked to the activation of BK channels in endothelium (Kawasaki *et al.* 2004). Also, RGD peptide is known to have agonist or antagonist activity depending on the dose (Tsao & Mousa, 1995). The hierarchy of responses, insoluble $\alpha5$ integrin Ab > FN > RGD, is consistent with the known affinities of $\alpha5\beta1$ integrin for the respective ligands. The control peptide (RAD), which does not ligate integrins (Silletti *et al.* 2000; Martinez-Lemus *et al.* 2005), was without a significant effect on K^+ current.

Our previous studies found that activation of $\alpha5\beta1$ integrin in VSM cells led to potentiation of Ca^{2+} current in part through activation of c-*Src* (Wu *et al.* 2001). Other studies have shown that the tyrosine kinase, c-*Src*, can phosphorylate the BK channel and lead to alterations in channel gating and/or Ca^{2+} sensitivity (Ling *et al.* 2000; Alioua *et al.* 2002). To test the possibility that the potentiation of the BK channel by $\alpha5\beta1$ integrin activation may involve c-*Src*, the soluble c-*Src* inhibitor PP2 (100 nM), was applied to the bath solution while recording whole-cell K^+ current. Under control conditions, PP2 caused ∼14% reduction in BK current amplitude and completely inhibited the potentiation of current following $\alpha5\beta1$ integrin activation (Fig. 2*D*). Application of the inactive analogue PP3 (100 nM) did not significantly reduce basal K^+ current or alter the amount of current potentiation induced by $\alpha5\beta1$ integrin activation.

Effect of $\alpha5\beta1$ integrin activation on single BK channel currents

Next, we investigated integrin-induced potentiation of BK current using single-channel recording methods. The activity of single BK channels was recorded either in cell-attached or excised, inside-out patches from freshly isolated arteriolar myocytes, with the cell or patch bathed in 140 mM K^+ solution to zero the membrane potential and equalize the K^+ gradient. The large single-channel conductance of BK channels was utilized as a marker of channel activity in our recordings and was confirmed using two separate methods: (1) Single-channel currents were recorded for several seconds at various membrane potentials between −80 and +80 mV, after which current amplitudes were detected using Pulse + Pulsefit and the average amplitudes of the events determined from Gaussian fits of the amplitude histogram (Sohma *et al.* 1996); (2) Alternatively, channel conductance was estimated from the amplitude(s) of the open large-conductance channel(s) during a voltage ramp

(from −100 to +100 mV; 1 s duration). Both methods were in excellent agreement when tested on the same patch. BK channels were identified by their characteristic gating behaviour and by exhibiting conductances between 220 and 250 pS as reported by other groups (Latorre *et al.* 1989).

Activating $\alpha5\beta1$ integrin while recording single-channel current proved to be somewhat difficult. We were unable to reliably form outside-out patches that would have permitted bath application of integrin ligands to the exterior surface of excised patches. However, it was possible to maintain cell-attached and inside-out patch recordings when the pipette was dipped in normal pipette solution to fill the tip for a distance of $< 100\ \mu$m, followed by back-filling with the same solution containing soluble FN. Under these recording conditions, diffusion of FN to the tip required 3–5 min, as assessed from pilot experiments using amphotericin B (commonly used for perforated patch recordings) in place of FN and by monitoring the time from initial gigaseal formation to the start of patch permeabilization. The same pipette-filling procedure allowed 3–5 min for the recording of control

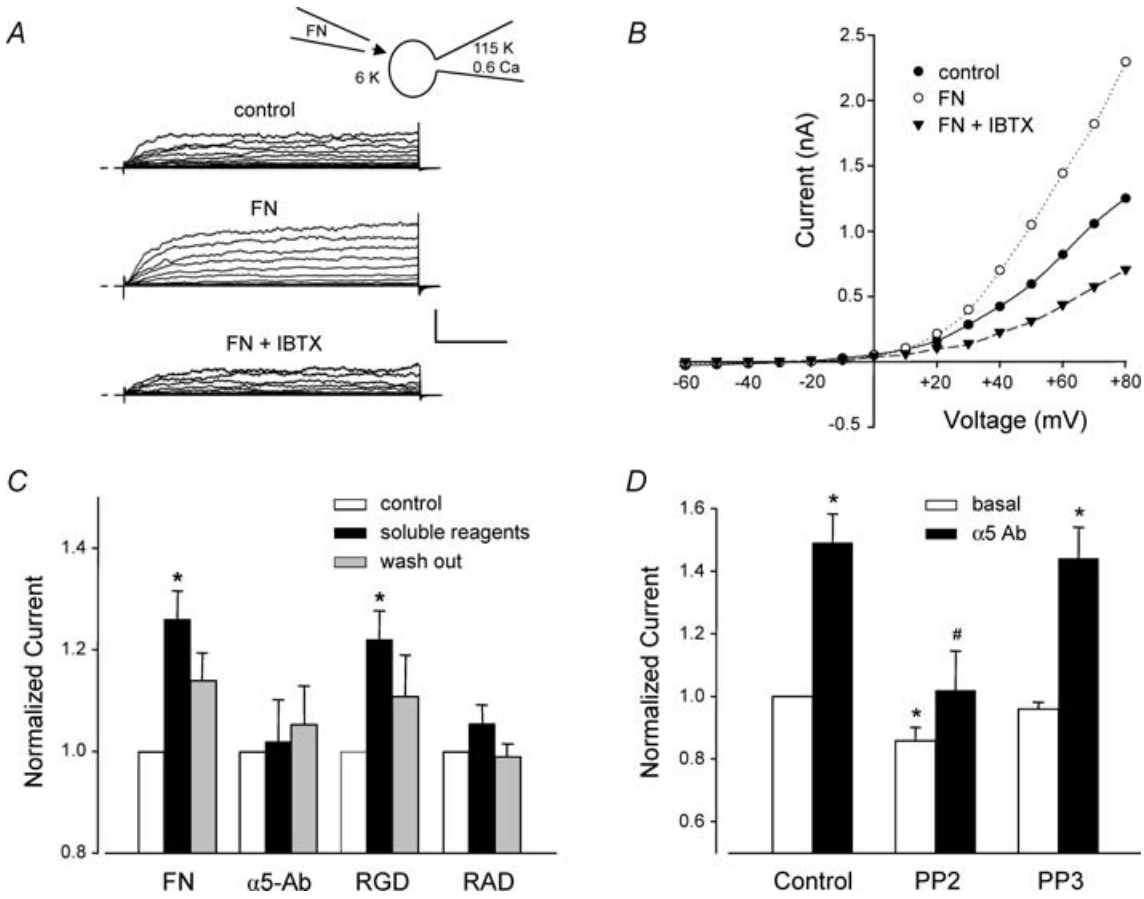

Figure 2. Effects of different $\alpha5\beta1$ integrin ligands on whole-cell VSM K^+ current
A, representative recordings of whole-cell K^+ currents before (control), 3 min after application of soluble FN (10 μg ml^{-1}), and after subsequent addition of IBTX (100 nM) to the bath. Calibration bar: 500 pA, 50 ms. Inset shows recording configuration for all panels. $V_h = -70$ mV. *B*, *I–V* curves derived from current tracings shown in panel *A*. *C*, summary of peak K^+ currents in response to a +50 mV voltage step in which the cells were treated with the following agents for 4 min: soluble FN fragment (10 μg ml^{-1}), soluble RGD peptide (100 μM), soluble $\alpha5$ integrin Ab (15 μg ml^{-1}), or soluble RAD (control peptide for RGD, 100 μM). $^*P < 0.05$ *versus* control. *D*, the soluble c-Src inhibitor PP2 (100 nM, $n = 8$) significantly blocked the potentiation of K^+ current by insoluble $\alpha5$-integrin Ab (measured at 5 min). Pretreatment of cells with PP2 (100 nM) significantly inhibited basal current and prevented enhancement of current after $\alpha5\beta1$ integrin activation. The inactive analogue PP3 (100 nM, $n = 8$) slightly but not significantly decreased basal BK current and did not significantly alter enhancement of current after $\alpha5\beta1$ integrin activation. All values were normalized to the value of control current at a test potential of +50 mV; $V_h = -60$ mV. For panels *A* and *B*, the bath solution was 140 mM Na^+, 6 mM K^+ + 4-AP (1 mM) + glibenclamide (500 nM); the pipette solution contained 115 mM K^+ and 0.6 μM Ca^{2+}. For panels *C* and *D* the bath solution was 136 Na^+ + 1 mM 4-AP + 500 nM glibenclamide; pipette solution: 115 K^+ with 100 nM Ca^{2+}. $^*P < 0.05$ *versus* control (basal current). #$P < 0.05$ *versus* control $\alpha5$-Ab.

channel activity before FN reached the patch. While this approach enabled us to test the effect of soluble FN, we could not test the effect of insoluble $\alpha5\beta1$ integrin Ab (i.e. on beads) or the effect of soluble $\alpha5\beta1$ integrin Ab crosslinked by an appropriate secondary Ab (Yamada *et al.* 1985; Elemer & Edgington, 1994) as we have previously shown is possible under whole-cell recording conditions (Wu *et al.* 1998).

Figure 3*A* shows data obtained from a cell-attached patch when the pipette was back-filled with FN ($15\,\mu g\,ml^{-1}$). At the top is a diagram of the preparation, illustrating the recording configuration with the cell bathed in 140 mM K^+ solution to zero the membrane potential ($V_h = +80$ mV). Immediately after seal formation (arrowhead in the top trace), basal channel activity was quite low and the infrequent openings shown probably represent a mixture of different K^+ channels. However after ~5 min, the open probability of a large amplitude channel increased dramatically (NP_o increased from 0.0032 to 0.23). The amplitude at +80 mV was consistent with current carried by a BK channel, but to confirm this, voltage ramps were used to estimate single-channel conductance. The lower inset shows an example of two ramps (−100 to +100 mV) applied during the first minute after seal formation and then after a sufficient amount of time for FN to diffuse to the membrane (respective times are indicated by open and closed symbols). At ~1 min, there were no channel openings at negative potentials but at ~5 min of recording, channel activity was evident at all potentials between −75 and +100 mV. The conductance of the larger amplitude openings was estimated to be 228 pS, which is consistent with a BK channel (representative of 4 cells). Figure 3*B* summarizes the NP_o values measured from similar protocols before and after FN ($n = 4$). On average, there was a 17-fold increase in NP_o under these recording conditions. Time controls made in other cells without FN in the pipette showed no significant changes in NP_o over the same time scale (0.077 ± 0.001 and 0.082 ± 0.001, respectively).

Under the experimental conditions used in Fig. 3, activation of $\alpha5\beta1$ integrin on the outer surface of the patch could initiate Ca^{2+} entry through L-type and other Ca^{2+} channels that might subsequently activate BK channels in the vicinity of the Ca^{2+} channel (Wang *et al.* 2005; Balasubramanian *et al.* 2007). However, the data in Figs 1 and 2 suggest that $\alpha5\beta1$ integrin activation can activate BK current under conditions where both voltage and intracellular Ca^{2+} are clamped (i.e. using whole-cell voltage clamp and cell dialysis with Ca^{2+}–EGTA from the pipette). Furthermore, inhibition of the response by PP2 (Fig. 2*D*) suggests that the sensitivity of the channel can be increased at a constant $[Ca^{2+}]_i$ by integrin-induced c-*Src* activity (Ling *et al.* 2000). We attempted to further test this idea by increasing the Ca^{2+} buffering on the internal surface of the cell-attached patch. Arteriolar myocytes were pre-loaded with the fast Ca^{2+} chelator BAPTA-AM ($10\,\mu M$) for 15 min and then superfused with 140 mM K^+ bath solution containing variable amounts of Ca^{2+}. When both bath and pipette solutions were Ca^{2+} free, BK channel openings were extremely rare at any voltage, even in the presence of FN ($n = 5$, data not shown). When the pipette solution was nominally Ca^{2+} free and the bath solution contained 1 mM Ca^{2+}, FN-induced K^+ channel openings were observed only at positive potentials during voltage ramps. With 1 mM $CaCl_2$ in the bath and 0.5 mM $CaCl_2$ in the pipette, BK channel openings were rare under control conditions, but FN diffusion to the pipette tip

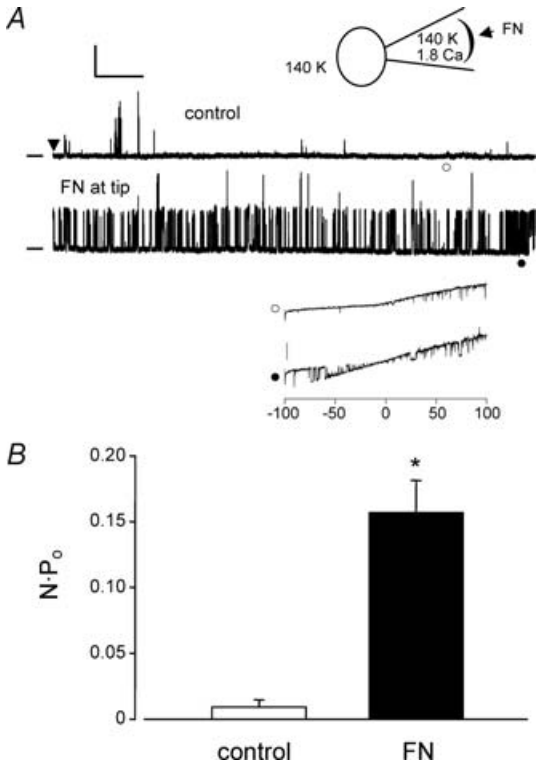

Figure 3. Effect of soluble FN on single-channel BK currents
A, cell-attached patch recording from a VSM cell bathed in solution containing 140 mM K^+ and 2 mM Ca^{2+} (represented by inset diagram). Pipette tip was filled for ~100 μm with 140 mM K^+ pipette solution containing 1.8 mM Ca^{2+}, and then back-filled with the same solution containing FN ($10\,\mu g\,ml^{-1}$). After gigaseal formation, single-channel K^+ currents were recorded at $V_h = +80$ mV. After allowing 5 min for diffusion of FN to the membrane, there was a dramatic increase in the activity of a large-conductance channel (lower trace), with NP_o increasing from 0.0032 to 0.23 in this patch. Calibration bar: 20 pA, 0.5 s. Zero current level is indicated by dash at left. Inset shows current recordings in response to two voltage ramps (from −100 to +100 mV, 1 s duration) performed at 1 min (○) and 5 min (●). Transient openings of a large-conductance K^+ channel were seen first only at positive voltages, but at 5 min, numerous channel openings were evident at both positive and negative voltage potentials. Calibration bar: 20 pA. Conductance of the channel was estimated to be 228 pS (from the lower *I–V* trace). *B*, graph of NP_o (mean ± S.E.M.) at +80 mV before and after FN diffusion to the cell surface ($n = 4$).

(3–5 min after gigaseal formation) induced the opening of a large-conductance channel at both negative and positive potentials. Figure 4*A* shows a recording of K^+ channel activity under the latter conditions, with the membrane potential held at +70 mV. For the first 4 min after gigaseal formation (denoted by the arrowhead in the top trace), very little channel activity was present. At ∼5 min, there was an abrupt opening of a much larger conductance K^+ channel with gating behaviour characteristic of a BK channel (the lower trace shows an expanded time scale). NP_o in this patch increased from 0.00026 (at 1 min) to 0.43 (at 5 min). After the channel opened, current was recorded at various holding potentials to determine channel conductance (not shown), and a conductance estimate of 242 pS was also made using a voltage ramp in the same patch. Figure 4*B* shows the single-channel *I–V* curve averaged from similar recordings made in two cells in which conductance averaged 230 pS. Figure 4*C* summarizes the change in NP_o for three cells under these conditions, where NP_o increased > 400-fold in response to FN. The large relative change in NP_o in Fig. 4*C* compared to that in Fig. 3 was due primarily to a lower basal NP_o caused by the increased Ca^{2+} buffering. The observation that no BK channel activity could be recorded under more stringent Ca^{2+} buffering conditions is consistent with a certain amount of external Ca^{2+} being permissive for increased BK channel activity in response to FN.

While the single-channel recordings in Figs 3 and 4 suggest that BK channels can be activated through a membrane-delimited signalling pathway following $\alpha5\beta1$ integrin engagement, a more definitive test would be to perform similar protocols in excised, inside-out (cell-free) patches. Figure 5 shows the results of such experiments. In Fig. 5*A*, a patch was excised from an arteriolar myocyte and bathed in 140 mM K^+ bath solution at a fixed internal [Ca^{2+}] of 0.8 μM. The pipette solution contained 140 mM K^+ and 1.8 mM Ca^{2+}. To minimize the potential contribution of other K^+ channels, the pipette also included 50 nM apamin (to block small-conductance, Ca^{2+}-activated K^+ channels) and

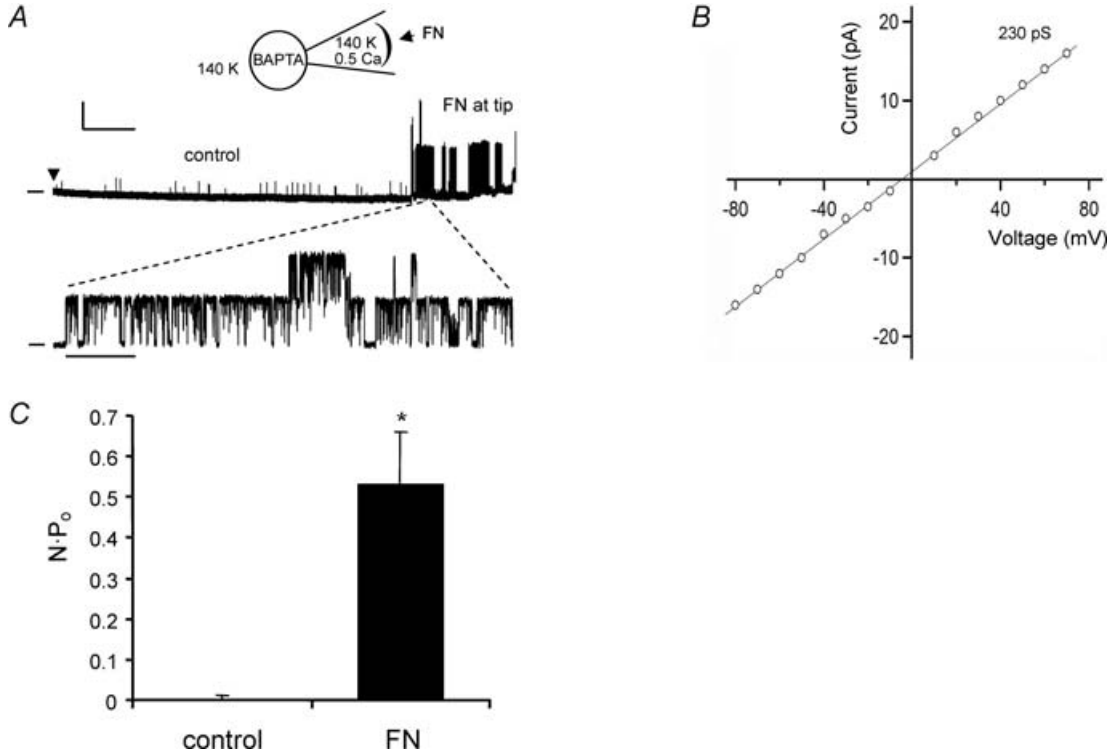

Figure 4. Effect of FN on single-channel BK currents in cells loaded with BAPTA
A, current recording from a cell-attached patch held at $V_h = +70$ mV with cell in 140 K^+ bath solution containing 1 mM Ca^{2+} (depicted by inset diagram). Cell was pre-loaded with BAPTA-AM (10 μM) for 15 min. The patch pipette tip was dipped into 140 K^+ pipette solution containing 0.5 mM Ca^{2+}, 50 nM apamin and 1 μM TRAM-34, then back-filled with the same solution containing FN (10 μg ml^{-1}). Calibration bar: 10 pA, 50 s. An expanded trace is shown in the lower panel, with at least 2 large-conductance channels evident. Time calibration bar: 1 s. Zero current level is indicated by dash at left. *B*, average *I–V* plot obtained from experiments similar to panel *A* with current amplitude measured ∼5 min after gigaseal formation at various holding potentials from −80 mV to +80 mV. The mean slope conductance of the channel was 230 pS ($n = 2$). *C*, average NP_o (mean ± S.E.M.) at +80 mV measured during the first (control) and fifth (FN) minutes using the same protocol as in panel *A*.

1 μM TRAM-34 (to block intermediate-conductance, Ca^{2+}-activated K^+ channels). FN was applied to the cell through the recording pipette as described for Figs 3 and 4. The top trace in Fig. 5*A* shows the baseline channel activity of an inside-out patch during the first minute following patch excision; NP_o was 0.091. The lower trace shows channel activity after ~5 min, allowing for FN to diffuse to the membrane; NP_o had increased to 0.3. Voltage steps were subsequently used to determine the *I–V* relationship for the channel, as shown in Fig. 5*B*. Conductance was 245 pS during the first minute and 255 pS during the fifth minute, consistent with the known behaviour of BK channels in symmetrical high K^+ solutions.

The increase in BK channel activity induced by FN under conditions when membrane potential and intracellular $[Ca^{2+}]$ were fixed is consistent with another mechanism regulating the channel. Subsequently, we tested whether c-Src was involved. Figure 5*C* shows a diagram of the preparation and a sample current recording. A patch was excised from an arteriolar myocyte and exposed to the same solutions as described in Fig. 5*A*. The baseline activity of a large-conductance channel was relatively low for the first few minutes, but increased at about the fifth minute. The inset shows two voltage ramps performed at the times indicated by the open and closed circles. The conductance for the larger unitary current amplitude

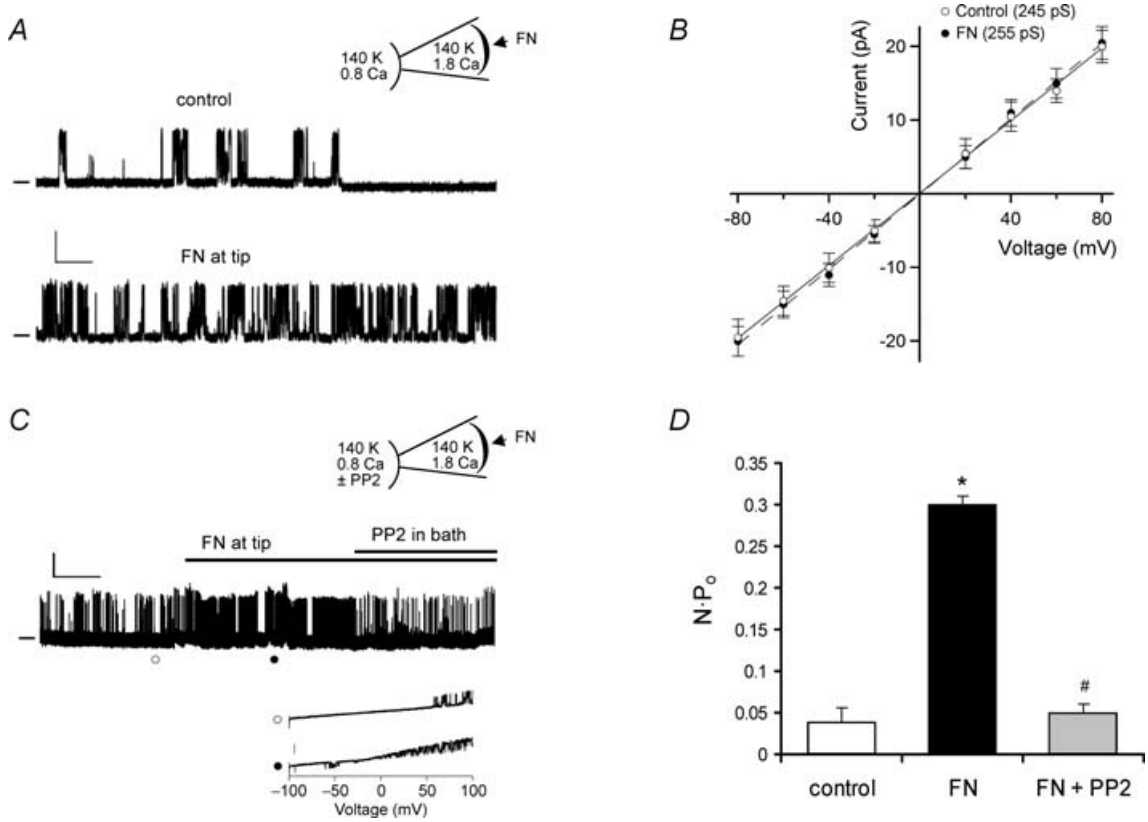

Figure 5. Effect of FN on single-channel BK currents in excised patches
A, current recording from an excised, inside-out patch at $V_h = +60$ mV with patch bathed in 140 K^+ bath solution containing 0.8 μM Ca^{2+} (represented by inset diagram). Pipette tip was filled for ~100 μm with 140 K^+ pipette solution containing 1.8 mM Ca^{2+}, 50 nM apamin, 1 μM TRAM-34 and then back-filled with the same solution containing FN (10 μg ml^{-1}). The upper trace (control) was acquired during the first min after gigaseal formation and the lower trace was acquired after ~5 min, allowing FN time to diffuse to the membrane. Calibration bar: 10 pA, 0.5 s. Zero current level is indicated by dash at left. *B*, *I–V* plot from single-channel currents obtained using same protocol as in panel *A* with current amplitudes measured at ~1 min and ~5 min after gigaseal formation at various holding potentials between −80 mV and +80 mV. *C*, current recording from an excised, inside-out patch at $V_h = +60$ mV with solutions as depicted in inset diagram. PP2 (1 μM) was added to the bath at ~5 min. Calibration bar: 10 pA, 1 min. Inset shows current recordings in response to two voltage ramps (from −100 to +100 mV, 1 s duration) performed at times indicated by ○ (upper trace) and ● (lower trace). Calibration bar for inset: 20 pA. Conductance of the channel in this patch was estimated to be 233 pS from the lower trace. *D*, summary data for NP_o measurements (mean ± S.E.M.) at +80 mV during control, FN, and FN + PP2 periods. The average conductance was 242 ± 5 pS for control; 237 ± 4 pS for FN and 238 ± 5 pS for FN + PP2, as estimated from voltage ramps as shown in *C*. For PP3 experiments using the same protocol, the values of NP_o were 0.04 ± 0.02 for control, 0.48 ± 0.06 for FN, 0.49 ± 0.07 for FN + PP3. $^*P < 0.05$ *versus* control. #$P < 0.05$ *versus* FN.

was 243 pS for control and 235 pS for FN. After channel activity had stabilized at a higher level, PP2 (1 μM) was added to the bath. In the presence of PP2, NP_o rapidly returned toward control levels. Figure 5*D* summarizes the changes in NP_o for this protocol ($n = 4$). On average, FN induced ~8-fold increase in NP_o and the potentiation of channel activity was almost completely reversed by PP2. The inactive analogue PP3 was without significant effect at the same concentration.

Integrin activation enhances activity of heterologously expressed BK channels

VSM cells contain a mixture of different K^+ channels whose activity might be altered directly or indirectly following integrin activation. Although the component of K^+ current potentiated by $\alpha5\beta1$ integrin activation was almost completely eliminated by the selective BK channel toxin inhibitor IBTX (Fig. 1) and single-channel currents activated by FN application had conductances consistent with those of BK channels (Figs 3–5), we sought to confirm our findings in a heterologous cell system that did not endogenously express BK channels. To do this, the pore-forming α-subunit of the mouse BK channel (m*Slo*) was transiently expressed in HEK 293 cells at low density so that whole-cell currents could be recorded without saturating the patch clamp amplifier. Parallel experiments using excised macropatch recordings at higher channel density were conducted in a separate study (Yang *et al.* 2008).

Figure 6*A* shows examples of whole-cell, K^+ current recordings in a non-transfected HEK cell, a cell transfected

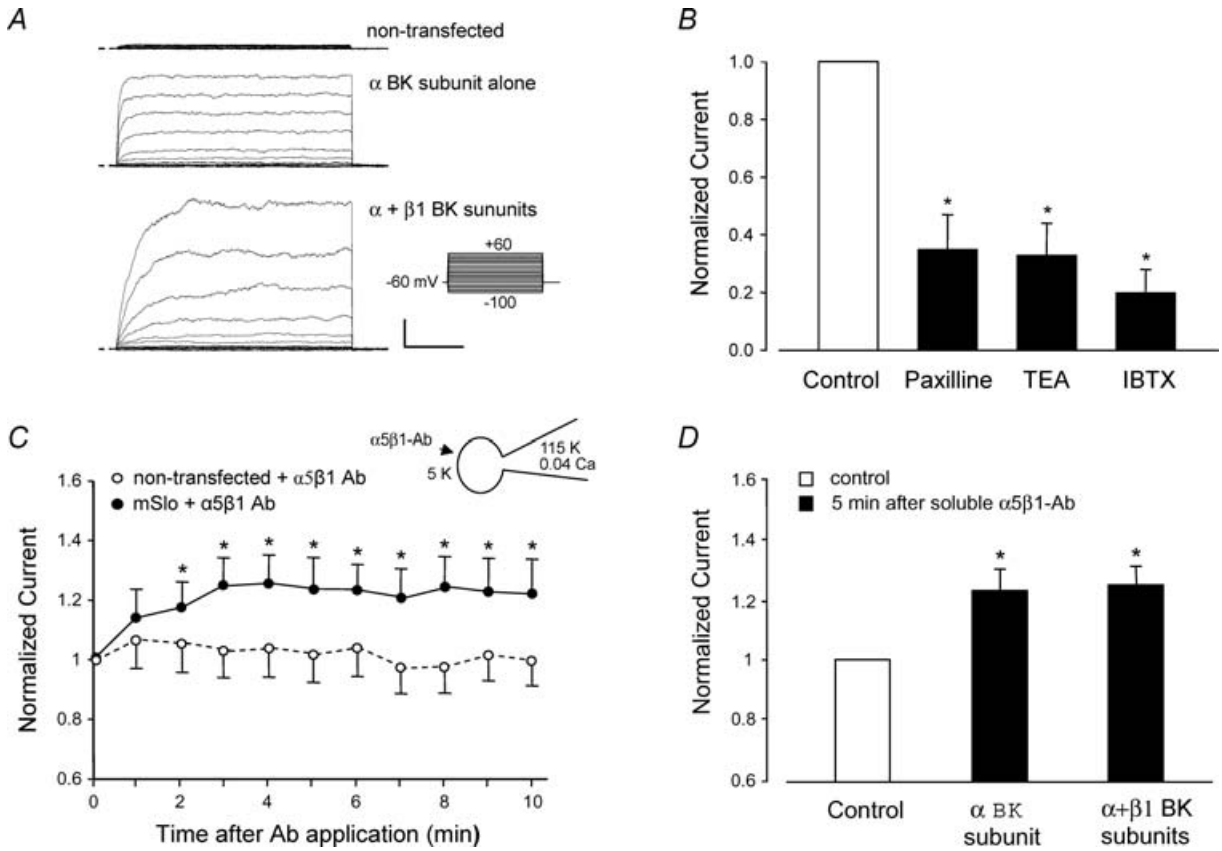

Figure 6. Activation of $\alpha5\beta1$ integrin increases current in heterologously expressed BK channels (m*Slo*)
A, whole-cell currents recorded from HEK 293 cells transiently transfected with cDNA for the murine brain BK α-subunit (m*Slo*). Top trace shows background current level in a representative non-transfected cell; middle trace shows current in cell expressing m*Slo* alone; lower trace shows current in cell expressing both m*Slo* and $\beta1$ BK channel subunits. Calibration bar: 500 pA, 50 ms. *B*, effects on peak m*Slo* currents (at +50 mV) of the BK channel inhibitors paxilline (10 μM), TEA (1 mM), or IBTX (100 nM) added to the bath. *C*, the time course of whole-cell m*Slo* current potentiation after application of soluble $\alpha5\beta1$ integrin Ab (JBS5, 15 μg ml^{-1}) to non-transfected ($n = 7$) or transfected HEK cells (BK α-subunit only, $n = 5$). The enhancement of m*Slo* current at +50 mV was first significant at 2 min and lasted > 10 min. The application of a soluble control Ab (IgG) did not produce a significant change in BK current (not shown). *D*, potentiation of m*Slo* current by $\alpha5\beta1$ integrin Ab in cells expressing m*Slo* alone ($n = 5$) or m*Slo* + $\beta1$ BK subunit ($n = 8$). Inset diagram in *C* shows recording configuration for all panels: whole-cell recording mode, $V_h = -60$ mV; bath solution: 136 mM Na^+; pipette solution: 115 mM K^+ and ~40 nM [Ca^{2+}].

with m*Slo* alone, and a cell transfected with both m*Slo* and $\beta1$ BK channel subunits. The common stimulation protocol is shown at the right. Non-transfected cells exhibited negligible outward current. m*Slo*-transfected cells showed a rapidly activating, non-inactivating outward K^+ current. Cells transfected with both BK channel subunits showed, on average, larger currents and that activated more slowly. These characteristics of heterologously expressed BK channels are in agreement with previous reports from other labs (McManus *et al.* 1995; Nimigean & Magleby, 1999; Cox & Aldrich, 2000). Figure 6*B* shows normalized whole-cell m*Slo* currents recorded before and after addition of the BK channel inhibitors paxilline (100 nM), TEA (1 mM) or IBTX (100 nM) to the bath, confirming that m*Slo* currents were sensitive to classic BK channel inhibitors.

We then tested whether m*Slo* current was potentiated by activation of $\alpha5\beta1$ integrin. HEK cells endogenously express $\alpha5\beta1$ integrin (Yang *et al.* 2008). Although soluble Ab does not activate this integrin in freshly isolated VSM cells (Fig. 2*C*), it does activate the integrin in HEK 293 cells (tSA 201 line), as previously reported (Gui *et al.* 2006), presumably due to the presence of the T surface antigen (and possible integrin crosslinking) in this transformed cell line. Using the whole-cell recording mode, soluble $\alpha5\beta1$ integrin antibody was applied to the cell from the bath. Figure 6*C* plots the time course of whole-cell m*Slo* current following application of soluble $\alpha5\beta1$ integrin Ab (JBS5, 15 μg ml^{-1}). Under these conditions, there was an ~25% increase in outward current in m*Slo*-transfected cells after $\alpha5\beta1$-Ab application, but no significant current increase in non-transfected cells. Furthermore, potentiation followed a time course similar to that of BK current potentiation in native VSM cells after $\alpha5\beta1$ integrin activation (Fig. 1*B*). A similar degree of whole-cell BK current potentiation was observed in cells transfected with both α and $\beta1$ BK channel subunits (Fig. 6*D*), indicating that only the α-subunit was essential for mediating the effect of integrin activation.

Discussion

Our results show that the activation of $\alpha5\beta1$ integrin on the surface of rat arteriolar smooth muscle cells leads to potentiation of BK channel activity through both a Ca^{2+}-dependent mechanism and a phosphorylation mechanism involving c-*Src*. In whole-cell recordings, ligation and clustering of $\alpha5\beta1$ integrin by insoluble $\alpha5\beta1$ antibody (Ab) resulted in ~30–50% increase in BK current amplitude, with the effect first being significant at 1 min and reaching a maximum at 4–5 min. Current potentiation was blocked by the BK channel inhibitor IBTX or by the c-*Src* inhibitor PP2. Soluble FN and RGD peptide each had effects qualitatively similar to insoluble $\alpha5\beta1$ antibody. In cell-attached and inside-out patches, application of the endogenous $\alpha5\beta1$ integrin ligand FN locally to the patch exterior led to large increases in the NP_o of single BK channels, suggesting that the signalling mechanism between the integrin and the channel occurred through a membrane-delimited pathway. Similarly, the enhancement in BK channel activity induced by FN was observed under conditions where intracellular Ca^{2+} was clamped, suggesting that at least part of the effect of integrin activation was mediated by an increase in BK channel Ca^{2+} sensitivity. The effects of $\alpha5\beta1$ integrin activation on BK current could be reproduced in HEK 293 cells expressing the BK channel α-subunit. These findings are consistent with previous observations that the vasodilatory effects of RGD peptide on rat skeletal muscle arterioles (Platts *et al.* 1998) were mediated by the activation of one or more K^+ channels. Our results show that ECM–integrin interactions can regulate VSM BK channels suggesting that this mechanism may play a role in the control of blood flow under both physiological and pathological conditions (Zhou *et al.* 2005).

Coordinated regulation of BK and Ca^{2+} channels by $\alpha5\beta1$ integrin

Previous work from our laboratory demonstrated that ligands of $\alpha5\beta1$ integrin (the FN receptor) and $\alpha v\beta3$ integrin (the vitronectin receptor) reciprocally regulate L-type Ca^{2+} current in myocytes isolated from rat skeletal muscle arterioles (Wu *et al.* 1998). Activation of $\alpha5\beta1$ integrin can evoke an ~70% increase in whole-cell L-type Ca^{2+} current in VSM (Wu *et al.* 2001) and > 2-fold change in whole-cell Cav1.2 current in HEK 293 cells heterologously expressing Cav1.2 channels (Gui *et al.* 2006). Integrin-induced potentiation of Cav1.2 current is mediated by phosphorylation of the channel α-subunit on two C-terminal residues by PKA and c-*Src*. Our finding in the present study that the soluble c-*Src* inhibitor, PP2, blocked BK current potentiation following $\alpha5\beta1$ integrin activation implies that c-*Src* is a key downstream mediator of integrin signalling to both channels. The specific role of c-*Src* in BK channel regulation under these conditions is the topic of a separate study (Yang *et al.* 2008). The activation of a channel that promotes vasodilatation (BK) and a channel that promotes vasoconstriction (Cav1.2) would seemingly lead to antagonistic effects on vascular tone. However, the time courses for integrin-induced potentiation of current in the two channels are different, with potentiation of BK channels being slightly delayed but more sustained (Fig. 1) relative to the potentiation of Cav1.2 channels (Wu *et al.* 1998). Therefore, the net effect of $\alpha5\beta1$ integrin activation in VSM would be a transient

increase in Ca^{2+} influx that is attenuated or terminated by BK-induced membrane hyperpolarization. Presumably, this influx subsequently triggers Ca^{2+} release and/or Ca^{2+}-dependent intracellular signalling mechanisms.

Integrin-induced membrane hyperpolarization has been reported in other cell types (Arcangeli *et al.* 1987, 1989; Hofmann *et al.* 2001), but our results provide the first evidence that BK channel activation may be a key underlying mechanism in VSM. Arcangeli and colleagues first reported that FN–integrin interactions elicited hyperpolarization of murine erythroleukaemia cells (Arcangeli *et al.* 1991), an effect presumably mediated by the activation of Ca^{2+}-activated K^+ channels (Arcangeli *et al.* 1987, 1989). The same group has also shown that the activation of $\beta1$ integrins in neuroblastoma and haemopoietic tumour cells leads to sustained activation of hERG K^+ current (Hofmann *et al.* 2001). $\alpha v\beta3$ integrin activation by vitronectin in cultured endothelial cells also induces membrane hyperpolarization mediated by outward BK current (Kawasaki *et al.* 2004). That result is consistent with, but not necessarily linked to, the observation that the $\alpha v\beta3$ integrin-blocking Ab, F11, prevents (attenuates) flow-induced dilatation of arterioles (Muller *et al.* 1997), a response known to be associated with K^+ channel activation (Platts *et al.* 1998).

Using single-channel recording methods in the present study, we were able to demonstrate that BK channel activity was potentiated as a consequence of integrin activation. We sought to answer at least two questions with single channel experiments: (1) Is the signalling between $\alpha5\beta1$ integrin and the BK channel membrane delimited, i.e. is the entire complement of signalling machinery contained within the patch? (2) Is the increase in channel activity explained simply by an increase in global/local $[Ca^{2+}]$ as a result of integrin-mediated Ca^{2+} entry or release, or is there also a shift in BK channel sensitivity to a given concentration of intracellular Ca^{2+}? The latter mechanism would implicate a possible channel phosphorylation mechanism, which has previously been shown to modify Ca^{2+} sensitivity of the BK channel (Reinhart *et al.* 1991; Taniguchi *et al.* 1993; Ling *et al.* 2000; Alioua *et al.* 2002). In single-channel recordings, the activation of BK channels could possibly be obscured by the presence of other native K^+, Cl^- and/or cation channels, especially in the absence of compounds to specifically block them. Indeed, we routinely observed the activity of outward currents through channels of various conductances under basal conditions (see Figs 3–5). For this reason, it was important to verify the single-channel conductance of any putative BK channel for which gating appeared to be increased in association with FN application; in each recording considered for further analysis, the conductance was well within the range previously reported for BK channels (Figs 3–5).

In cell-attached patches, BK channel activity was significantly increased after localized application of FN to the patch exterior via the recording pipette. To detect the effects of FN against a background of basal BK channel activity, which could vary widely from patch to patch, the pipette tip was filled with FN-free solution, while the remainder of the pipette was back-filled with FN-containing solution. Adjusting the amount of tip filling gave variable amounts of time for 'control' recordings before FN diffused to the surface of the patch. FN-induced BK channel gating in this protocol demonstrates that all of the enzymatic machinery for channel activation is contained in the vicinity of the membrane patch where BK channel activity was measured. However, intracellular $[Ca^{2+}]$ was, again, not controlled and the increase in BK channel activity could have reflected a local change in Ca^{2+} due to FN-stimulated Ca^{2+} entry/release within the patch environment. When local Ca^{2+} changes were minimized by pre-loading the cells with the fast Ca^{2+} chelator BAPTA, a large increase in BK channel activity still occurred in response to patch-specific FN application. The left-ward shift in the *I–V* relationship was suggestive of an increase in Ca^{2+} sensitivity, although we had no way to verify the extent to which intracellular $[Ca^{2+}]$ remained constant. It is interesting to note, however, that a minimal level of Ca^{2+} was needed in the recording pipette under such conditions to even record basal channel activity. The strongest evidence for integrin-induced BK channel potentiation being at least partially mediated by a shift in Ca^{2+} sensitivity came from excised, inside-out patch recordings, where $[Ca^{2+}]$ on the inner surface of the patch remained fixed while FN was applied to the outer surface of the patch through the recording pipette. Under those conditions, integrin-induced potentiation of BK channel activity was still consistently observed (Figs 4 and 5), but at a lower $[Ca^{2+}]$ than reported by Ling (Ling *et al.* 2000), possibly due to the presence of the $\beta1$ BK channel subunit in native VSM cells that would enhance the Ca^{2+} sensitivity of the channel. Furthermore, the effect of FN in the same recording configuration was almost completely blocked by PP2 (Fig. 5). The effect of $\alpha5\beta1$ integrin activation on BK channel Ca^{2+} sensitivity, and the role of c-Src in that process, are issues that are explored in more detail in a separate study (Yang *et al.* 2008).

It is interesting that FN produced, on average, a 26% increase in whole-cell BK current (Fig. 2*A*), but produced much larger (10- to 20-fold) increases in BK single channel activity (quantified as NP_o in excised patches) (Figs 3*B* and 5*D*). There are a number of likely explanations for this apparent discrepancy. First, cytosolic free Ca^{2+} was held at a higher concentration in excised patch *versus* whole-cell recordings – a condition under which integrin activation would be expected to lead to a larger increase in the activity of single-channel events (Yang *et al.* 2008). Second, one would expect that the single-channel data

shown here represent only a subset of the response of the entire BK channel population in a given cell in which FN was observed to have an effect. Since we had no independent method of verifying whether FN reached the extracellular surface of every membrane patch tested, we were able to quantify the effect of FN *only* in patches where (1) BK channels were observed to be present before FN application (Fig. 5*A*) or (2) FN stimulated BK channel activity in the absence of basal channel activity (Fig. 4*A*). In fact, we observed no response to FN in about 40% of total patches examined and therefore did not include those cells in the NP_o analysis. Thus, the single-channel recordings shown here only illustrate the effect of FN on a portion of BK channels in a single cell, such that any recorded macroscopic whole-cell current will reflect a mixed population of stimulated and unstimulated BK channels. If colocalization of the channel and integrin is necessary for channel modulation, some channels would predictably be unaffected by FN–integrin binding, since it is unlikely that all BK channels in a given smooth muscle cell colocalize with $\alpha5\beta1$ integrin. Despite these caveats, our experiments demonstrate that all of the functional signalling components between the $\alpha5\beta1$ integrin and the BK channel are contained within the patch and that the increase in channel activity is mediated in part by a shift in Ca^{2+} sensitivity, due to the activity of c-*Src*.

Physiological relevance of BK channel regulation by ECM

The blood vessel wall is composed of a number of different extracellular matrix proteins, including collagen, fibronectin and laminin (Weber & McFadden, 1997; Bonacci *et al.* 2006; Lebleu *et al.* 2007). Matrix composition is reported to change as the vessel wall is remodelled in disease states such as hypertension, diabetes, ischaemia-reperfusion injury and atherosclerosis (Cagliero *et al.* 1988; Roth *et al.* 1993; Bezie *et al.* 1998; Brownlee, 2000; Intengan & Schiffrin, 2000). For example, osteopontin, fibrinogen and vitronectin – ECM proteins not normally found in the vessel wall at significant levels – are deposited during the formation of an atherosclerotic plaque. With wall remodelling, there are also corresponding changes in both the number and type of integrins expressed by VSM and endothelium (Roth *et al.* 1993; Regoli & Bendayan, 1997; Intengan *et al.* 1999). These changes in wall composition occur in parallel with impaired vascular reactivity (Hultgardh-Nilsson & Durbeej, 2007; Strom *et al.* 2007).

A possible explanation for changes in vascular reactivity under these conditions involves alterations in the signalling between adhesion molecules and vascular ion channels. Indeed, a number of studies have now shown that integrin ligands can acutely regulate the tone of blood vessels (Mogford *et al.* 1997; Muller *et al.* 1997; Platts *et al.* 1998), in part through the role that integrins play in mechanotransduction (Martinez-Lemus *et al.* 2005; Heerkens *et al.* 2007; Lal *et al.* 2007). In addition, matrix degradation subsequent to chronic remodelling, inflammation and vascular wall injury results in the release of cryptic matrix fragments (matricryptins), some of which are vasoactive (Mogford *et al.* 1997; Bayless *et al.* 2000; Davis *et al.* 2000). In this context, $\alpha v\beta3$ integrin has been proposed to function as an injury receptor that may detect the presence of proteins such as vitronectin and osteopontin (Davis *et al.* 2000). Vitronectin is known to activate BK current through $\alpha v\beta3$ integrin in vascular endothelium (Kawasaki *et al.* 2004). Therefore, it is reasonable to expect that changes in the vascular ECM-integrin composition, and the consequent changes in the signalling pathways downstream from those integrins, including BK channel activation, underlie part of the altered vascular reactivity associated with many vascular diseases.

References

Akbarali HI, Thatte H, He XD, Giles WR & Goyal RK (1999). Role of HERG-like K^+ currents in opossum esophageal circular smooth muscle. *Am J Physiol Cell Physiol* **277**, C1284–C1290.

Alioua A, Mahajan A, Nishimaru K, Zarei MM, Stefani E & Toro L (2002). Coupling of c-Src to large conductance voltage- and Ca^{2+}-activated K^+ channels as a new mechanism of agonist-induced vasoconstriction. *Proc Natl Acad Sci U S A* **99**, 14560–14565.

Arcangeli A, Becchetti A, Del Bene MR, Wanke E & Olivotto M (1991). Fibronectin-integrin binding promotes hyperpolarization of murine erythroleukemia cells. *Biochem Biophys Res Commun* **177**, 1266–1272.

Arcangeli A, Becchetti A, Mannini A, Mugnai G, De Filippi P, Tarone G, Del Bene MR, Barletta E, Wanke E & Olivotto M (1993). Integrin-mediated neurite outgrowth in neuroblastoma cells depends on the activation of potassium channels. *J Cell Biol* **122**, 1131–1143.

Arcangeli A, Riccarda Del Bene M, Poli R, Ricupero L & Olivotto M (1989). Mutual contact of murine erythroleukemia cells activates depolarizing cation channels, whereas contact with extracellular substrata activates hyperpolarizing Ca^{2+}-dependent K^+ channels. *J Cell Physiol* **139**, 1–8.

Arcangeli A, Wanke E, Olivotto M, Camagni S & Ferroni A (1987). Three types of ion channels are present on the plasma membrane of Friend erythroleukemia cells. *Biochem Biophys Res Commun* **146**, 1450–1457.

Balasubramanian L, Ahmed A, Lo CM, Sham JS & Yip KP (2007). Integrin-mediated mechanotransduction in renal vascular smooth muscle cells: activation of calcium sparks. *Am J Physiol Regul Integr Comp Physiol* **293**, R1586–R1594.

Bayless KJ, Salazar R & Davis GE (2000). RGD-dependent vacuolation and lumen formation observed during endothelial cell morphogenesis in three-dimensional fibrin matrices involves the $\alpha_v\beta_3$ and $\alpha_5\beta_1$ integrins. *Am J Pathol* **156**, 1673–1683.

Becchetti A, Arcangeli A, Del Bene MR, Olivotto M & Wanke E (1992). Response to fibronectin–integrin interaction in leukaemia cells: delayed enhancing of a K^+ current. *Proc Biol Sci* **248**, 235–240.

Bezie Y, Lamaziere JM, Laurent S, Challande P, Cunha RS, Bonnet J & Lacolley P (1998). Fibronectin expression and aortic wall elastic modulus in spontaneously hypertensive rats. *Arterioscler Thromb Vasc Biol* **18**, 1027–1034.

Bonacci JV, Schuliga M, Harris T & Stewart AG (2006). Collagen impairs glucocorticoid actions in airway smooth muscle through integrin signalling. *Br J Pharmacol* **149**, 365–373.

Braun AP & Sy L (2001). Contribution of potential EF hand motifs to the calcium-dependent gating of a mouse brain large conductance, calcium-sensitive K^+ channel. *J Physiol* **533**, 681–695.

Brayden JE & Nelson MT (1992). Regulation of arterial tone by activation of calcium-dependent potassium channels. *Science* **256**, 532–535.

Brenner R, Perez GJ, Bonev AD, Eckman DM, Kosek JC, Wiler SW, Patterson AJ, Nelson MT & Aldrich RW (2000). Vasoregulation by the $\beta 1$ subunit of the calcium-activated potassium channel. *Nature* **407**, 870–876.

Brownlee M (2000). Negative consequences of glycation. *Metabolism* **49**, 9–13.

Cagliero E, Maiello M, Boeri D, Roy S & Lorenzi M (1988). Increased expression of basement membrane components in human endothelial cells cultured in high glucose. *J Clin Invest* **82**, 735–738.

Clark EA & Brugge JS (1995). Integrins and signal transduction pathways: the road taken. *Science* **268**, 233–239.

Cox DH & Aldrich RW (2000). Role of the $\beta 1$ subunit in large-conductance Ca^{2+}-activated K^+ channel gating energetics. Mechanisms of enhanced Ca^{2+} sensitivity. *J Gen Physiol* **116**, 411–432.

Davis GE, Bayless KJ, Davis MJ & Meininger GA (2000). Regulation of tissue injury responses by the exposure of matricryptic sites within extracellular matrix molecules. *Am J Pathol* **156**, 1489–1498.

Davis MJ, Wu X, Nurkiewicz TR, Kawasaki J, Davis GE, Hill MA & Meininger GA (2001). Integrins and mechanotransduction of the vascular myogenic response. *Am J Physiol Heart Circ Physiol* **280**, H1427–H1433.

Davis MJ, Wu X, Nurkiewicz TR, Kawasaki J, Gui P, Hill MA & Wilson E (2002). Regulation of ion channels by integrins. *Cell Biochem Biophys* **36**, 41–66.

Elemer GS & Edgington TS (1994). Two independent sets of monoclonal antibodies define neoepitopes linked to soluble ligand binding and leukocyte adhesion functions of activated αM $\beta 2$. *Circ Res* **75**, 165–171.

Gui P, Wu X, Ling S, Stotz SC, Winkfein RJ, Wilson E, Davis GE, Braun AP, Zamponi GW & Davis MJ (2006). Integrin receptor activation triggers converging regulation of Cav1.2 calcium channels by c-Src and protein kinase A pathways. *J Biol Chem* **281**, 14015–14025.

Hamill OP, Marty A, Neher E, Sakmann B & Sigworth FJ (1981). Improved patch-clamp techniques for high-resolution current recording from cells and cell-free membrane patches. *Pflugers Arch* **391**, 85–100.

Heerkens EH, Izzard AS & Heagerty AM (2007). Integrins, vascular remodeling, and hypertension. *Hypertension* **49**, 1–4.

Hofmann G, Bernabei PA, Crociani O, Cherubini A, Guasti L, Pillozzi S, Lastraioli E, Polvani S, Bartolozzi B, Solazzo V, Gragnani L, Defilippi P, Rosati B, Wanke E, Olivotto M & Arcangeli A (2001). HERG K^+ channels activation during B_1 integrin-mediated adhesion to fibronectin induces an up-regulation of $\alpha_v\beta_3$ integrin in the preosteoclastic leukemia cell line FLG 29.1. *J Biol Chem* **276**, 4923–4931.

Hultgardh-Nilsson A & Durbeej M (2007). Role of the extracellular matrix and its receptors in smooth muscle cell function: implications in vascular development and disease. *Curr Opin Lipidol* **18**, 540–545.

Intengan HD, Deng LY, Li JS & Schiffrin EL (1999). Mechanics and composition of human subcutaneous resistance arteries in essential hypertension. *Hypertension* **33**, 569–574.

Intengan HD & Schiffrin EL (2000). Structure and mechanical properties of resistance arteries in hypertension: role of adhesion molecules and extracellular matrix determinants. *Hypertension* **36**, 312–318.

Jackson WF & Blair KL (1998). Characterization and function of Ca^{2+}-activated K^+ channels in arteriolar muscle cells. *Am J Physiol Heart Circ Physiol* **274**, H27–H34.

Kawasaki J, Davis GE & Davis MJ (2004). Regulation of Ca^{2+}-dependent K^+ current by $\alpha v\beta 3$ integrin engagement in vascular endothelium. *J Biol Chem* **279**, 12959–12966.

Lal H, Verma SK, Smith M, Guleria RS, Lu G, Foster DM & Dostal DE (2007). Stretch-induced MAP kinase activation in cardiac myocytes: differential regulation through $\beta 1$-integrin and focal adhesion kinase. *J Mol Cell Cardiol* **43**, 137–147.

Latorre R, Oberhauser A, Labarca P & Alvarez O (1989). Varieties of calcium-activated potassium channels. *Annu Rev Physiol* **51**, 385–399.

Lebleu VS, Macdonald B & Kalluri R (2007). Structure and function of basement membranes. *Exp Biol Med (Maywood)* **232**, 1121–1129.

Ling S, Woronuk G, Sy L, Lev S & Braun AP (2000). Enhanced activity of a large conductance, calcium-sensitive K^+ channel in the presence of Src tyrosine kinase. *J Biol Chem* **275**, 30683–30689.

McManus OB, Helms LM, Pallanck L, Ganetzky B, Swanson R & Leonard RJ (1995). Functional role of the β subunit of high conductance calcium-activated potassium channels. *Neuron* **14**, 645–650.

Martinez-Lemus LA, Crow T, Davis MJ & Meininger GA (2005). $\alpha v\beta 3$- and $\alpha 5\beta 1$-integrin blockade inhibits myogenic constriction of skeletal muscle resistance arterioles. *Am J Physiol Heart Circ Physiol* **289**, H322–H329.

Mogford JE, Davis GE & Meininger GA (1997). RGDN peptide interaction with endothelial $\alpha 5\beta 1$ integrin causes sustained endothelin-dependent vasoconstriction of rat skeletal muscle arterioles. *J Clin Invest* **100**, 1647–1653.

Mogford JE, Davis GE, Platts SH & Meininger GA(1996). Vascular smooth muscles $\alpha v\beta 3$ integrin mediates arteriolar vasodilation in response to RGD peptides. *Circ Res* **79**, 821–826.

Muller JM, Chilian WM & Davis MJ (1997). Integrin signaling transduces shear stress-dependent vasodilation of coronary arterioles. *Circ Res* **80**, 320–326.

Nelson MT & Quayle JM (1995). Physiological roles and properties of potassium channels in arterial smooth muscle. *Am J Physiol Cell Physiol* **268**, C799–C822.

Nimigean CM & Magleby KL (1999). The β subunit increases the Ca^{2+} sensitivity of large conductance Ca^{2+}-activated potassium channels by retaining the gating in the bursting states. *J Gen Physiol* **113**, 425–440.

Platts SH, Mogford JE, Davis MJ & Meininger GA (1998). Role of K^+ channels in arteriolar vasodilation mediated by integrin interaction with RGD-containing peptide. *Am J Physiol Heart Circ Physiol* **275**, H1449–H1454.

Regoli M & Bendayan M (1997). Alterations in the expression of the $\alpha3\beta1$ integrin in certain membrane domains of the glomerular epithelial cells (podocytes) in diabetes mellitus. *Diabetologia* **40**, 15–22.

Reinhart PH, Chung S, Martin BL, Brautigan DL & Levitan IB (1991). Modulation of calcium-activated potassium channels from rat brain by protein kinase A and phosphatase 2A. *J Neurosci* **11**, 1627–1635.

Roth T, Podesta F, Stepp MA, Boeri D & Lorenzi M (1993). Integrin overexpression induced by high glucose and by human diabetes: potential pathway to cell dysfunction in diabetic microangiopathy. *Proc Natl Acad Sci U S A* **90**, 9640–9644.

Silletti S, Mei F, Sheppard D & Montgomery AM (2000). Plasmin-sensitive dibasic sequences in the third fibronectin-like domain of L1-cell adhesion molecule (CAM) facilitate homomultimerization and concomitant integrin recruitment. *J Cell Biol* **149**, 1485–1502.

Sohma Y, Harris A, Wardle CJ, Argent BE & Gray MA (1996). Two barium binding sites on a maxi K^+ channel from human vas deferens epithelial cells. *Biophys J* **70**, 1316–1325.

Strom A, Fredrikson GN, Schiopu A, Ljungcrantz I, Soderberg I, Jansson B, Carlsson R, Hultgardh-Nilsson A & Nilsson J (2007). Inhibition of injury-induced arterial remodelling and carotid atherosclerosis by recombinant human antibodies against aldehyde-modified apoB-100. *Atherosclerosis* **190**, 298–305.

Swayze RD & Braun AP (2001). A catalytically inactive mutant of type I cGMP-dependent protein kinase prevents enhancement of large conductance, calcium-sensitive K^+ channels by sodium nitroprusside and cGMP. *J Biol Chem* **276**, 19729–19737.

Taniguchi J, Furukawa KI & Shigekawa M (1993). Maxi K^+ channels are stimulated by cyclic guanosine monophosphate-dependent protein kinase in canine coronary artery smooth muscle cells. *Pflugers Arch* **423**, 167–172.

Toro L, Wallner M, Meera P & Tanaka Y (1998). Maxi-K_{Ca}, a unique member of the voltage-gated K channel superfamily. *News Physiol Sci* **13**, 112–117.

Tsao PW & Mousa SA (1995). Thrombospondin mediates calcium mobilization in fibroblasts via its Arg-Gly-Asp and carboxyl-terminal domains. *J Biol Chem* **270**, 23747–23753.

Wang J, Shimoda LA, Weigand L, Wang W, Sun D & Sylvester JT (2005). Acute hypoxia increases intracellular $[Ca^{2+}]$ in pulmonary arterial smooth muscle by enhancing capacitative Ca^{2+} entry. *Am J Physiol Lung Cell Mol Physiol* **288**, L1059–L1069.

Weber DJ & McFadden PN (1997). Injury-induced enzymatic methylation of aging collagen in the extracellular matrix of blood vessels. *J Protein Chem* **16**, 269–281.

Wu X, Davis GE, Meininger GA, Wilson E & Davis MJ (2001). Regulation of the L-type calcium channel by $\alpha5\beta1$ integrin requires signaling between focal adhesion proteins. *J Biol Chem* **276**, 30285–30292.

Wu X, Mogford JE, Platts SH, Davis GE, Meininger GA & Davis MJ (1998). Modulation of calcium current in arteriolar smooth muscle by $\alpha v\beta3$ and $\alpha5\beta1$ integrin ligands. *J Cell Biol* **143**, 241–252.

Yamada KM, Akiyama SK, Hasegawa T, Hasegawa E, Humphries MJ, Kennedy DW, Nagata K, Urushihara H, Olden K & Chen WT (1985). Recent advances in research on fibronectin and other cell attachment proteins. *J Cell Biochem* **28**, 79–97.

Yang Y, Wu X, Wu JB, Sheng JZ, Ling S, Braun AP, Davis GE & Davis MJ(2008). $\alpha5\alpha1$ integrin activation increases BK channel current and Ca^{2+} sensitivity through c-Src mediated channel phosphorylation. *J Biol Chem*.

Zhou R, Liu L & Hu D (2005). Involvement of BKCa α subunit tyrosine phosphorylation in vascular hyporesponsiveness of superior mesenteric artery following hemorrhagic shock in rats. *Cardiovasc Res* **68**, 327–335.

Acknowledgements

We thank David Durtschi and Judy Davidson for their technical assistance. We are also grateful to Drs David Murchison and William Griffith for advice concerning several of the patch clamp protocols. This work was supported by NIH grants HL-072989 and HL-089784.